SPIKES FOR SINGULARLY PERTURBED REACTION-DIFFUSION SYSTEMS AND CARRIER'S PROBLEM

MICHAEL J. WARD

Dept. of Mathematics,
University of British Columbia,
Vancouver, B.C., Canada V6T 1Z2
E-mail: ward@math.ubc.ca

1. Introduction

For a two-component reaction-diffusion system, Turing [97] in 1952 used a linear stability analysis to show that a spatially homogeneous steady-state solution that is stable in the absence of diffusion can be destablilized when the ratio of the diffusion coefficients is sufficiently large. This diffusion induced instability of the homogeneous state leads to various types of stable spatial patterns. Spike patterns are those where one or both of the chemical species concentrate, or localize, at certain points in the domain. There has been considerable progress over the past thirty years in developing weakly nonlinear theories to analyze small amplitude patterns that emerge from an initially spatially homogeneous solution. However, there are many open problems that relate to the stability and dynamics of fully nonlinear, but localized structures, in reaction-diffusion systems. In the survey chapter on pattern formation by Knobloch (see [61]), he remarks that "The question of stability of finite amplitude structures, be they periodic or localized, and their bifurcation is a major topic that requires new insights". In this survey we make an effort in this direction by giving some results for the existence, stability, and dynamics, of spike patterns to a few reaction-diffusion systems, including the Gierer-Meinhardt (GM) model [36], the Gray-Scott (GS) model [37], and the Schnakenburg (SC) model [90]. Specific open problems are also mentioned.

The GM model has been used to model a range of localization processes in nature, including morphogenesis and the formation of sea-shell patterns (cf. [70], [71]). In dimensionless form, the GM model is given by

$$a_t = \varepsilon^2 \triangle a - a + \frac{a^p}{h^q}\,, \quad x \in \Omega\,; \quad \partial_n a = 0\,, \quad x \in \partial\Omega\,, \tag{1.1a}$$

$$\tau h_t = D \triangle h - h + \frac{a^m}{\varepsilon^N h^s}\,, \quad x \in \Omega\,; \quad \partial_n h = 0\,, \quad x \in \partial\Omega\,. \tag{1.1b}$$

Here Ω is a bounded simply-connected domain in $\mathbb{R}^N$, a and h are the activator and inhibitor concentrations, $\varepsilon^2 \ll 1$ and D are the two diffusivities, τ is a reaction-time constant, and ∂_n denotes the outward normal derivative. The exponents (p, q, m, s) in the GM model are assumed to satisfy

$$p > 1, \qquad q > 0, \qquad m > 0, \qquad s \geq 0, \qquad \zeta \equiv \frac{mq}{p-1} - (s+1) > 0\,. \tag{1.2}$$

For $N > 3$, we assume that $p < p_c = (N+2)/(N-2)$, where p_c is the critical Sobolev exponent.

The Gray-Scott system, introduced in [37] and popularized in the numerical study of [86], models an irreversible reaction involving two reactants in a gel reactor, where the reactor is maintained in contact with a reservoir of one of the two chemicals in the reaction. In the nondimensional variables of [74], this system can be written in one spatial dimension as

$$v_t = \varepsilon^2 v_{xx} - v + A u v^2\,, \quad |x| < 1\,; \quad v_x(\pm 1, t) = 0\,, \tag{1.3a}$$

$$\tau u_t = D u_{xx} + (1-u) - u v^2\,, \quad |x| < 1\,; \quad u_x(\pm 1, t) = 0\,. \tag{1.3b}$$

Here $D > 0$, $\tau > 1$, $\varepsilon \ll 1$, and $A > 0$. Two ranges of the feed-rate parameter A are of interest: the high feed-rate regime where $A = O(1)$ and the low feed-rate regime where $A = O(\varepsilon^{1/2})$. In this latter regime, we introduce the new variables

$$A = \varepsilon^{1/2} \tilde{A}\,, \qquad v = \varepsilon^{-1/2} \nu\,. \tag{1.4}$$

In terms of (1.4), (1.5) is transformed to

$$\nu_t = \varepsilon^2 \nu_{xx} - \nu + \tilde{A} u \nu^2\,, \quad |x| < 1\,; \quad \nu_x(\pm 1, t) = 0\,, \tag{1.5a}$$

$$\tau u_t = D u_{xx} + (1-u) - \varepsilon^{-1} u \nu^2\,, \quad |x| < 1\,; \quad u_x(\pm 1, t) = 0\,. \tag{1.5b}$$

The Schnakenberg model [90] is another well-known two-component reaction-diffusion system. In non-dimensional form, and in one spatial di-

mension, this system is given by (cf. [107]),

$$u_t = \varepsilon^2 u_{xx} - u + vu^2\,, \quad |x| < 1\,; \quad u_x(\pm 1, t) = 0\,, \tag{1.6a}$$

$$\tau v_t = Dv_{xx} + \frac{1}{2} - \frac{b}{\varepsilon} vu^2\,, \quad |x| < 1\,; \quad v_x(\pm 1, t) = 0\,. \tag{1.6b}$$

In this survey we will only consider the semi-strong interaction limit where $\varepsilon \ll 1$ and $D = O(1)$. In this limit, only one of the two chemical species in (1.1), (1.5), and (1.6), becomes localized. For each of these problems, we will find that the localizing chemical can be well-approximated by dilations of the radially symmetric ground-state solution $w(\rho)$, with $\rho = |y|$, where $w(\rho)$ is the unique solution to

$$w'' + \frac{(N-1)}{\rho} w' - w + w^p = 0\,, \quad \rho \geq 0\,, \tag{1.7a}$$

$$w(0) > 0\,, \quad w'(0) = 0\,, \quad w \sim c\rho^{-(N-1)/2} e^{-\rho}\,, \quad \text{as} \quad \rho \to \infty\,. \tag{1.7b}$$

where $p > 1$ and c is a positive constant. There exists a unique solution to (1.7) when $N = 1$ and $N = 2$, while for $N \geq 3$ we require that $p < p_c$ (cf. [65]. The one-dimensional problem with $N = 1$, plays an important role in our survey. In this case, with $\rho = y$, we readily calculate that

$$w(y) = \left(\frac{p+1}{2}\right)^{1/(p-1)} \left(\cosh\left[\frac{(p-1)y}{2}\right]\right)^{-2/(p-1)}\,, \quad c = (2p+2)^{1/(p-1)}\,. \tag{1.8}$$

For the special case $p = 2$ and $N = 1$, we get $w(y) = \frac{3}{2}\mathrm{sech}^2(y/2)$.

The topics in this survey are organized into sections of increasing problem complexity. In Sec. 2 we consider scalar nonlinear problems. We first focus on constructing k-spike equilibria to nonlinear boundary value problems of the type originally considered in [13]. Then, we describe some results for spikes in scalar quasilinear elliptic problems. In Sec. 3 we study the stability and dynamics of spikes for certain scalar, but nonlocal, problems. One such problem arises from the shadow limit associated with (1.1). In Sec. 4 we survey some bifurcation and dynamical phenomena that occur for one-spike solutions to the reaction-diffusion system (1.1). Finally, in Sec. 5 we give some equilibrium and stability results for multi-spike patterns of the reaction-diffusion systems (1.1), (1.5), (1.3), and (1.6).

2. Spike Equilibria for Scalar Problems

In this section we begin by constructing asymptotic solutions for

$$\varepsilon^2 u'' + Q(u) = 0\,, \qquad -1 < x < 1\,, \tag{2.1}$$

with various boundary conditions at $x = \pm 1$. The assumptions on $Q(u)$ are that $Q(u)$ is smooth and that it has only two zeroes, s and s_b, with $s < s_b$, where $Q^{'}(s) < 0$, and $Q^{'}(s_b) > 0$. In addition we assume that there exists a $u_m > s_b$ such that $\int_s^{u_m} Q(\eta)\, d\eta = 0$. In Fig. 1 we plot such a $Q(u)$, and in Fig. 2 we plot the corresponding phase-plane u_z versus u, where $z = x/\varepsilon$, showing a saddle point at $u = s$ and a separatrix structure.

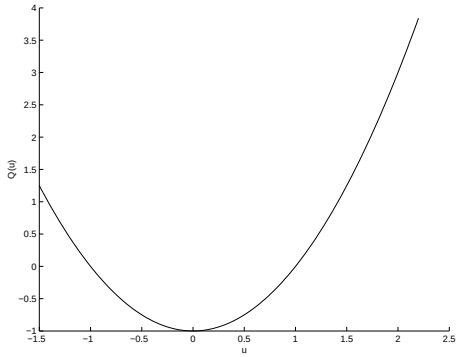

Figure 1. Plot of $Q(u)$ versus u with $Q(s) = 0$, $Q^{'}(s) < 0$, $Q(s_b) = 0$, and $Q^{'}(s_b) > 0$. There, exists a $u_m > s_b$ such that $\int_s^{u_m} Q(\eta)\, d\eta = 0$. Here $s = -1$ and $s_b = 1$.

The separatrix corresponds to a homoclinic solution $w(y)$ to (2.1) on $-\infty < y < \infty$, with $w(\pm\infty) = s$. Up to an arbitrary phase-shift, $w(y)$ satisfies

$$w^{''} + Q(w) = 0\,, \quad -\infty < y < \infty\,, \tag{2.2a}$$

$$w^{'}(0) = 0\,, \quad w(0) > 0\,; \quad w(y) \sim s + ce^{-\sigma y}\,, \quad |y| \to \infty\,. \tag{2.2b}$$

Here, $\sigma > 0$ and $c > 0$ are defined by

$$\sigma = \left[-Q^{'}(s)\right]^{1/2}\,, \quad \log c = \log(u_m - s) + \int_{u_m}^{s} \left[\frac{-\sigma}{[-2\,V(\eta)]^{1/2}} + \frac{1}{\eta - s}\right] d\eta\,, \tag{2.2c}$$

where $V(\eta) \equiv \int_{u_m}^{\eta} Q(\theta)\, d\theta$. This homoclinic solution leads to the existence of spike layer solutions for (2.1), where the spikes are localized near certain points in the domain. Depending on the boundary conditions for (2.1), there may be boundary layers near one or both endpoints that correspond to pieces of the homoclinic orbit.

A phase-plane analysis of (2.1) for various boundary conditions was made in [84] and [88]. The main observation is that by using the stretching

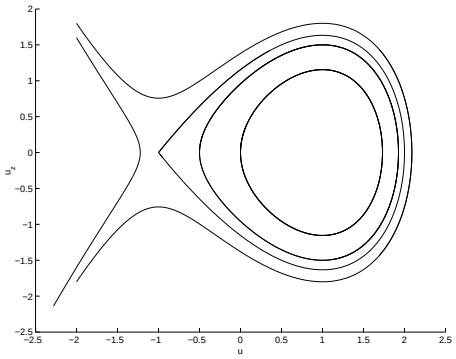

Figure 2. Plot of the phase-plane u_z versus u, with $z = x/\varepsilon$, for a $Q(u)$ that admits spike-type solutions.

$y = x/\varepsilon$ in (2.1), it is clear that boundary and internal layer solutions for (2.1) correspond to trajectories in the phase-plane that are close to the separatrix in Fig. 2 and are away from the saddle point region near $u = s$. Since the solution spends a long time near the saddle point and a comparably shorter time to make a complete or partial circuit around the separatrix, it is clear that $u \sim s$ on $-1 \leq x \leq 1$ except for $O(\varepsilon)$ transitions, or spike layers, located near the endpoints or at some interior points in the domain. This geometrical picture is very useful for obtaining qualitative information regarding the admissible spike configurations. In particular, it shows that for the boundary data $u = s$ at $x = \pm 1$, solutions with two or more interior spikes are impossible for (2.1) since any trajectory must necessarily lie outside the closed region bounded by the separatrix. Despite the simplicity of the geometrical picture afforded by the phase-plane, it does not readily yield detailed quantitative information regarding questions such as determining the locations of the spikes for arbitrary boundary data, the possibility of bifurcation behavior, and determining the number of solutions that exist for a fixed but small ε. Furthermore, the phase-plane does not generalize to the singularly perturbed quasilinear elliptic problems in two or more spatial dimensions. Therefore, it is desirable to develop an asymptotic method to construct spike layer solutions to (2.1) that can be extended to the multi-dimensional case.

The first example illustrating the difficulty in applying the method of matched asymptotic expansions to treat (2.1) was given by Carrier and Pearson (see pages 202-205 of [13]) for the special nonlinearity $Q(u) =$

$u^2 - 1$, and with $u(\pm 1) = 0$. For this reason, we refer to (2.1) as Carrier's problem. Near each endpoint there are two possible boundary layer solutions. Superimposed on these boundary layer solutions, they tried to construct a solution with one interior spike. However, as shown in [13], a routine application of the method of matched asymptotic expansions fails to determine the interior spike location x_0. In the vicinity of $x = x_0$, it is easy to see that u has the form

$$u(x) \sim 2w\left[\sqrt{2}\varepsilon^{-1}(x - x_0)\right] - 1\,, \tag{2.3}$$

where $w(y)$ is given in (1.8) with $p = 2$. This failure in determining x_0 is not restricted to the choice $Q(u) = u^2 - 1$ but is typical for the class of problems (2.1). An extension of the method of matched asymptotic expansions was used in [66] to determine the spike locations for $Q(u) = u^2 - 1$. There it was shown that the failure of a routine application of the method of matched asymptotic expansions in determining the spike locations was a result of ignoring exponentially small terms in the expansion of the solution. By extending this method to retain and match the dominant exponentially small terms, it was shown how to find the correct spike layer locations for $Q(u) = u^2 - 1$. Another analytical approach to determine the spike locations for $Q(u) = u^2 - 1$ was given in [51]. They employed a variational principle, with trial functions from the matched asymptotic expansion solution, and determined the spike locations by making the variation stationary with respect to the spike layer locations. More recently, for the nonlinearity $Q(u) = u^2 - 1$ a rigorous shooting method has been developed in [85] for constructing spike layer solutions, and for determining the number of such solutions for a fixed ε with $\varepsilon \ll 1$. Another rigorous approach based on Green's functions is given in [52]. One limitation of these approaches are that they rely heavily on analytical formulae that are available only for $Q(u) = u^2 - 1$, and they are inherently methods that will work only in one space dimension.

In [100], an analytical method called the *projection method*, was used to determine the spike layer locations for (2.1) for various boundary conditions. As shown in [100], the indeterminacy in constructing interior spike solutions for (2.1) is a result of the occurrence of exponentially small eigenvalues in the spectrum of the linearized operator. In this sense, the linearized problem is exponentially ill-conditioned. The projection method, which combines traditional matched asymptotic analysis with spectral theory, exploits this exponential ill-conditioning by imposing limiting solvability conditions on the solution to the linearized equation. In this sense the projection

method has much in common with a Lyapunov-Schmidt approach to study the linearized equation. Although this method is formal, it does not require any detailed knowledge of the explicit form of the homoclinic orbit and so can treat an arbitrary $Q(u)$ of the form shown in Fig. 1. In addition, it can be extended to treat related problems in several space dimensions.

In addition to Carrier's problem, there are other classes of singularly perturbed boundary-value problems where a straightforward application of the method of matched asymptotic expansions fails to determine the solution uniquely as a result of neglecting important exponentially small terms. Such problems include boundary layer resonance phenomena for turning point problems [67], heteroclinic interfaces in reaction-diffusion systems, certain viscous shock waves for convection-diffusion problems, the Cahn-Hillard equation etc. These problem are all exponentially ill-conditioned and the projection method can be used to eliminate the indeterminacy. A survey of these other problems is given in [102].

2.1. *Interior Spike Solutions: No Boundary Layers*

We now outline the projection method for constructing a solution to

$$\varepsilon^2 u'' + Q(u) = 0\,, \qquad -1 < x < 1\,, \tag{2.4a}$$

$$\varepsilon u'(1) + \kappa_r\,[u(1) - s] = 0\,; \qquad \varepsilon u'(-1) - \kappa_l\,[u(-1) - s] = 0\,, \tag{2.4b}$$

with one interior spike and with no boundary layers near $x = \pm 1$. Here $\kappa_r \geq 0$ and $\kappa_l \geq 0$ and s is the saddle-point location for $Q(u)$. In the phase-plane u_z versus u, where $z = x/\varepsilon$, these special boundary conditions geometrically represent straight line segments originating from the saddle-point $u = s$. Each of these lines is either locally inside or outside the loop bounded by the separatrix. This geometrical fact will have an implication regarding the location of a spike for (2.4).

The first step in the projection method is to look for an approximate solution to (2.4) in the form

$$u(x) = w\left[\varepsilon^{-1}(x - x_0)\right] + R(x)\,, \tag{2.5}$$

where x_0, with $|x_0| < 1$, is to be found, and the error $R(x)$ is assumed to be small. We substitute (2.5) into (2.4) and linearize. Assuming that x_0 is not $O(\varepsilon)$ close to ± 1, we can use the far-field behavior of $w(y)$ in (2.2b) to estimate the residuals in satisfying the boundary conditions in (2.4b). In

this way, we obtain that R satisfies

$$LR \equiv \varepsilon^2 R^{''} + Q^{'}(w)R = 0\,, \qquad -1 < x < 1\,, \tag{2.6a}$$

$$\varepsilon R^{'}(1) + \kappa_r R(1) \sim ce^{-\sigma y_r}(\sigma - \kappa_r)\,, \tag{2.6b}$$

$$\varepsilon R^{'}(-1) - \kappa_l R(-1) \sim ce^{\sigma y_l}(\kappa_l - \sigma)\,. \tag{2.6c}$$

Here we have defined $y_r \equiv \varepsilon^{-1}(1 - x_0)$ and $y_l = -\varepsilon^{-1}(1 + x_0)$.

Next, we consider the associated eigenvalue problem

$$L\phi \equiv \varepsilon^2\phi'' + Q'(w)\,\phi = \lambda\phi\,, \quad -1 < x < 1\,, \tag{2.7a}$$

$$\varepsilon\phi'(1) + \kappa_r\,\phi(1) = 0\,; \quad \varepsilon\phi'(-1) - \kappa_l\phi(-1) = 0\,. \tag{2.7b}$$

For $\varepsilon > 0$ fixed, there exists a countably infinite number of eigenvalues λ_j of (2.7) for $j = -1, 0, 1, \ldots$. The corresponding eigenfunctions form a complete set with respect to the space of square integrable functions. However, since $\varepsilon \ll 1$, there is an eigenvalue of (2.7), labeled by λ_0, which tends to zero as $\varepsilon \to 0$, and the corresponding (unnormalized) eigenfunction ϕ_0 is nearly proportional to $w^{'}(y)$, where $y = \varepsilon^{-1}(x - x_0)$. Since w is a spike, the derivative $w^{'}$ has exactly one zero-crossing. Hence, by standard Sturm-Liouville oscillation theory, we expect that λ_0 is the second largest eigenvalue in the spectrum. The principle, or equivalently, largest eigenvalue, labeled by λ_{-1}, tends to a positive value as $\varepsilon \to 0$. This is discussed more fully in Sec. 3 when we analyze the stability of spike layer solutions.

Roughly speaking, the exponential ill-conditioning results from a slight break of a translation invariance that occurs for Carrier's problem posed in the infinite line. On the infinite line, where there is translation invariance, $w^{'}$ is an exact eigenfunction corresponding to a zero eigenvalue. For our finite-domain problem where the spike is localized near $x = x_0$ the translation invariance is broken only through the interaction of the far-field behavior of $w(y)$ with the boundaries at $x = \pm 1$. Near the boundaries, $w - s$ is exponentially small, and thus this interaction is exponentially weak. As we now show, this weak interaction perturbs the zero eigenvalue of translation by exponentially small terms.

We now calculate λ_0. Applying Green's identity to ϕ_0 and $w^{'}$, we get

$$\frac{\lambda_0}{\varepsilon}\left(\phi_0, w^{'}\right) = -\phi_0(1)\left[\varepsilon w^{''}(y_r) - \kappa_r w^{'}(y_r)\right] + \phi_0(-1)\left[\varepsilon w^{''}(y_l) - \kappa_l w^{'}(y_l)\right]\,, \tag{2.8}$$

where the inner product (f, g) is defined by $(f, g) \equiv \int_{-1}^{1} fg\,dx$. Using the far-field behavior for $w(y)$ as $|y| \to \infty$ from (2.2b), (2.8) reduces to

$$\lambda_0\left(\phi_0, w^{'}\right) \sim -\varepsilon\phi_0(1)c\sigma\,(\sigma - \kappa_r)\,e^{-\sigma\kappa_r} + \varepsilon\phi_0(-1)c\sigma\,[\sigma - \kappa_l]\,e^{\sigma y_l}\,. \tag{2.9}$$

To determine $\phi_0(\pm 1)$, we use boundary layer theory to calculate ϕ_0 as

$$\phi_0(x) = w^{'}\left[\varepsilon^{-1}(x-x_0)\right] + \phi_r[\varepsilon^{-1}(1-x)] + \phi_l[\varepsilon^{-1}(x+1)]\,, \qquad (2.10)$$

where $\phi_l(\eta) \to 0$ and $\phi_r(\eta) \to 0$ as $\eta \to +\infty$. Since $Q^{'}(u) \sim Q^{'}(s) = -\sigma^2$ near $x = \pm 1$, we calculate from (2.1) that $\phi_l(\eta) = b_l e^{-\sigma\eta}$ and $\phi_r(\eta) = b_r e^{-\sigma\eta}$ for some coefficients b_l and b_r to be determined. We then substitute (2.10) into the boundary conditions (2.7b), and we use the far-field behavior (2.2b) to calculate $w^{'}$ at $x = \pm 1$. In this way we determine b_l and b_r, and from this we calculate

$$\phi_0(1) \sim -\frac{2c\sigma^2}{\kappa_r+\sigma} e^{-\sigma\varepsilon^{-1}(1-x_0)}\,, \quad \phi_0(-1) \sim \frac{2c\sigma^2}{\kappa_l+\sigma} e^{-\sigma\varepsilon^{-1}(1+x_0)}\,. \quad (2.11)$$

Substituting (2.11) into (2.9), and using (2.10) to asymptotically evaluate $\left(\phi_0, w^{'}\right) \sim \varepsilon \int_{-\infty}^{\infty} w^{'2}(y)\,dy$, we obtain the following result:

Proposition 2.1. *For $\varepsilon \ll 1$, the spectrum of the linearized problem (2.6) around a one-spike solution has an exponentially small eigenvalue λ_0 with*

$$\lambda_0 \sim -\frac{2c^2\sigma^3}{\int_{-\infty}^{\infty} w'^2\,dy}\left[\left(\frac{\kappa_r-\sigma}{\kappa_r+\sigma}\right)e^{-2\sigma y_r} + \left(\frac{\kappa_l-\sigma}{\kappa_l+\sigma}\right)e^{2\sigma y_l}\right]\,, \qquad (2.12)$$

where $y_r \equiv \varepsilon^{-1}(1-x_0)$ and $y_l = -\varepsilon^{-1}(1+x_0)$. The corresponding eigenfunction ϕ_0 is given by (2.10).

Next, we select the correct value of x_0 by imposing a limiting solvability condition on the solution to the linearized problem. We expand R in (2.6) in terms of the normalized eigenfunctions ϕ_j of (2.7). Using Green's second identity, we readily derive that

$$R = \sum_{j=-1}^{\infty} \frac{C_j}{\lambda_j}\phi_j\,, \quad C_j = -c\varepsilon\left[e^{-\sigma y_r}(\sigma-\kappa_r)\phi_j(1) - e^{\sigma y_l}(\kappa_l-\sigma)\phi_j(-1)\right]\,. \qquad (2.13)$$

Since $\lambda_0 \to 0$ as $\varepsilon \to 0$, a necessary condition for (2.6) to have a solution in this limit is that $C_0 \to 0$ as $\varepsilon \to 0$. This limiting solvability condition, which ensures that the projection of the error R onto the eigenspace associated with the exponentially small eigenvalue is zero, yields an equation for x_0. Setting $C_0 = 0$, and using (2.11) for $\phi_0(\pm 1)$, we obtain that

$$-e^{-2\sigma y_r}\left(\frac{\sigma-\kappa_r}{\sigma+\kappa_r}\right) \sim e^{2\sigma y_l}\left(\frac{\kappa_l-\sigma}{\sigma+\kappa_l}\right)\,. \qquad (2.14)$$

Solving (2.14) for x_0, we obtain the following result:

Proposition 2.2. *Let $\varepsilon \ll 1$ and suppose that $(\sigma-\kappa_r)(\sigma-\kappa_l) > 0$. Then, a solution to (2.4) with one interior spike satisfies $u \sim w\left[\varepsilon^{-1}(x-x_0)\right]$, where $w(y)$ is the homoclinic solution satisfying (2.2), and x_0 satisfies*

$$x_0 \sim -\frac{\varepsilon}{4\sigma}\log\left[\left(\frac{\kappa_r-\sigma}{\kappa_l-\sigma}\right)\left(\frac{\kappa_l+\sigma}{\kappa_r+\sigma}\right)\right]. \tag{2.15}$$

We now make several remarks. From (2.15), we see that an interior one-spike solution does not exist when $(\sigma-\kappa_r)(\sigma-\kappa_l) < 0$. This condition is readily seen from the phase-plane shown in Fig. 2. When $\kappa_r = \kappa_l$, we get $x_0 = 0$ as expected. Secondly, Eq. (2.15) also suggests a sensitivity of the solution to small changes in the data. In particular, if $\kappa_l = 0$ and $\kappa_r = \sigma - e^{-\nu/\varepsilon}$, for some $\nu > 0$, the spike layer location x_0 is perturbed by $O(1)$ as $\varepsilon \to 0$. In fact, as shown in Sec. 2.3 below, other types of extreme sensitivity to exponentially small perturbations in Carrier's problem are possible as a result of the exponential ill-conditioning. Finally, the exponential ill-conditioning leads to significant numerical difficulties when trying to compute spike layer solutions to (2.4) using finite difference schemes. As a result of the large condition number of the linearized problem, small residuals in Newton's method do not generally imply that the iterations have converged to a close approximate solution. In particular, suppose that $Q(u) = -u + u^2$, $\kappa_r = \kappa_l = 0$, and $\varepsilon = 0.05$. Then, we calculate that $\sigma = 1$, $c = 6$, and $\int_{-\infty}^{\infty} w'^2\, dy = 6/5$. Therefore, from (2.12), we obtain

$$\lambda_0 \sim 120 e^{-2/\varepsilon} = 5.1 \times 10^{-16}. \tag{2.16}$$

This shows that the condition number of the system is on the order $O(10^{16})$, and hence even with 16 digit floating point computations, the solution will be sensitive to roundoff error. With extended precision computations, which retain 32 digits in the computation, the negative effects of this ill-conditioning can be alleviated somewhat, but only for slightly smaller values of ε. Exponential ill-conditioning, and the numerical consequences, is discussed further in [67], [94], [93], and [102]. Numerical difficulties for the related problem of Euler buckling for large applied loads, modeled by $u'' + \lambda \sin u = 0$ for $\lambda \gg 1$, has been studied recently in [31].

Next, we follow Sec. 3 of [100] and show how to construct multi-spike solutions to (2.4) having n interior spikes at some unknown x_j for $j = 0, \ldots, n-1$, where $-1 < x_0 < x_1 < \ldots < x_{n-1} < 1$. In the remainder of this section we label the inter-spike separations d_j by $d_j = x_j - x_{j-1}$ for $j = 0, \ldots, n$, where we have labeled $x_{-1} = -1$, and $x_n = 1$. We assume that

the spikes are well-separated in the sense that $d_j \gg O(\varepsilon)$ for $j = 0, \ldots, n$. We look for an n-spike solution to (2.4) in the form

$$u \sim u_c(x) \equiv \sum_{j=0}^{n-1} w\left[\varepsilon^{-1}(x - x_j)\right] - (n-1)\, s\,. \tag{2.17}$$

We substitute $u = u_c + R$ into (2.4), where $R \ll 1$. In analogy with (2.6), we obtain that R satisfies

$$\varepsilon^2 R^{''} + Q^{'}(u_c)\, R = E \equiv \sum_{i=0}^{n-1} Q\left[w(y_i)\right] - Q(u_c)\,, \tag{2.18a}$$

$$\varepsilon\, R^{'}(1) + \kappa_r\, R(1) \sim -c\,(\kappa_r - \sigma) e^{-\sigma\varepsilon^{-1} d_n}\,, \tag{2.18b}$$

$$\varepsilon\, R^{'}(-1) - \kappa_l\, R(-1) \sim -c\,(\sigma - \kappa_l) e^{-\sigma\varepsilon^{-1} d_0}\,. \tag{2.18c}$$

Here we have defined y_i by $y_i \equiv \varepsilon^{-1}(x - x_i)$, for $i = 0, \ldots, n-1$.

The eigenvalue problem associated with (2.18) is (2.7), where $Q^{'}(w)$ in (2.7a) is replaced by $Q^{'}(u_c)$. When the spikes are well-separated, there are n eigenvalues, labeled by λ_j for $j = -n, -n+1, \ldots, -1$ that tend to a common positive value as $\varepsilon \to 0$. These are the largest eigenvalues in the spectrum of the linearization. The next largest group of eigenvalues are the exponentially small eigenvalues λ_j for $j = 0, \ldots, n-1$ that result from the broken translation invariance. The corresponding eigenfunction near the core of the j^{th} spike is $\phi_j \sim w^{'}(y_j)$ for $j = 0, \ldots, n-1$. The solution to (2.18) is expanded in terms of all of the normalized eigenfunctions ϕ_j as $R = \sum_{j=-n}^{\infty} C_j \lambda_j^{-1} \phi_j$. Using Green's identity we derive

$$C_j = (E, \phi_j) - \varepsilon\left[(\varepsilon\, R^{'}(1) + \kappa_r\, R(1))\phi_j(1) - (\varepsilon\, R^{'}(-1) - \kappa_l\, R(-1))\phi_j(-1)\right]\,. \tag{2.19}$$

Here $(f, g) \equiv \int_{-1}^{1} f g\, dx$. A necessary condition for there to be a solution to (2.18) in the limit $\varepsilon \to 0$, is that the projection of R onto the subspace spanned by ϕ_j, for $j = 0, \ldots, n-1$, vanishes. Setting $C_j = 0$ for $j = 0, \ldots, n-1$, we obtain n coupled algebraic equations for x_j given by

$$(E, \phi_j) \sim B_j \equiv \varepsilon\, c\left[(\sigma - \kappa_r) e^{-\sigma\varepsilon^{-1} d_n}\, \phi_j(1) + (\sigma - \kappa_l) e^{-\sigma\varepsilon^{-1} d_0}\, \phi_j(-1)\right]\,, \tag{2.20}$$

for $j = 0, \ldots, n-1$.

To determine explicit equations for x_j, we must evaluate the inner product term and the boundary term B_j in (2.20). For well-separated spikes, the residual E is exponentially small on $-1 < x < 1$. Since $\phi_j \sim w^{'}(y_j)$

near $x = x_j$, it follows that the dominant contribution to the inner product term (E, ϕ_j) arises from the region near $x = x_j$. To determine this contribution we must retain the dominant exponentially small terms in E near $x = x_j$. These terms arise from the nearest neighbor spikes located at $x = x_{j+1}$ and $x = x_{j-1}$ when $j = 1, \ldots, n-2$. The spikes at x_0 and x_{n-1}, which are closest to the boundary, have only one nearest neighbor. A detailed calculation as given in §3 of [100] shows that

$$(E, \phi_j) \sim \begin{cases} 2\varepsilon\, c^2\sigma^2\, e^{-\sigma\varepsilon^{-1}d_1}\,, & j = 0\,, \\ 2\varepsilon\, c^2\sigma^2 \left(e^{-\sigma\varepsilon^{-1}d_{j+1}} - e^{-\sigma\varepsilon^{-1}d_j} \right), & j = 1, \ldots, n-2\,, \\ -2\varepsilon\, c^2\sigma^2 e^{-\sigma\varepsilon^{-1}d_{n-1}} & j = n-1\,. \end{cases} \tag{2.21}$$

Next, we asymptotically calculate the boundary term B_j in (2.20). The dominant terms in B_j for $j = 0, \ldots, n-1$ arise when $j = 0$ or $j = n-1$. To compute B_0 and B_{n-1} we calculate $\phi_0(-1)$ and $\phi_{n-1}(1)$ in a similar way as was done above for a one-spike solution. We readily obtain that

$$\phi_0(-1) \sim \frac{2\sigma^2 c}{\kappa_l + \sigma} e^{-\sigma\varepsilon^{-1}d_0}\,, \qquad \phi_{n-1}(1) \sim -\frac{2\sigma^2 c}{\kappa_r + \sigma} e^{-\sigma\varepsilon^{-1}d_n}\,. \tag{2.22}$$

From (2.20), we get that

$$B_0 \sim 2\sigma^2 c^2\, \varepsilon \left(\frac{\sigma - \kappa_l}{\sigma + \kappa_l} \right) e^{-2\sigma\varepsilon^{-1}d_0}\,, \quad B_{n-1} \sim -2\sigma^2 c^2\, \varepsilon \left(\frac{\sigma - \kappa_r}{\sigma + \kappa_r} \right) e^{-2\sigma\varepsilon^{-1}d_n}\,. \tag{2.23}$$

For $j = 1, \ldots, n-2$, B_j is of an exponential order smaller than (E, ϕ_j). Therefore, in (2.20) we can set $B_j = 0$ for $j = 1, \ldots, n-2$.

Substituting (2.23) and (2.21) into (2.20), we get that (2.20) reduces to

$$e^{-\sigma\varepsilon^{-1}(d_1 - 2d_0)} \sim \left(\frac{\sigma - \kappa_l}{\sigma + \kappa_l} \right), \quad e^{-\sigma\varepsilon^{-1}(d_{n-1} - 2d_n)} \sim \left(\frac{\sigma - \kappa_r}{\sigma + \kappa_r} \right). \tag{2.24a}$$

$$e^{-\sigma\varepsilon^{-1}d_{j+1}} \sim e^{-\sigma\varepsilon^{-1}d_j}\,, \qquad j = 1, \ldots, n-2\,. \tag{2.24b}$$

It is clear from (2.24a) that there are no n-spike solutions to (2.4) when either $(\sigma - \kappa_l) < 0$ or $(\sigma - \kappa_r) < 0$. This is also readily seen from the phase-plane shown in Fig. 2. Only when $(\sigma - \kappa_l) > 0$ and $(\sigma - \kappa_r) > 0$ are both satisfied is the trajectory inside the region bounded by the separatrix, which then allows for n-spike solutions with $n \geq 2$. By solving (2.24) explicitly, we obtain the following result for the spike locations:

Proposition 2.3. *Let $\varepsilon \ll 1$ and suppose that $(\sigma - \kappa_r) > 0$ and $(\sigma - \kappa_l) > 0$.*

Then, for $n \geq 2$, there is an n-spike solution to (2.4) of the form

$$u \sim u_c(x) \equiv \sum_{j=0}^{n-1} w\left[\varepsilon^{-1}(x - x_j)\right] - (n-1)\, s\,, \tag{2.25}$$

where x_j is given by

$$x_j \sim -1 + \frac{(2j+1)}{n} + \frac{\varepsilon}{2}\left[\eta_l - \frac{1}{2n}(\eta_r + \eta_l)(1+2j)\right]\,, \quad j = 0, \ldots, n-1\,. \tag{2.26}$$

Here η_l and η_r are defined by

$$\eta_l \equiv \sigma^{-1}\log\left(\frac{\sigma - \kappa_l}{\sigma + \kappa_l}\right)\,, \quad \eta_r \equiv \sigma^{-1}\log\left(\frac{\sigma - \kappa_r}{\sigma + \kappa_r}\right)\,. \tag{2.27}$$

For the Neumann problem where $\kappa_l = \kappa_r = 0$, (2.26) shows that $x_j = -1 + (2j-1)/n$, for $j = 0, \ldots, n-1$, so that $d_j = 2/n$ for $j = 1, \ldots, n-1$ and $d_0 = d_n = 1/n$. This symmetric spike spacing for the Neumann problem also follows readily from the "time-map" associated with the phase-plane.

2.2. *Interior Spike Solutions: Boundary Layers*

We now construct n-spike solutions to (2.1) for the boundary data

$$u(-1) = u_L\,, \quad u(1) = u_R\,, \tag{2.28}$$

where $s < u_L, u_R < u_m$ (see Fig. 1). A composite expansion for an n-spike solution has the form

$$u \sim u_c(x) \equiv \sum_{j=0}^{n-1} w\left[\varepsilon^{-1}(x - x_j)\right] - (n-1)\, s + \left[w_L\left(\varepsilon^{-1}(x+1)\right) - s\right] + \left[w_R\left(\varepsilon^{-1}(1-x)\right) - s\right]\,. \tag{2.29}$$

The boundary layer terms $w_L(\xi)$ and $w_R(\xi)$ for $\xi \geq 0$ at the left and right endpoints, respectively, are portions of the homoclinic orbit, which satisfy

$$w_L'' + Q(w_L) = 0\,, \quad w_L(0) = u_L\,, \quad w_L(\xi) \sim s + c_L e^{-\sigma\xi} \quad \text{as } \xi \to \infty\,, \tag{2.30a}$$

$$w_R'' + Q(w_R) = 0\,, \quad w_R(0) = u_R\,, \quad w_R(\xi) \sim s + c_R e^{-\sigma\xi} \quad \text{as } \xi \to \infty\,, \tag{2.30b}$$

for some constants $c_L > 0$ and $c_R > 0$. From the phase-plane, it is clear that there are two solutions to each of (2.30a) and (2.30b). One solution decreases monotonically to s, while the other first increases to u_m and then decreases to s. Therefore, there are two values for c_L and for c_R.

We substitute $u = u_c + R$ into (2.1), where $R \ll 1$. In analogy with (2.18), we obtain that R satisfies

$$\varepsilon^2 R'' + Q'(u_c)\, R = E \equiv \sum_{i=0}^{n-1} Q\left[w(y_i)\right] - Q(u_c) + Q[w_R(-y_n)] + Q\left[w_L(y_{-1})\right] , \tag{2.31a}$$

$$R(-1) \sim -ce^{-\sigma\varepsilon^{-1}d_0} ; \quad R(1) \sim -ce^{-\sigma\varepsilon^{-1}d_n} . \tag{2.31b}$$

Here $y_i \equiv \varepsilon^{-1}(x - x_i)$, for $i = -1, \ldots, n$, where $x_{-1} \equiv -1$ and $x_n \equiv 1$. By eliminating the projection of R onto the eigenspace associated with the exponentially small eigenvalues, the spike layer locations satisfy

$$(E, \phi_j) \sim B_j \equiv \varepsilon^2\, c \left(e^{-\sigma\varepsilon^{-1}d_n}\, \phi_j'(1) - e^{-\sigma\varepsilon^{-1}d_0}\, \phi_j'(-1) \right), \;\; j = 0, \ldots, n-1 , \tag{2.32}$$

where $\phi_j \sim w'(y_j)$ near the j^{th} spike.

The analysis of (2.32) differs in two main respects from the analysis in Sec. 2.1. Firstly, to evaluate (E, ϕ_j), we note that the interior spikes closest to the endpoints, corresponding to $j = 0$ and $j = n-1$, now have two nearest neighbors instead of only one. Specifically, for the spike at $x = x_0$, the nearest neighbors are the spike at $x = x_1$ and the boundary layer solution w_L. A similar situation occurs for the spike nearest the right endpoint. Secondly, it can be shown that for each $j = 0, \ldots, n-1$ the boundary term B_j in (2.32) is asymptotically smaller than (E, ϕ_j). In contrast, for the problem in Sec. 2.1, the contribution from B_0 and B_{n-1} had to be retained. Therefore, we can set $B_j = 0$ for $j = 0, \ldots, n-1$ in (2.32), to obtain that the layer locations asymptotically satisfy $(E, \phi_j) \sim 0$. By calculating (E, ϕ_j) asymptotically as in Sec. 7.1 of [100], we obtain, in analogy with (2.24), that the inter-spike separations d_j satisfy

$$ce^{-\sigma\varepsilon^{-1}d_1} \sim c_L e^{-\sigma\varepsilon^{-1}d_0} ; \quad c_R e^{-\sigma\varepsilon^{-1}d_n} \sim ce^{-\sigma\varepsilon^{-1}d_{n-1}} . \tag{2.33a}$$

$$e^{-\sigma\varepsilon^{-1}d_{j+1}} \sim e^{-\sigma\varepsilon^{-1}d_j} , \qquad j = 1, \ldots, n-2 . \tag{2.33b}$$

By solving (2.33) explicitly, we obtain the following result:

Proposition 2.4. *Let $\varepsilon \ll 1$ and consider (2.1) with the Dirichlet conditions $u(-1) = u_L$ and $u(1) = u_R$, where $s < u_L, u_R < u_m$. Then, there is an n-spike solution of the form*

$$u \sim u_c(x) \equiv \sum_{j=0}^{n-1} w\left[\varepsilon^{-1}(x - x_j)\right] - (n-1)\, s + \left[w_L\left(\varepsilon^{-1}(x+1)\right) - s\right] + \left[w_R\left(\varepsilon^{-1}(1-x)\right) - s\right] , \tag{2.34}$$

where w_L and w_R are boundary layer functions satisfying (2.30). For this problem, there are are four possible sets $(x_0, \ldots, x_n)$ of spike-layer locations, which for $j = 0, \ldots, n-1$ satisfy

$$x_j \sim -1 + \frac{2}{n+1}(1+j) + \frac{\varepsilon}{\sigma(n+1)}\left[\log\left(\frac{c^{1-n}c_L^n}{c_R}\right) + j\,\log\left(\frac{c^2}{c_R c_L}\right)\right]. \tag{2.35}$$

There are two values for c_L and for c_R defined in (2.30).

Therefore, for Dirichlet conditions we get $d_j = 2/(n+1) + O(\varepsilon)$ for $j = 0, \ldots, n$, whereas for the problem considered in Sec. 2.1, we found that $d_j = 2/n + O(\varepsilon)$ for $j = 1, \ldots, n-1$, with $d_0 = 1/n + O(\varepsilon)$, $d_n = 1/n + O(\varepsilon)$. Although (2.35) was was derived only for the case $n > 1$, the result (2.35) turns out to be correct even for one spike where $n = 1$.

We now give an explicit example to illustrate this result. We consider Carrier's original problem with $Q(u) = u^2 - 1$, $u_L = 0$, and $u_R = 0$. For this example, we can calculate w, w_L and w_R explicitly, to obtain that

$$\sigma = \sqrt{2}\,, \quad c = 12\,, \quad c_L = 12e^{-\kappa_1\sqrt{2}}\,, \quad c_R = 12e^{-\kappa_2\sqrt{2}}\,, \tag{2.36}$$

where κ_1 and κ_2 can be either $\pm\sqrt{2}\cosh^{-1}(\sqrt{3}) = \pm\sqrt{2}\log(\sqrt{3}+\sqrt{2})$. Then, from (2.35), we obtain four different sets of spike layer locations for $j = 0, \ldots, n-1$ given by

$$x_j \sim -1 + \frac{2(j+1)}{n+1} \pm \sqrt{2}\varepsilon\log(\sqrt{3}+\sqrt{2})\,, \tag{2.37a}$$

$$x_j \sim -1 + \frac{2(j+1)}{n+1} \pm \sqrt{2}\varepsilon\log(\sqrt{3}+\sqrt{2}) \mp \frac{2\varepsilon(j+1)}{n+1}\sqrt{2}\log(\sqrt{3}+\sqrt{2})\,. \tag{2.37b}$$

This example was given at the end of Sec. 7.1 of [100]. A rigorous proof of this result has only been obtained recently in Theorem 3 of [85]. For $n = 2$, the two solutions corresponding to (2.37a) are shown in Fig. 3.

Finally, we consider a situation where there is a boundary layer at only one of the endpoints. We consider (2.1) with $u(-1) = u_L$ and $u'(1) = 0$, and we look for an n-spike solution where there is no boundary layer at $x = 1$. Using the projection method, we readily obtain that the inter-spike separations d_j satisfy $ce^{-\sigma\varepsilon^{-1}d_1} \sim c_L e^{-\sigma\varepsilon^{-1}d_0}$, and $e^{-\sigma\varepsilon^{-1}d_{n-1}} \sim e^{-2\sigma\varepsilon^{-1}d_n}$, together with (2.33b). By solving this system explicitly, we obtain the following result:

Proposition 2.5. *Let $\varepsilon \ll 1$ and consider (2.1) with the boundary conditions $u(-1) = u_L$ and $u'(1) = 0$. Then, there is an n-spike solution to this*

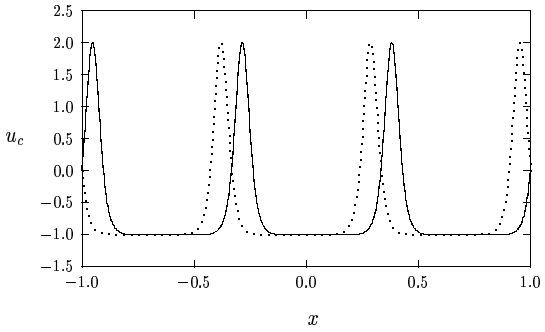

Figure 3. Plot of u_c, given in (2.34), versus x for a two-spike solution for $Q(u) = u^2 - 1$ with $\varepsilon = 0.03$. The two curves correspond to the two choices in (2.37a).

problem with no boundary layer near $x = 1$ of the form

$$u \sim u_c(x) \equiv \sum_{j=0}^{n-1} w\left[\varepsilon^{-1}(x - x_j)\right] - (n-1)\, s + \left[w_L\left(\varepsilon^{-1}(x+1)\right) - s\right] . \tag{2.38}$$

Here w_L is the boundary layer function satisfying (2.30). For this problem, there are are two possible sets $(x_0, \ldots, x_n)$ of spike-layer locations, which for $j = 0, \ldots, n-1$ satisfy

$$x_j \sim -1 + \frac{4(j+1)}{2n+1} + \frac{2\varepsilon}{\sigma(2n+1)}\left[\log\left(\left(\frac{c}{c_L}\right)^{\frac{1}{2}-n}\right) + j\,\log\left(\frac{c}{c_L}\right)\right] . \tag{2.39}$$

There are two values of c_L defined in (2.30).

Therefore, for this Neumann/Dirichlet problem, the inter-layer separations satisfy $d_j = 4/(2n+1) + O(\varepsilon)$ for $j = 0, \ldots, n-1$, and $d_n = 2/(2n+1) + O(\varepsilon)$. For the special case where $n = 1$, we get $x_0 = 1/3$.

2.3. *Exponential Sensitivity to the Data*

We now consider two types of perturbations of Carrier's problem, where a seemingly minor modification of (2.1) leads to a dramatic effect on the solution behavior. This extreme sensitivity is a result of the exponential ill-conditioning of (2.1) for interior spike solutions.

We first construct spike solutions to (2.1) with $n \geq 2$ interior spikes, when exponentially small terms are added to certain Dirichlet boundary

conditions. Specifically, we consider (2.1) with

$$u(-1) = s + A\,e^{-\sigma\varepsilon^{-1}/n}\,, \quad u(1) = s + A\,e^{-\sigma\varepsilon^{-1}/n}\,. \tag{2.40}$$

Here $A > 0$ and is $O(1)$ as $\varepsilon \to 0$. This problem models the initial formation of boundary layers near the endpoints. For the special case $Q(u) = u^2 - 1$, and for two interior spikes, such a problem was analyzed using variational methods in [51], where it was shown that a bifurcation can occur if A exceeds a threshold. The general case for arbitrary $n \geq 2$, and for arbitrary $Q(u)$ of the form shown in Fig. 1, was treated using the projection method in §6.1 of [100], where the following result was obtained:

Proposition 2.6. *Let $\varepsilon \ll 1$ and consider (2.1) with the boundary conditions (2.40). Consider an n-spike solution of the form (2.25) with $n \geq 2$. These equilibria exhibit a saddle-node bifurcation structure as A is varied. In particular, there are four possible sets $(x_0, \ldots, x_n)$ of spike-layer locations when $A > 2c$, two sets when $A_s(n) < A < 2c$, and no such sets when $A < A_s(n)$. Here $A_s(n)$ is defined by*

$$A_s(n) = 2\,c\left(\frac{n}{n+1}\right)\left(\frac{n-1}{n+1}\right)^{(1-n)/2n}\,, \quad n = 2, 3, \ldots\,. \tag{2.41}$$

Therefore, by perturbing the boundary conditions by exponentially small terms, new solutions can be created by saddle-node bifurcations. To illustrate this result, let $Q(u) = u^2 - 1$. Then, $c = 12$, and $A_s(2) = 21.06$ from (2.41). Therefore, for $\varepsilon \ll 1$, we predict that there are no two-spike solutions to (2.1) with boundary conditions (2.40) when $0 < A < 21.06$.

The next problem considers the effect of modifying a coefficient in the differential operator in (2.1) by an exponentially small but spatially varying term. In [46] a solution with one interior spike was constructed for

$$\frac{\varepsilon^2}{\kappa}\left(\kappa u'\right)' + Q(u) = 0\,, \quad -1 < x < 1\,; \quad u'(\pm 1) = 0\,, \tag{2.42a}$$

where, for some constants ν and $q > 0$, $\kappa = \kappa(x;\varepsilon)$ has the form

$$\kappa(x;\varepsilon) = 1 + \varepsilon^{\nu} g(x) e^{-\varepsilon^{-1} q}\,. \tag{2.42b}$$

Here $g(x)$ is a smooth function. In [46] the projection method was used to determine the location of a spike for an interior one-spike solution with no boundary layers. The result is summarized as follows:

Proposition 2.7. *Let $\varepsilon \ll 1$ and consider a solution to (2.42) with one interior spike. The solution is given asymptotically by $u \sim w\left[\varepsilon^{-1}(x - x_0)\right]$,*

where $w(y)$ solves (2.2). The spike location x_0 is a root of $h(x_0) = 0$, where

$$h(x_0) \equiv \frac{2\varepsilon c^2}{\beta_0}\left(e^{-2\sigma\varepsilon^{-1}(1-x_0)} - e^{-2\sigma\varepsilon^{-1}(1+x_0)}\right) - \varepsilon^{\nu+2}e^{-q/\varepsilon}g'(x_0)\,. \quad (2.43)$$

Here $\beta_0 \equiv \int_{-\infty}^{\infty} w'^2(y)\,dy$.

For $0 < q < q_c$, it is possible that (2.43) has multiple roots, which corresponds to multiple interior one-spike solutions. To illustrate this, let $g(x) = x^2/2$, and $Q(u) = -u + u^2$, for which $\sigma = 1$, $c = 6$, and $\beta_0 = 6/5$. A simple calculation shows that $x_0 = 0$ is always a solution, and that we have a pitchfork bifurcation when $q = q_c$, where

$$q_c = 2 + (\nu+2)\varepsilon\log\varepsilon - \varepsilon\log(240)\,. \quad (2.44)$$

For $0 < q < q_c$, there are three roots to (2.43) on $-1 < x_0 < 1$, whereas for $q > q_c$ there is only one such root. Therefore, by perturbing Carrier's problem by an exponentially small but spatially varying term new interior one-spike solutions may be generated by a pitchfork bifurcation.

2.4. *Related Problems: One Space Dimension*

There have been several related studies of spike solutions in ODE's, including problems with spatially varying coefficients [1], [69], and problems involving two components [53]. In addition, there are some further questions that remain to be explored.

Question 2.1. Can one give a rigorous analytical proof, along the lines of [85], of the asymptotic results in Propositions 2.1–2.7 without using the details of the phase-plane?

Question 2.2. For a given $\varepsilon \ll 1$ fixed, can one determine a bound on the number $N(\varepsilon)$ of internal spikes for Carrier's problem (2.1) with various boundary conditions?

For the case $Q(u) = u^2 - 1$, it was proved in [85] that $N(\varepsilon) < 0.41\varepsilon^{-1} + 1$ for $\varepsilon \ll 1$. What is the result for other nonlinearities $Q(u)$?

Question 2.3. Can one numerically compute multi-spike solutions to (2.1) for $\varepsilon \ll 1$, and with various boundary conditions, in a reliable manner despite the exponential ill-conditioning?

This is a key open problem. Standard numerical methods for (2.1) are subject to a loss of precision as a result of the ill-conditioning. However, for

Carrier's other problem where $Q(u)$ is modified to allow for heteroclinic, rather than homoclinic, solutions, an exact nonlinear WKB transformation was introduced in [87] and used to numerically compute multi-layer solutions for $\varepsilon \ll 1$. The sensitivity of these solutions to exponentially small perturbations in the boundary data was also studied numerically with this approach. A distinct advantage of the WKB transformed problem is that it is well-conditioned as $\varepsilon \to 0$. Our question is whether it is possible to use a related change of variables to remove the ill-conditioning associated with (2.1). In particular, can one compute solutions by re-casting (2.1) in terms of the distance function? If successful, such a method could be extended to numerically treat the quasilinear multi-dimensional problems of Sec. 2.5.

Question 2.4. What is the global bifurcation diagram for multi-spike solutions as ε is increased?

For $\varepsilon \gg 1$, multi-spike solutions are born from a bifurcation at infinity. For a few choices of $Q(u)$, branches of n-spike solutions were computed numerically in [88] as ε is decreased from a large positive value. It was found that each n-spike branch undergoes a saddle-node bifurcation at some $O(1)$ value of ε. Does this generic feature holds for other $Q(u)$? Can such a path following method in ε allow one to compute solutions for $\varepsilon \ll 1$?

Finally, we mention a modification of Carrier's original problem. This problem concerns constructing multi-bump solutions for

$$\varepsilon^2 u'' + u^2 - 1 + 2b(1-x^2)u = 0\,, \quad -1 < x < 1\,; \quad u(\pm 1) = 0\,. \qquad (2.45)$$

It was proved in [1] that if $\varepsilon \ll 1$, $b > 0$, $n \geq 2$, and if u has minima at x_k, for $k = 1, \ldots, n$, where $-1 < x_1 < \ldots < x_n < 1$, then $|x_k| < M\varepsilon|\log\varepsilon|$ for some $M > 0$ independent of ε. Therefore, (2.45) admits multi-bump solutions clustered near $x = 0$. A similar, but formal, result was obtained in [69]. This result is natural in that (2.45) can be written as a nonlinear Schrodinger equation $\varepsilon^2 u'' - 1 + u^2 - V(x)u = 0$, where the potential $V(x) = 2b(x^2 - 1)$ has a global minimum at $x = 0$ when $b > 0$. The possibility of multi-bump solutions near non-degenerate minima of $V(x)$ is well-known (cf. [99], [22]). We conjecture that a one-spike solution to Carrier's original problem with $b = 0$ will undergo a pitchfork bifurcation at $x_0 = 0$ when b is raised to an exponentially small value. The bifurcation should be similar to that for problem (2.42). This leads to the next question.

Question 2.5. What are the bifurcation properties of k-spike solutions with $k \geq 1$ to (2.45) when b is exponentially small?

2.5. *Spikes for Quasilinear Elliptic PDE*

In this subsection, we construct spike solutions for

$$\varepsilon^2 \triangle u + Q(u) = 0\,, \quad x \in \Omega\,; \quad \partial_n u = 0 \quad x \in \partial\Omega\,, \tag{2.46}$$

where Ω is a bounded, simply-connected, domain in $\mathbb{R}^N$, with $N > 1$. We assume that $Q(s) = 0$, with $Q^{'}(s) < 0$, and that there exists a unique radially symmetric ground-state solution $w(\rho)$, with $\rho = |y|$, that satisfies

$$w^{''} + \frac{(N-1)}{\rho} w^{'} + Q(w) = 0\,, \quad \rho \geq 0\,; \quad w(0) > 0\,, \tag{2.47a}$$

$$w^{'}(0) = 0\,, \quad w \sim s + c\rho^{-(N-1)/2} e^{-\sigma\rho}\,, \quad \text{as} \quad \rho \to \infty\,, \tag{2.47b}$$

where $c > 0$ and $\sigma = \left[-Q^{'}(s)\right]^{1/2}$. An important example is $Q(u) = -u + u^p$ for $1 < p < p_c$, where $p_c = \frac{N+2}{N-2}$ is the Sobolev exponent for $N \geq 3$, and $p_c = \infty$ if $N = 2$. For this case, $w(\rho)$ satisfies (1.7). Equation (2.46) is the multi-dimensional version of Carrier's problem (2.1), where $w(\rho)$ replaces the homoclinic solution $w(y)$.

The study of spike solutions to (2.46) was largely initiated in the pioneering work of Ni and Takagi (cf. [68], [76], [77]). An earlier survey of results for (2.46), and for some related problems, is given in [78].

We now follow [78] and give a rough summary of the results of [76] and [77], characterizing the "least-energy solution" of (2.46) for $Q(u) = -u + u^p$, and with $u > 0$ in Ω. For this problem, the energy functional for (2.46) is

$$J_\varepsilon(u) = \frac{1}{2} \int_\Omega \left(\varepsilon^2 |\nabla u|^2 + u^2\right)\, dx - \frac{1}{p+1} \int_\Omega u_+^{p+1}\, dx\,, \tag{2.48}$$

where $u_+ = \max(u, 0)$. As argued in [76] and [77], J_ε has a minimum when restricted to the set of solutions of (2.46) with $u > 0$ in Ω. This minimizing solution is called the "least-energy solution". Since an interior spike solution has, asymptotically, twice the energy of a boundary spike solution, the least-energy solution must be a one-spike solution centered at some point on $\partial\Omega$. To determine the actual point $\xi_\varepsilon \in \partial\Omega$ where the spike concentrates, a two-term expansion for J_ε as $\varepsilon \to 0$ is required. For a spike centered at $\xi_\varepsilon \in \partial\Omega$, it was shown in [77] that

$$J_\varepsilon(u) = \varepsilon^N \left(\frac{1}{2} I(w) - C\varepsilon H\left(\xi_\varepsilon\right) + o(\varepsilon)\right)\,, \tag{2.49}$$

where C is a positive constant independent of ε, and $I(w)$ is defined by

$$I(w) = \int_{\mathbb{R}^N} \left[\frac{1}{2}\left(|\nabla w|^2 + w^2\right) - \frac{1}{p+1} w^p\right]\, dy\,. \tag{2.50}$$

Here $H(\xi_\varepsilon)$ is the mean curvature of $\partial\Omega$ at ξ_ε. By minimizing (2.50), the following result was proved in [76], [77]:

Proposition 2.8. *Consider (2.46) with $u > 0$ in Ω and $Q(u) = -u + u^p$, where $1 < p < p_c$. Then, for $\varepsilon \ll 1$, this problem has a least-energy solution u_ε with exactly one global maximum point at ξ_ε. Moreover, $\xi_\varepsilon \in \partial\Omega$, and $H(\xi_\varepsilon) \to \max_{\partial\Omega} H$ as $\varepsilon \to 0$, where H is the mean curvature of $\partial\Omega$.*

Recently, there has been much work characterizing other types of boundary spike solutions that have a higher energy. The theory for this class of solutions is now rather complete. In Theorem 1.2 of [109] it was proved that (2.46) admits a boundary spike-layer solution that concentrates at any non-degenerate critical point of the mean curvature $H(P)$ with $P \in \partial\Omega$. In [39] a boundary k-spike solution was constructed where the spikes are separated by $O(1)$ as $\varepsilon \to 0$, and where each spike concentrates at a different local maximum point of the mean curvature $H(P)$. In [42] it was shown that for any integer $k > 0$, there exists boundary k-peak solutions to (2.46) where the peaks all cluster near a local minimum point of $H(P)$. This clustering effect is qualitatively similar to the spike-clustering phenomena for the one-dimensional problem (2.45) described in Sec. 2.4. Boundary spike solutions, together with asymptotic estimates for the eigenvalues of the linearization that tend to zero as $\varepsilon \to 0$, are also given in [111] and [4].

Next, we describe some results for interior k-spike solutions to (2.46). These solutions have the form

$$u \sim \sum_{j=1}^{k} w\left[\varepsilon^{-1}|x - \xi_j|\right], \tag{2.51}$$

for some $\xi_j \in \Omega$ for $j = 1, \ldots, k$ to be found. As for Carrier's problem in Sec. 2.1–2.3, since $w(|y|)$ decays exponentially as $|y| \to \infty$, the linerarization of (2.46) around an interior spike solution is exponentially ill-conditioned.

For an interior one-spike solution, it was shown formally in [101], and proved rigorously in [110], that the spike concentrates at a local maximum of the distance function. The result and method used in [101] is described more precisely below. Geometrically, this one-spike result for (2.46) is asymptotically equivalent to that given in Proposition 2.2 for the one-dimensional problem in the sense that an interior spike for (2.46) concentrates at a point in Ω that is farthest from the boundary. In [41] a solution to (2.46) that has one boundary spike and one interior spike was constructed. It was found that the location of the interior spike is moved an $O(1)$ distance from the center of the largest inscribed sphere for Ω in the

direction away from the boundary spike. Such a mixed boundary/interior spike solution is the multi-dimensional equivalent of the result in Proposition 2.5 for Carrier's problem, where for $\varepsilon^2 u'' + Q(u) = 0$ with $u(-1) = u_L$ and $u'(1) = 0$, an interior spike is located not at the midpoint $x_0 = 0$ but instead at $x_0 = 1/3$.

For an interior k-spike solution of (2.46), with $k \geq 1$, the following result with relatively minor technical differences, was given in [59], [40], and [3]:

Proposition 2.9. *Equation (2.46) admits an interior k-spike solution given asymptotically by (2.51), where the concentration points $\xi_{1\varepsilon}, \ldots, \xi_{k\varepsilon}$ tend to local maximum points of $\psi(\xi_1, \ldots, \xi_k)$ as $\varepsilon \to 0$, where*

$$\psi(\xi_1, \ldots, \xi_k) \equiv \min_{i,j,l=1,\ldots,k|j\neq l} \left(dist(\xi_i, \partial\Omega), \frac{1}{2}|\xi_j - \xi_l| \right). \tag{2.52}$$

Notice that this result is geometrically very similar to the analogous result in (2.24) for a k-spike solution to Carrier's problem with Neumann boundary conditions. The main difference in the multi-dimensional case is that, depending on the topology of Ω, there can be many different choices for the set of spike locations. From Proposition 2.9, it is clear that the spike locations are asymptotically equivalent to a corresponding geometric ball-packing problem. The next result, given in Corollary 1.8 of [3], makes this equivalence precise.

Proposition 2.10. *Let $S_1, \ldots, S_k \in \Omega$ be nonoverlapping spheres of the same radius d, and assume that $S_1, \ldots, S_k$ are packed in such a way that when considered as rigid bodies in a rigid container Ω, the set $\xi_1, \ldots, \xi_k$ of their centers becomes also a rigid body. Then, for $\varepsilon > 0$ sufficiently small, (2.46) has a solution with k spikes that localize at $\xi_1, \ldots, \xi_k$.*

In Fig. 2–6 of [3], many illustrations of this "rigid-body" geometrical construction are shown. In particular, in Fig. 5 of [3], several possibilities are shown for packing eight small spheres of a common radius inside a spherical domain Ω.

Although the basic theory for spike solutions of (2.46) is rather well established, there are two questions that should be explored.

Question 2.6. Formulate a numerical method to compute interior k-spike solutions to (2.46) for $\varepsilon \ll 1$ that overcomes the exponential ill-conditioning. What are the global bifurcation branches of solutions to (2.46) as a function of the topology of Ω and of ε, for both $\varepsilon \ll 1$ and $\varepsilon \gg 1$?

Question 2.7. Using techniques in computational geometry, investigate how the topology of Ω influences the geometrical ball-packing characterization given in Proposition 2.10 for a k-spike solution of (2.46) with k large. Can one estimate the number of solutions for ε small but fixed?

In [101], a multi-dimensional extension of the projection method, as outlined in Sec. 2, was used to determine an interior spike location. We now sketch this method for a one-spike solution of

$$\varepsilon^2 \triangle u + Q(u) = 0\,, \quad x \in \Omega\,; \quad \varepsilon \partial_n u + b(u - s) = 0\,, \quad x \in \partial\Omega\,. \tag{2.53}$$

Here $\Omega \in \mathbb{R}^2$, and $b = b(\xi) \geq 0$, where ξ is arclength along the smooth boundary $\partial\Omega$. We look for an interior one-spike solution of the form $u \sim w\left[\varepsilon^{-1}|x - x_0|\right] + R$, where $R \ll 1$. Using the far-field behavior of w in (2.47b), we find that R satisfies

$$L_\varepsilon R \equiv \varepsilon^2 \triangle R + Q'(w) R = 0\,, \quad x \in \Omega\,, \tag{2.54a}$$

$$\varepsilon\, \partial_n R + bR \sim -c\varepsilon^{1/2} r^{-1/2} e^{-\sigma\varepsilon^{-1} r} \left[b - \sigma \hat{r}\cdot\hat{n}\right]\,. \tag{2.54b}$$

Here $c > 0$ and $\sigma > 0$ are defined in (2.47b). Moreover, $r = |x - x_0|$, $\hat{r} = (x - x_0)/r$, and $\hat{n}$ is the unit outward normal to $\partial\Omega$.

Next, we consider the eigenvalue problem

$$L_\varepsilon \phi = \lambda \phi\,, \quad x \in \Omega\,; \quad \varepsilon \partial_n \phi + b\phi = 0\,. \tag{2.55}$$

This problem has two exponentially small eigenvalues, where the corresponding eigenfunctions ϕ_j for $j = 1, 2$, have the form

$$\phi_j \sim \partial_{x_j} w\left[\varepsilon^{-1}|x - x_0|\right] + \phi_{Lj}\,, \quad j = 1, 2\,. \tag{2.56}$$

Here ϕ_{Lj} is a boundary layer function localized near $\partial\Omega$ that allows the boundary condition in (2.55) to be satisfied. To estimate λ_j, for $j = 1, 2$, we then use Green's identity for ϕ_j and $\partial_{x_j} w$, to derive

$$\lambda_j \left(\partial_{x_j} w, \phi_j\right) = -\varepsilon \int_{\partial\Omega} \phi_j \left(\varepsilon\, \partial_n + b\right)\left[\partial_{x_j} w\right]\, d\xi\,, \quad j = 1, 2\,, \tag{2.57}$$

where $(u, v) \equiv \int_\Omega uv\, dx$. In [101], ϕ_{Lj} was calculated from a boundary layer analysis, which then determines ϕ_j on $\partial\Omega$. In this way, we get

$$\lambda_j \sim -\frac{c^2\sigma^3}{\pi\beta} \int_{\partial\Omega} \left(\frac{x_j - x_{0j}}{r}\right)^2 r^{-1} e^{-2\sigma\varepsilon^{-1} r}\, \frac{\left[b - \sigma\hat{r}\cdot\hat{n}\right]\left[1 + \hat{r}\cdot\hat{n}\right]}{\sigma + b}\, d\xi\,, \tag{2.58}$$

for $j = 1, 2$. Here $\beta \equiv \int_0^\infty w'^2 \rho\, d\rho$. This surface integral defining λ_j is of Laplace type, and so can be calculated asymptotically in terms of the points on $\partial\Omega$ closest to x_0. Therefore, it is clear that λ_j for $j = 1, 2$ is

exponentially small as $\varepsilon \to 0$. Thus, the problem of determining x_0 is exponentially ill-conditioned. Notice the close similarity in the derivation of (2.58) with that given in (2.8)–(2.12) for Carrier's problem in a one dimensional domain.

To determine the spike location we expand R in terms of the normalized eigenfunctions of (2.55) as $R = \sum_{j=0}^{\infty} C_j \lambda_j^{-1} \phi_j$, where

$$C_j = \varepsilon \int_{\partial\Omega} \phi_j \, (\varepsilon \, \partial_n + b) \, w \, d\xi \, . \tag{2.59}$$

The coefficients C_j for $j = 1, 2$ can be calculated from the far-field behavior of w in (2.47b) and from the behavior of ϕ_j on $\partial\Omega$ as obtained from the boundary layer analysis described above. Since $\lambda_j \to 0$ exponentially for $j = 1, 2$, the corresponding limiting solvability condition is that $C_j \to 0$ for $j = 1, 2$. In this way, it was found in [101] that the spike location x_0 is given by a root of the vector-valued function $I(x_0)$, where

$$I(x_0) \equiv \int_{\partial\Omega} r^{-1} \, e^{-2\sigma\varepsilon^{-1} r} \, [1 + \hat{r}\cdot\hat{n}] \, \left(\frac{b - \sigma \hat{r}\cdot\hat{n}}{\sigma + b} \right) \hat{r} \, d\xi \, . \tag{2.60}$$

The following result, obtained by balancing "forces" as described in the rigid body characterization of Proposition 2.10 of [3], was obtained in [101]:

Proposition 2.11. *Assume that there exists a unique largest inscribed circle B for Ω, with center at x_{in} and radius r_{in}, that makes exactly two-point contact with $\partial\Omega$ at $x(\xi_i) \in \partial\Omega$ for $i = 1, 2$. Suppose that $b_i - \sigma$ has the same sign at each contact point and that $\kappa_i r_{in} > -1$ for $i = 1, 2$, where $b_i \equiv b(\xi_i)$ and where κ_i is the curvature of $\partial\Omega$ at ξ_i. Then, x_0 lies on the chord joining $x(\xi_1)$ and $x(\xi_2)$. Moreover, for $\varepsilon \to 0$, x_0 satisfies*

$$x_0(\varepsilon) = x_{in} + \frac{\varepsilon}{8\sigma} x_0^1 \hat{n}_2 + O(\varepsilon^2) \, , \tag{2.61a}$$

where

$$x_0^1 = 2 \log \left[\left(\frac{b_1 - \sigma}{b_1 + \sigma} \right) \left(\frac{b_2 + \sigma}{b_2 - \sigma} \right) \right] + \log \left(\frac{1 + \kappa_2 r_{in}}{1 + \kappa_1 r_{in}} \right) \, , \quad \hat{n}_2 \equiv \hat{n}(\xi_2) \, . \tag{2.61b}$$

Notice that if $(b_1 - \sigma)(b_2 - \sigma) < 0$, then (2.60) has no root near $x_{\rm in}$. This condition is qualitatively similar to the condition given in Proposition 2.2 for Carrier's problem. A similar result for when the largest inscribed circle makes three-point contact with $\partial\Omega$ was given in [101].

There are several rigorous results for an interior spike solution for (2.53). For the Dirichlet problem with $b = \infty$, it was proved in [79] that there

is a least-energy solution where a one-spike solution concentrates at the maximum of the distance function. This result can be obtained by letting $b \to \infty$ in (2.61). In [8] an interior spike for 2.53) was analyzed in a half-space when b is near the critical value $b = \sigma$. As $b \to \sigma^+$, the spike was found to approach the boundary. The sensitivity of the spike location for b near σ is certainly suggested from (2.61b).

For the Neumann problem, the result in Proposition 2.10 shows that there is a plethora of interior spike solutions. However, as for Carrier's problem in one spatial dimension, interior multi-spike solutions for the Dirichlet problem with $u = s$ on $\partial\Omega$ should not exist. This leads to the next question.

Question 2.8. What are the bifurcation properties of interior k-spike solutions for (2.53) with $k \geq 2$ spikes under the Dirichlet boundary conditions $u = s + Ae^{-\alpha\varepsilon^{-1}}$ for some $\alpha > 0$ and $A > 0$. When $A = 0$, there should be no such solutions. Do the solutions have a saddle-node bifurcation behavior similar to that described in Proposition 2.6 for Carrier's problem?

Question 2.9. For general Dirichlet data with $u = u_b(\xi) > s$ on $\partial\Omega$ can one construct a solution to $\varepsilon^2\triangle u + Q(u) = 0$ that concentrates on the entire boundary of $\partial\Omega$ and that has $k \geq 1$ interior spikes? We conjecture that, in analogy with Proposition 2.4, the interior spikes now concentrate at local maximum points of

$$\psi(\xi_1, \ldots, \xi_k) \equiv \min_{i,j,l=1,\ldots,k|j\neq l} (\mathrm{dist}(\xi_i, \partial\Omega), |\xi_j - \xi_l|) \ . \tag{2.62}$$

A related problem where localization occurs is for the nonlinear Schrodinger equation (cf. [38], [22] and [99])

$$\varepsilon^2\triangle u - V(x)u + u^p = 0\,, \quad x \in \Omega\,; \quad \partial_n u = 0 \quad x \in \partial\Omega\,. \tag{2.63}$$

Here $V(x)$ is a smooth positive potential with $V(x) > V_0 > 0$ in Ω, and p is subcritical. This is the multi-dimensional counterpart of the modified Carrier problem (2.45). It is well-known that there exists spike solutions of (2.63) that localize near non-degenerate local maxima and minima of $V(x)$. Equation (2.63) also admits spike-clustering phenomena where k spikes all cluster near a minimum of $V(x)$ (cf. [99]). It would be interesting to compare the spike phenomena for (2.63) for an exponentially shallow potential with that for the quasilinear problem (2.46). This leads to the next question.

Question 2.10. What are bifurcation properties of spike solutions for (2.63) for a potential of the form $V(x) = 1 + e^{-\sigma/\varepsilon}\hat{V}(x)$, where $\sigma > 0$?

The spike locations should be determined from a competition between the distance function and the localizing effect of the potential $\hat{V}(x)$.

Another problem where localization occurs is in the construction of hot-spot solutions for Bratu's problem

$$\triangle u + \lambda e^u = 0\,, \quad x \in \Omega\,; \quad u = 0\,, \quad x \in \partial\Omega\,. \tag{2.64}$$

Here Ω is a bounded, simply-connected, domain in $\mathbb{R}^2$. The qualitative feature of hot-spot solutions is that $u \to \infty$ as $\lambda \to 0$ in a localized region near some $x = \xi_j$, for $j = 1, \ldots, k$ while $u = O(1)$ as $\lambda \to 0$ away from these points. Using complex analysis, a system of equations for the hot-spot locations ξ_j, for $j = 1, .., k$, was derived in [75]. An alternative method based on singular perturbation theory was used in [101]. The following result characterizes the hot-spot locations:

Proposition 2.12. *For $\varepsilon \to 0$, the hot-spot locations $\xi_1, \ldots, \xi_k$ for (2.64) satisfy the coupled system*

$$\nabla R_d(x;\xi_j)|_{x=\xi_j} + \sum_{i\neq j}^{k} \nabla G_d(x;\xi_i)|_{x=\xi_i} = 0\,. \quad j = 1, \ldots, k\,. \tag{2.65}$$

Here $G_d(x;\xi)$ is the Dirichlet Green's function, with $R_d(x;\xi)$ as its regular part, so that

$$\triangle G_d = -\delta(x-\xi) \quad x \in \Omega\,; \quad G_d = 0\,, \quad x \in \partial\Omega\,, \tag{2.66}$$

and

$$R_d(x,\xi) = G_d(x,\xi) + \frac{1}{2\pi}\log|x-\xi|\,. \tag{2.67}$$

Therefore, the criteria determining the hot-spot locations for (2.64) is very different from that given in Proposition 2.9 for the spike locations of (2.46). This difference arises from a logarithmic, or Coulomb-type, singularity in the far-field behavior of the local hot-spot profile (cf. [101]). For a one hot-spot solution, the hot-spot location satisfies $\nabla R_d(x;\xi_1) = 0$ at $x = \xi_1$. For a convex domain Ω, R_d is convex (cf. [12]), and so there is only one hot-spot location. This criterion for a hot-spot solution with $k = 1$ is actually very similar to the criterion developed in Sec. 4 that determines the location of a spike for the full GM model (1.1).

3. Spikes for Nonlocal Scalar Problems

In this section we begin by examining the stability of the equilibrium spike solutions constructed in Sec. 2. Consider the time-dependent problem

$$u_t = \varepsilon^2 \triangle u - u + u^p\,, \quad x \in \Omega\,; \quad \partial_n u = 0 \quad x \in \partial\Omega\,. \tag{3.1}$$

Here Ω is a bounded domain in R^N, and p is a subcritical exponent.

Let w_ε be an interior one-spike equilibrium solution to (3.1). The center of the spike x_0 satisfies $\mathrm{dist}(x_0, \partial\Omega) = O(1)$ as $\varepsilon \to 0$. By linearizing (3.1), we find that the stability of this solution is determined by the spectrum of

$$L_\varepsilon \phi_\varepsilon \equiv \varepsilon^2 \triangle \phi_\varepsilon - \phi_\varepsilon + p w_\varepsilon^{p-1} \phi_\varepsilon = \lambda^\varepsilon \phi_\varepsilon\,, \quad \partial_n \phi_\varepsilon = 0\,. \tag{3.2}$$

Letting $\varepsilon \to 0$, and defining $y = \varepsilon^{-1}(x - x_0)$, we have that $w_\varepsilon \to w$, where $w(|y|)$ satisfies (1.7). In this way, we obtain

$$L_0 \phi \equiv \triangle \phi - \phi + p w^{p-1} \phi = \lambda \phi\,, \quad \phi \to 0 \quad \text{for} \quad |y| \to \infty\,. \tag{3.3}$$

We refer to L_0 as the local operator, and (3.3) as the *infinite-line local eigenvalue problem*. The consequence of the exponential decay of $w(|y|)$ as $|y| \to \infty$ is that (3.3) is independent of the shape of Ω, of ε, and of x_0. A key result for (3.3), obtained in [68], is the following:

Proposition 3.1. *Consider (3.3) written as $L_0\phi_l = \nu\phi_l$ for $\phi_l \in H^1(\mathbb{R}^N)$. This problem admits the eigenvalues $\nu_0 > 0$, $\nu_1 = \cdots = \nu_N = 0$, and $\nu_{N+k} < 0$ for $k \geq 1$. The eigenvalue ν_0 is simple, and the corresponding eigenfunction is radially symmetric with constant sign.*

This result was proved in Theorem 2.12 of [68]. Therefore, there is exactly one unstable eigenvalue $\nu_0 > 0$ for (3.3). The eigenfunctions corresponding to the zero eigenvalues are the translation modes $\phi_j = \partial_{y_j} w(|y|)$ for $j = 1, \ldots, N$. Each of these modes has exactly one nodal line.

In the one-dimensional case, the following more precise result for the spectrum of (3.3) was obtained in [27] using hypergeometric functions:

Proposition 3.2. *Let $J = J(p)$ be a positive integer such that $J < (p+1)/(p-1) \leq J+1$. Then, for $\phi_l \in H^1(R)$, the infinite-line local eigenvalue problem $L_0\phi_l = \nu\phi_l$ has $J+1$ discrete eigenvalues given by*

$$\nu_j = \frac{1}{4}\left[(p+1) - j(p-1)\right]^2 - 1\,, \qquad j = 0, \ldots, J\,. \tag{3.4}$$

The continuous spectrum of L_0 lies in the range $-\infty < \nu < -1$.

This result is Proposition 5.6 of [27]. Notice that $\nu_0 > 0$, $\nu_1 = 0$, and $\nu_j \in (-1, 0)$ for $2 \le j \le J$. However, when $p \ge 3$, then $J = 1$, and there are no discrete eigenvalues in the interval $(-1, 0)$. Alternatively, there are many discrete eigenvalues that appear in $(-1, 0)$ as $p \to 1^+$. When $p = 2$, the only discrete eigenvalues are $\nu_0 = 5/4$, $\nu_1 = 0$, and $\nu_2 = -3/4$.

Although, for $\varepsilon \ll 1$, it is clear that the discrete eigenvalues of the infinite-line local eigenvalue problem should be exponentially close to corresponding eigenvalues of (3.2), a rigorous result to this effect is rather technical. The formal analysis in Sec. 2.1 leading to Proposition 2.1 determines the exponentially small change in the translation mode $\nu_1 = 0$ as a result of the finite domain. The underlying idea is that if the infinite-line local eigenvalue problem has a discrete eigenvalue corresponding to an eigenfunction with an exponential decay as $|y| \to \infty$, then this eigenvalue should be perturbed by only exponentially small terms by the finite domain. An analysis incorporating this idea was made in [17], where it was proved (see Theorem 3.1 of [17]) that the first three eigenvalues of (3.2) are exponentially close to those of (3.3) in the sense that

$$\lambda_0^\varepsilon = \frac{1}{4}(p-1)(p+3) + O\left(e^{-2/\varepsilon}\right), \tag{3.5a}$$

$$\lambda_1^\varepsilon = \frac{4c^2}{\left(\int_{-\infty}^{\infty} w'^2(y)\,dy\right)} e^{-2/\varepsilon}\left(1 + O(e^{-1/\varepsilon})\right), \tag{3.5b}$$

$$\lambda_2 = \frac{1}{4}(p-1)(p-5) + O\left(e^{-(3-p)/\varepsilon}\right), \qquad \text{when } \; p < 3\,. \tag{3.5c}$$

Here c and $w(y)$ are defined in (1.8). Equation (3.5b) is also readily obtained by setting $\kappa_l = \kappa_r = 0$ in (2.12) of Proposition 2.1 in Sec. 2.

Since (3.3) has a strictly positive eigenvalue, there is an eigenvalue of (3.2) that remains positive for $\varepsilon \ll 1$. Therefore, an interior one-spike equilibrium solution is unstable for (3.1). Similarly, an equilibrium solution of (3.1) with k interior and well-separated spikes will be unstable due to the existence of k positive eigenvalues that tend to ν_0 as $\varepsilon \to 0$. The existence of one unstable eigenvalue should also occur for an interior one-spike solution of subcritical quasilinear problems of the general form

$$u_t = \varepsilon^2 \triangle u + Q(u)\,, \quad x \in \Omega\,; \quad \partial_n u = 0 \quad x \in \partial\Omega\,. \tag{3.6}$$

Here $Q(u)$ has the form shown in Fig. 1. This leads to our first question.

Question 3.1. Can one characterize the discrete spectrum of the linearization of (3.6) around an interior one-spike solution for more general $Q(u)$?

Since (3.1) will not have stable equilibrium spike solutions, it is natural to ask whether stability can occur for systems of reaction-diffusion equations that admit spike solutions. The simplest type of coupling in a two-component reaction-diffusion system is to consider the so-called shadow limit where the diffusion coefficient of one of the species is taken to infinity and the reaction-time constant for the same species is set to zero. Several examples to illustrate this limit are given below. Before discussing these systems in any detail, we first illustrate qualitatively the mechanism through which a spike can be stabilized by the shadow problem.

The shadow limiting process on a reaction-diffusion system typically leads to a nonlocal scalar PDE of the form

$$u_t = \varepsilon^2 \triangle u + Q(u\,;\sigma_\varepsilon)\,, \quad x \in \Omega\,; \quad \partial_n u = 0\,, \quad x \in \partial\Omega\,, \tag{3.7a}$$

$$\sigma_\varepsilon \equiv \int_D g(u\,;\varepsilon)\,dx\,. \tag{3.7b}$$

Suppose that (3.7) has a radially symmetric localized equilibrium solution of the form $u = u_q\left(\varepsilon^{-1}|x - x_0|\right)$ where $u_q(|y|) \to s$ exponentially as $|y| \to \infty$, for some constant s. Here, we assume that $x_0 \in D$ with $\mathrm{dist}(x_0, \partial\Omega) = O(1)$ as $\varepsilon \to 0$. Then, the stability of this solution is determined by the spectrum of the finite-domain nonlocal eigenvalue problem

$$M_\varepsilon \phi_\varepsilon \equiv \varepsilon^2 \triangle \phi_\varepsilon + Q_u \phi_\varepsilon + Q_\sigma \int_\Omega g_u \phi_\varepsilon\,dx = \lambda^\varepsilon \phi_\varepsilon\,, \quad x \in \Omega\,, \tag{3.8a}$$

$$\partial_n \phi_\varepsilon = 0\,, \quad x \in \partial\Omega\,. \tag{3.8b}$$

where the coefficients in the differential operator are evaluated at u_q. The stability of the spike on an $O(1)$ time-scale follows if we can show that there are no $O(1)$ eigenvalues that satisfy $\mathrm{Re}(\lambda) > 0$. Since the coefficients in the differential operator depend only on $y = \varepsilon^{-1}|x - x_0|$, we look for localized eigenfunctions $\Phi(y)$, which decay as $|y| \to \infty$. Therefore, it is natural to try to compare the spectrum of (3.8) with that of

$$M_0\Phi \equiv \triangle\Phi + Q_u\Phi + Q_\sigma \varepsilon^N \int_{\mathbb{R}^N} g_u \Phi\,dy = \lambda\Phi\,, \quad y \in \mathbb{R}^N\,, \quad \Phi \to 0 \quad y \to \infty\,. \tag{3.9}$$

Here the derivatives are with respect to the y variable. This problem is referred to as the infinite-line nonlocal eigenvalue problem.

We first note that the spectrum of (3.9) has N zero eigenvalues with corresponding eigenfunctions $\Phi_j(y) = \partial_{y_j} u_q(|y|)$, for $j = 1, \ldots, N$. For these functions the nonlocal term in (3.9) vanishes identically since g_u is radially symmetric in $|y|$. As a result of the exponential decay of u_q, the discrete

eigenvalues of (3.9) should be exponentially close to corresponding eigenvalues of the finite-domain nonlocal eigenvalue problem (3.8). This suggests that there are N eigenvalues of (3.8) that will be exponentially small, and whose eigenfunctions $\phi_{j\varepsilon}$ can be approximated by $\phi_{j\varepsilon} = \partial_{x_j} u_q + \phi_{bj}$, where ϕ_b is a boundary layer function localized near $\partial\Omega$ that allows the no-flux condition (3.8b) to be satisfied. Notice that the boundary layer calculation is in the same spirit as that done in Sec. 2.1 for Carrier's problem.

Secondly, we note that if we neglect the nonlocal term in (3.9), the resulting local eigenvalue problem will have one eigenvalue that is strictly positive corresponding to an eigenfunction Φ_l that is of one sign. Since in general $\int_\Omega g_u \Phi_l \, dy \neq 0$, the nonlocal term in (3.9) will perturb this eigenpair significantly. The key step in the analysis is reduced to determining whether the nonlocal term in (3.9) is sufficiently strong to push this positive eigenvalue associated with the local problem into the left half-plane $\mathrm{Re}(\lambda) < 0$. Since (3.8) only perturbs this eigenvalue by exponentially small terms, it remains strictly in the left half-plane for the finite-domain nonlocal problem. If this spectral condition holds, it would follow that an interior one-spike equilibrium solution is *metastable* in the sense that the eigenvalues in the spectrum of the finite-domain nonlocal problem (3.8) that have the largest real parts are exponentially small as $\varepsilon \to 0$. The corresponding eigenfunctions are closely approximated by the translation modes $\partial_{y_j} u_q(|y|)$, for $j = 1, \ldots, N$.

This rough sketch outlines the mechanism through which the nonlocal term can eliminate one unstable eigenvalue of the corresponding local eigenvalue problem and ensure stability on an $O(1)$ time-scale. Depending on the sign of the exponentially small eigenvalues, an interior one-spike solution may not stable on an exponentially long time-scale. However, these exponentially small eigenvalues will lead to the existence of a metastable time-dependent behavior for an interior one-spike solution.

As mentioned above, the key step in the analysis is to find conditions for which there are no eigenvalues of (3.9) with $\mathrm{Re}(\lambda) > 0$. In general, eigenvalue problems of the type (3.9) and (3.8) are difficult to analyze since they are in general not self-adjoint, and hence complex eigenvalues are possible. To illustrate this possibility, consider the eigenvalue problem (3.8) in one space dimension when $\Omega = [-1, 1]$ and $x_0 = 0$. The resulting problem has the general form

$$\varepsilon^2 \phi_{xx} + (A(x/\varepsilon) - \lambda)\,\phi = \delta B(x/\varepsilon) \int_{-1}^{1} C(x/\varepsilon)\phi \, dx\,, \quad -1 < x < 1\,, \tag{3.10}$$

with $\phi_x(\pm 1) = 0$. Here δ is a parameter measuring the strength of the nonlocal term. This eigenvalue problem is not self-adjoint unless $B(x) = kC(x)$ for some constant k. For fixed ε, many properties of self-adjoint eigenvalue problems of the class (3.10) were obtained in [35] and [9].

Consider the example of [50] where $\varepsilon = 1$, $A(x) \equiv 0$, and

$$B(x) \equiv 2.5 + \cos(\pi x) + 2\cos(2\pi x) \qquad C(x) \equiv 1.1 - \frac{1}{2}\cos(\pi x) + \frac{1}{2}\cos(2\pi x)\ . \tag{3.11}$$

Moveable eigenvalues are those eigenvalues of the local problem that are perturbed by the nonlocal term. Fixed eigenvalues refer to those eigenvalues of the local problem that remain independent of δ, since their eigenfunctions are orthogonal to $C(x)$. For this example, the only moveable eigenvalues are those for which the eigenfunctions lie in the subspace spanned by

$$\phi = s_0 + s_1\cos(\pi x) + s_2\cos(2\pi x)\ , \tag{3.12}$$

for some s_0, s_1, and s_2. Substituting (3.11) and (3.12) into (3.10) where $\varepsilon = 1$, we get the matrix eigenvalue problem $(\Lambda - \delta D)\,\boldsymbol{s} = \lambda \boldsymbol{s}$, where

$$\Lambda \equiv \begin{pmatrix} 0 & 0 & 0 \\ 0 & -\pi^2 & 0 \\ 0 & 0 & -4\pi^2 \end{pmatrix}\ , \quad D \equiv \begin{pmatrix} 5.5 & -1.25 & 1.25 \\ 2.2 & -0.5 & 0.5 \\ 2.2 & -0.5 & 0.5 \end{pmatrix}\ , \quad \boldsymbol{s} \equiv \begin{pmatrix} s_0 \\ s_1 \\ s_2 \end{pmatrix}\ . \tag{3.13}$$

The real parts of the eigenvalues as a function of δ are shown in Fig. 4. In this figure, the dotted lines correspond to the fixed eigenvalues $-k^2\pi^2/4$ for $k = 1$ and $k = 3$, corresponding to the eigenfunctions $\phi = \cos(k\pi(x+1)/2)$ for $k = 1, 3$. This simple example shows that nonlocal non self-adjoint eigenvalue problems of the form (3.10) can have complex eigenvalues through the collision of two moveable eigenvalues.

An important class of nonlocal infinite-line eigenvalue problems that arises in determining the stability of spike solutions in several different systems is the following nonlocal non self-adjoint problem:

$$M_0\Phi \equiv L_0\Phi - \alpha w^p\left(\frac{\int_{\mathbb{R}^N} w^{m-1}\Phi\, dy}{\int_{\mathbb{R}^N} w^m\, dy}\right) = \lambda\Phi\,, \quad y \in \mathbb{R}^N\,; \quad \Phi \to 0 \ \ |y| \to \infty\,. \tag{3.14a}$$

Here $w(|y|)$ satisfies (1.7), and L_0 is the local operator

$$L_0\Phi \equiv \triangle\Phi - \Phi + pw^{p-1}\Phi\,. \tag{3.14b}$$

We assume that $m > 1$ and $1 < p < p_c$, where p_c is the critical Sobolev exponent. Notice that $\partial_{y_j} w(|y|)$ lies in the kernel of M_0 for $j = 1, \ldots, N$,

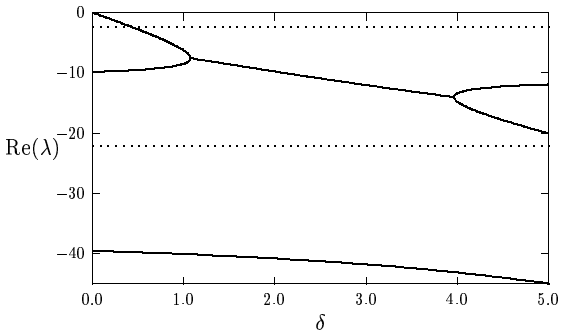

Figure 4. The real parts of the eigenvalues of (3.13) (solid curves) versus δ. Two of them are complex when $1.076 < \delta < 3.970$. The dotted lines are two fixed eigenvalues $\lambda = -\pi^2/4$ and $\lambda = -9\pi^2/4$, not contained in (3.13), which are independent of δ.

and so $\lambda = 0$ is a fixed eigenvalue. There are two key formulae for L_0, obtained by a direct calculation, that are needed below

$$L_0^{-1} w^p = \frac{w}{p-1}\,; \qquad L_0^{-1} w = \frac{w}{p-1} + \frac{1}{2} y \cdot \nabla w\,. \tag{3.15}$$

For the one-dimensional case $N = 1$, where $w(y)$ is given explicitly in (1.8), the following spectral results for (3.14) hold:

Proposition 3.3. *Let $\Phi \in H^1(R)$, and consider any nonzero eigenvalue λ_0 of (3.14). Then, we have the following:*

- *For $0 \le \alpha < p-1$ we have $Re(\lambda_0) > 0$.*
- *Now suppose $\alpha > p-1$. Then, if either $m = 2$ and $1 < p \le 5$, or, $m = p+1$ and $p > 1$, we have $Re(\lambda_0) < 0$.*
- *If $p > 1$ and $m = p$, then we have $Re(\lambda_0) < 0$ when $p-1 < \alpha \le p$.*

The proof of the first result for $0 \le \alpha < p-1$ is given in Appendix E of [47]. The proof of the second result for $\alpha > p-1$ is given in Lemma A and Theorem 1.4 of [108]. The third result is proved in Theorem 1 of [115]. For the multidimensional case where $N > 1$, the following results are known:

Proposition 3.4. *Let $\Phi \in H^1(\mathbb{R}^N)$, and consider any nonzero eigenvalue λ_0 of (3.14). Then, we have the following:*

- *For $0 \le \alpha < p-1$ we have $Re(\lambda_0) > 0$.*

- *Now suppose* $\alpha > p-1$. *Then, if either* $m = 2$ *and* $1 < p \leq 1+4/N$, *or,* $m = p+1$ *and* $1 < p < p_c$, *where* p_c *is the critical Sobolev exponent, we conclude that* $Re(\lambda_0) < 0$.
- *Let* $m = p$. *If* $2 \leq p \leq 5$ *when* $N = 2$, *or* $2 \leq p \leq 3$ *when* $N = 3$, *then we have* $Re(\lambda_0) < 0$ *when* $\alpha = 2p$.

The proof of the first two results are given in [108], and the proof of the third result for $\alpha = p$ is given in Theorem 5.6 of [91]. Notice that when $m = p+1$, the operator is self-adjoint. Qualitatively, these results show that the nonlocal term may eliminate the unstable eigenvalue of the local operator only when α is large enough.

We now comment on the bounds in these results. The lower bound $\alpha = p-1$ for stability in the second result of Propositions 3.3 and 3.4 cannot be improved since from (3.15) we readily calculate that $M_0 w = 0$ when $\alpha = p-1$. The upper bound for α in the third result of Proposition 3.3 is not sharp as stated in [115]. The upper bound on p for $m = 2$ in the second result of Proposition 3.3 is indeed sharp as the next result shows.

Proposition 3.5. *Let* $\Phi \in H^1(R)$, $m = 2$, *and suppose that* $p > 5$ *in (3.14). Then, there exists an* α_m *with* $\alpha_m > p-1$ *such that there are exactly two positive real eigenvalues in the interval* $(0, \nu_0)$ *for any* α *with* $(p-1) < \alpha < \alpha_m$. *In addition, there exists a value* α_h, *with* $\alpha_h > \alpha_m$ *such that for* $\alpha_m < \alpha < \alpha_h$, *there is a pair of complex conjugate eigenvalues in the unstable right half-plane* $Re(\lambda) > 0$. *When* $\alpha = \alpha_h$, *there is a pair of complex conjugate eigenvalues on the imaginary axis.*

This result was proved in Proposition 2.7 of [50]. In addition, a detailed numerical study of the spectrum of (3.14) for different values of m and p was given in Sec. 2.2 and Sec. 2.3 of [50].

For any $p \geq 3$ and with $\alpha = 0$, Proposition 3.2 shows that there is only one discrete nonzero eigenvalue of M_0. Proposition 3.5 shows that there are two discrete eigenvalues in the right half-plane for some range of α when $p > 5$. The numerical computations of [50] show that an extra eigenvalue is created out of the edge of the continuous spectrum at a certain value of α. The two discrete moveable eigenvalues then coalesce producing a complex conjugate pair as in the simple example (3.13). This leads to the next question.

Question 3.2. Find other ranges of p, m, and N where any nonzero eigenvalue of (3.14) will have $\mathrm{Re}(\lambda) < 0$? Can one characterize any edge bifurca-

tions for (3.14) from the continuous spectrum? A detailed numerical study for $N > 1$ is an open problem.

The analysis leading to Proposition 3.3–3.5 relies rather heavily on special properties of the nonlinearity $Q(u) = -u+u^p$, most notably the explicit formulae (3.15). This leads to the following question.

Question 3.3. Can one characterize the discrete spectrum of more general problems of the form (3.9) around an interior one-spike solution?

Although the proofs of Propositions 3.3–3.5 are too involved to discuss here in detail, we can still give a qualitative idea on how some of these results are obtained. To do so, we reformulate (3.14) by letting $\psi(y)$ be the solution to

$$L_0\psi \equiv \psi'' - \psi + pw^{p-1}\psi = \lambda\psi + w^p\,; \qquad \psi \to 0 \quad \text{as} \quad |y| \to \infty\,. \tag{3.16}$$

Then, the eigenfunctions of (3.14) can be written as

$$\Phi = \alpha\psi J\,, \qquad J \equiv \frac{\int_{\mathbb{R}^N} w^{m-1}\Phi\, dy}{\int_{\mathbb{R}^N} w^m\, dy}\,. \tag{3.17}$$

We then multiply both sides of (3.17) by w^{m-1} and integrate over $\mathbb{R}^N$. Assuming, that $\int_{\mathbb{R}^N} w^{m-1}\Phi\, dy \neq 0$, we then obtain that the eigenvalues of (3.14) with even eigenfunctions are the roots of $g(\lambda) = 0$, where

$$g(\lambda) \equiv \frac{1}{\alpha} - f(\lambda)\,, \qquad f(\lambda) \equiv \frac{\int_{\mathbb{R}^N} w^{m-1}\,(L_0-\lambda)^{-1}\, w^p\, dy}{\int_{\mathbb{R}^N} w^m\, dy}\,. \tag{3.18}$$

The function $g(\lambda)$ is analytic in the right half-plane except at the simple pole $\lambda = \nu_0$, where ν_0 is the unique positive eigenvalue of L_0. A simple calculation of the winding number shows that the number M of zeroes of $g(\lambda)$ in $\mathrm{Re}(\lambda) > 0$ is

$$M = 1 + \frac{1}{\pi}\left[\arg g\right]_{\Gamma_I}\,. \tag{3.19}$$

Here $\left[\arg g\right]_{\Gamma_I}$ denotes the change in the argument of $g(\lambda)$ along the semi-infinite imaginary axis $\Gamma_I = i\lambda_I$, $0 \le \lambda_I < \infty$, traversed in the downwards direction. Therefore, to calculate M, we need only determine properties of $g(\lambda)$ on the positive imaginary axis.

We let $\lambda = i\lambda_I$ and we separate real and imaginary parts by writing $g(i\lambda_I) = \tilde{g}_R(\lambda_I) + i\tilde{g}_I(\lambda_I)$. A simple calculation shows that the eigenvalues

of (3.14) along the positive imaginary axis are the roots of the coupled system $\tilde{g}_R = \tilde{g}_I = 0$, given by

$$\tilde{g}_R(\lambda_I) \equiv \frac{1}{\alpha} - \tilde{f}_R(\lambda_I)\,, \qquad \tilde{g}_I(\lambda_I) \equiv -\tilde{f}_I(\lambda_I)\,, \tag{3.20a}$$

where $\tilde{f}_R$ and $\tilde{f}_I$ are defined by

$$\tilde{f}_R(\lambda_I) \equiv \frac{\int_{\mathbb{R}^N} w^{m-1} L_0 \left[L_0^2 + \lambda_I^2\right]^{-1} w^p\, dy}{\int_{\mathbb{R}^N} w^m\, dy}\,, \tag{3.20b}$$

$$\tilde{f}_I(\lambda_I) \equiv \frac{\lambda_I \int_{\mathbb{R}^N} w^{m-1} \left[L_0^2 + \lambda_I^2\right]^{-1} w^p\, dy}{\int_{\mathbb{R}^N} w^m\, dy}\,. \tag{3.20c}$$

The following local and global properties of $\tilde{f}_R$ and $\tilde{f}_I$ have been established:

Proposition 3.6. *The function $\tilde{f}_R$ in (3.20b) has the asymptotic behavior*

$$\tilde{f}_R(\lambda_I) \sim \frac{1}{p-1} - \kappa_c \lambda_I^2 + \cdots\,,\ \text{as } \lambda_I \to 0\,; \quad \tilde{f}_R(\lambda_I) = 0\left(\lambda_I^{-2}\right)\,,\ \text{as } \lambda_I \to \infty\,. \tag{3.21}$$

Here $\kappa_c > 0$ if $m = 2$, or, if $m = p+1$ and $1 < p < 1 + 4/N$. When $m = 2$ the function $\tilde{f}_R(\lambda_I)$ is monotone decreasing for $\lambda_I > 0$. The function $\tilde{f}_I$ in (3.20c) has the asymptotic behavior

$$\tilde{f}_I(\lambda_I) \sim \frac{\lambda_I}{p-1}\left[\frac{1}{p-1} - \frac{N}{2m}\right] + O(\lambda_I^3)\,, \quad \text{as} \quad \lambda_I \to 0\,, \tag{3.22}$$

with $\tilde{f}_I(\lambda_I) = 0\left(\lambda_I^{-1}\right)$ as $\lambda_I \to \infty$. When either, $m = 2$ and $1 < p \le 1 + 4/N$, or, when $m = p+1$ and $1 < p < p_c$, where p_c is the critical Sobolev exponent, we have the global result that $\tilde{f}_I(\lambda_I) > 0$ for $\lambda_I > 0$.

The local behavior of $\tilde{f}_R$ was derived in Eq. (4.3) of [106]. The condition $\tilde{f}_R' < 0$ for $m = 2$ was derived in the proof of Theorem 2.3 of [106]. The local behavior of $\tilde{f}_I$ was derived in Eq. (4.2) of [106]. The proof that $\tilde{f}_I > 0$ for $m = 2$ and $1 < p \le 1 + 4/N$ is rather difficult, and was obtained in Theorem 2.3 of [106]. The condition $\tilde{f}_I > 0$ for $m = p+1$ and $1 < p < p_c$ is readily seen by writing $\tilde{f}_I$ as $\tilde{f}_I(\lambda_I) = \lambda_I C(\lambda_I)$, where

$$C(\lambda_I) \equiv \frac{\int_{\mathbb{R}^N} w^p \left[L_0^2 + \lambda_I^2\right]^{-1} w^p\, dy}{\int_{\mathbb{R}^N} w^{p+1}\, dy}\,. \tag{3.23}$$

We readily calculate using (3.15) that

$$C^{'}(\lambda_I) = -2\lambda_I \frac{\int_{\mathbb{R}^N} \left[\left(L_0^2 + \lambda_I^2 \right)^{-1} w^p \right]^2 dy}{\int_{\mathbb{R}^N} w^{p+1}\, dy} < 0\,, \tag{3.24a}$$

$$C(0) = \frac{1}{p-1} \left[\frac{1}{p-1} - \frac{N}{2(p+1)} \right]. \tag{3.24b}$$

Thus, for $1 < p < p_c$, we have that $C(0) > 0$ together with $C^{'}(\lambda_I) < 0$ for $\lambda_I > 0$, and $C(\lambda_I) \to 0^+$ as $\lambda_I \to \infty$. Hence $C(\lambda_I) > 0$ for $\lambda_I > 0$, which establishes that $\tilde{f}_I > 0$ for $\lambda_I > 0$ when $m = p+1$ and $1 < p < p_c$.

Next, we use the properties of g on the imaginary axis to calculate M from (3.19). The following result is readily derived by using (3.20)–(3.22) to calculate $[\arg g]_{\Gamma_I}$:

Proposition 3.7. *Let $\alpha > p-1$. Suppose that at each root of $\tilde{g}_R = 0$, we have that $\tilde{f}_I > 0$. Then, $M = 0$, and there are no eigenvalues of (3.14) in $Re(\lambda) > 0$. Alternatively, suppose that $0 < \alpha < p-1$, and that $\tilde{f}_R$ is monotone decreasing for $\lambda_I > 0$. Then, $M = 1$ and so there is a unique real positive eigenvalue of (3.14).*

Notice that if $\alpha > p-1$, then $\tilde{g}_R(0) < 0$ and $\tilde{g}_I(0) = 0$. As $\lambda_I \to \infty$, we have $\tilde{g}_R \to \alpha^{-1} > 0$ and $\tilde{g}_I \to 0$. Hence, if whenever we have a root of $\tilde{g}_R = 0$ it follows that $\tilde{g}_I < 0$, we conclude that $[\arg g]_{\Gamma_I} = -\pi$, and consequently $M = 0$ from (3.19). Note that $\tilde{g}_I < 0$ is guaranteed whenever $\tilde{f}_I > 0$ for all $\lambda_I > 0$. As seen in Proposition 3.6, this condition is guaranteed for two cases: $m = 2$ and $1 < p \leq 1 + 4/N$, or, $m = p+1$ and $1 < p < p_c$. This criterion then establishes the second statements in Proposition 3.3 and Proposition 3.4. Alternatively, if $0 < \alpha < p-1$ and $\tilde{f}_R^{'} < 0$, then $\tilde{g}_R > 0$ for $\lambda_I > 0$. Consequently, $[\arg g]_{\Gamma_I} = 0$, and hence $M = 1$. This is the first statement in Proposition 3.3 and Proposition 3.4 under a slightly weaker hypothesis. Eliminating the hypothesis that $\tilde{f}_R$ is monotone decreasing, it is readily seen, upon looking for roots of $g(\lambda) = 0$ on the positive real axis, that $M \geq 1$ when $0 < \alpha < p-1$. Finally, we comment on the idea behind Proposition 3.5. For $m = 2$, we have from Proposition 3.6 that $\tilde{f}_R^{'} < 0$ for $\lambda_I > 0$, and hence there exists a unique root to $\tilde{g}_R = 0$ when $\alpha > p-1$. If we can guarantee that $\tilde{g}_I > 0$, or equivalently $\tilde{f}_I < 0$, at this root, then we have $[\arg g]_{\Gamma_I} = +\pi$, and so $M = 2$. For $N = 1$, $m = 2$, and $p > 5$, the local behavior in Proposition 3.6 shows that $\tilde{f}_I < 0$ for $\lambda_I > 0$ sufficiently small. Hence, there is some range of α with $\alpha > p-1$ for which $M = 2$. This is the essence of Proposition 3.5.

The result in Proposition 3.7 gives a simple criterion to determine sufficient conditions for nonzero eigenvalues of (3.14) to satisfy $\mathrm{Re}(\lambda) < 0$. This leads to the following question.

Question 3.4. Can one find other ranges of m, p, and N, to ensure that the positivity condition on $\tilde{f}_I$ given in Proposition 3.7 holds? With this condition any nonzero eigenvalue of (3.14) has $\mathrm{Re}(\lambda) < 0$ when $\alpha > p - 1$.

One of the earliest analyses of metastability for a shadow system was given in [64]. Another activator-inhibitor system that exhibits metastability was given in [5] and [6]. In the next few subsections we give a few explicit examples of the stability and dynamics of spikes for shadow systems.

3.1. *The Shadow Gierer-Meinhardt Model*

Our first example of a shadow system is obtained by letting $D \to \infty$ in the GM model (1.1) to get

$$a_t = \varepsilon^2 \triangle a - a + a^p/h^q\,, \quad x \in \Omega\,; \quad \partial_n a = 0\,, \qquad x \in \partial\Omega\,, \tag{3.25a}$$

$$\tau h_t = -h + \frac{\varepsilon^{-N}}{|\Omega|}\int_\Omega \frac{a^m}{h^s}\,dx\,. \tag{3.25b}$$

In (3.25b), $|\Omega|$ denotes the volume of Ω. In this section we will consider the case where the reaction-time constant τ in (3.25b) is zero. The possibility of Hopf bifurcations when $\tau > 0$ is discussed in the next section.

An interior one-spike equilibrium solution to (3.25) in $\mathbb{R}^N$ is given by

$$a = h^{q/(p-1)} w\left[\varepsilon^{-1}|x - x_0|\right]\,, \quad h = \left(\frac{\omega_N}{|\Omega|}\int_0^\infty w^m \rho^{N-1}\,d\rho\right)^{-1/\zeta}\,. \tag{3.26}$$

Here ζ is given in (1.2), ω_N is the surface area of the unit N-dimensional sphere, and $w(\rho)$ satisfies (1.7). The finite-domain nonlocal eigenvalue problem of the form (3.8), obtained by linearizing (3.25) around this equilibrium solution, is

$$M_\varepsilon = \epsilon^2 \triangle \phi_\varepsilon + (-1 + p w^{p-1})\phi_\varepsilon - \frac{mq\epsilon^{-N} w^p}{s+1}\left(\frac{\int_\Omega w^{m-1}\phi\,dx}{\int_\Omega w^m\,dx}\right) = \lambda^\varepsilon \phi_\varepsilon\,, \tag{3.27}$$

where $\partial_n \phi_\varepsilon = 0$ on $\partial\Omega$. The corresponding infinite-line nonlocal eigenvalue problem is

$$M_0 \Phi \equiv L_0 \Phi - \frac{mq}{s+1} w^p \left(\frac{\int_{\mathbb{R}^N} w^{m-1}\Phi\,dy}{\int_{\mathbb{R}^N} w^m\,dy}\right) = \lambda \Phi\,, \tag{3.28}$$

with $\Phi \to 0$ as $|y| \to \infty$, and L_0 defined in (3.14b).

From (3.14), and the condition (1.2) on the exponents (p, q, m, s), we see that $\alpha = mq/(s+1) > p-1$. From the second statement of Proposition 3.4 we conclude that for any nonzero eigenvalue of (3.28), we have that $\mathrm{Re}(\lambda) < 0$ when $m = 2$ and $1 < p \leq 1 + 4/N$, or when $m = p+1$ and $1 < p < p_c$, where p_c is the critical Sobolev exponent. Therefore, under these conditions, the nonlocal term has pushed the unstable eigenvalue of the local operator L_0 into the stable left half-plane. Since the discrete eigenvalues of (3.28) are exponentially close to corresponding eigenvalues of (3.27), we conclude from the discussion following (3.8) that an interior one-spike solution to the shadow GM model will be metastable.

Then, by using the projection method in a similar way as was done in Sec. 2, the derivation in Sec. 2.5 of [44] yields the estimate (2.58) for the exponentially small eigenvalues of (3.27). Therefore, to leading order, the contribution of the nonlocal term in (3.27) is subdominant to that of the boundary layer calculation given in Sec. 2.5. Then, by using the projection method for the time-dependent problem, the following result for the metastable motion of an interior one-spike solution for the shadow GM model was obtained in [44]:

Proposition 3.8. *Let $\varepsilon \to 0$, and assume that either $m = 2$ and $1 < p \leq 1 + 4/N$, or $m = p+1$ and $1 < p < p_c$, where p_c is the critical Sobolev exponent. Then, a one-spike solution for the shadow GM model (3.25) with $\tau = 0$ is given asymptotically by $a(x,t) \sim h^{q/(p-1)} w\left(\varepsilon^{-1}|x - x_0(t)|\right)$, where $x_0(t)$ satisfies the differential equation*

$$x_0' \sim \frac{\varepsilon N c^2}{\beta_N \omega_N} \int_{\partial\Omega} \hat{r}\, r^{1-N} e^{-2r/\varepsilon} (1 + \hat{r}\cdot\hat{n})\, \hat{r}\cdot\hat{n}\, d\partial\Omega\,, \quad \beta_N \equiv \int_0^\infty w'^2 \rho^{N-1}\, d\rho\,. \tag{3.29}$$

Here $r = |x - x_0|$, $\hat{r} = (x - x_0)/r$, $\hat{n}$ is the unit outward normal to $\partial\Omega$, and c is defined in (1.7b). Next, assume that there is a unique point x_m on $\partial\Omega$, where r is minimized. Then, the spike moves exponentially slowly in a straight line towards x_m and the distance $r_m(t) \equiv |x_m - x_0(t)|$ satisfies

$$r_m' \sim -\xi r_m \left(\frac{\varepsilon}{r_m}\right)^{(N+1)/2} H(r_m)\, e^{-2r_m/\varepsilon}\,, \quad \xi \equiv \frac{2Nc^2}{\omega_N \beta_N} \pi^{(N-1)/2}\,. \tag{3.30}$$

In terms of the principal radii of curvature R_i, $i = 1, \ldots, N-1$ of $\partial\Omega$ at x_m, the function $H(r_m)$ is defined by $H(r_m) \equiv \left(1 - \frac{r_m}{R_1}\right)^{-1/2} \cdots \left(1 - \frac{r_m}{R_{N-1}}\right)^{-1/2}$.

This result was first derived formally in Proposition 2 and Corollary 2 of [44] and was later proved rigorously in [14]. Metastability will also occur for other (p, q, m, s) whenever we can guarantee that for any nonzero eigenvalue of (3.28) we have $\mathrm{Re}(\lambda) < 0$ (see Question 3.2 above).

This analysis shows that an interior one-spike solution to the shadow GM model with $\tau = 0$ is ultimately unstable, and the spike will drift exponentially slowly towards the closest point on the boundary. An open problem concerns how the spike attaches to the boundary of the domain.

Question 3.5. Analyze the time-dependent motion of a spike when $\mathrm{dist}(x_0, \partial\Omega) = O(\varepsilon)$. How does a spike attach itself to the boundary?

We remark that if we were to change the boundary conditions from Neumann to the Robin condition

$$\varepsilon \partial_n a + \kappa a = 0\,, \quad x \in \partial\Omega\,, \tag{3.31}$$

where $\partial_n a$ is the outward normal derivative, then from Eq. (2.58) of Sec. 2.5 we would expect that the exponentially small eigenvalues of (3.27) will all be negative when $\kappa > 1$ (see Proposition 2.1 for the analogous formula in one-dimension). Therefore, when $\kappa > 1$ an interior one-spike equilibrium solution will be stable. This leads to the next question.

Question 3.6. Consider (3.25) (with $\tau = 0$) and with the Robin condition (3.31) for a with $k > 1$. Prove that an interior one-spike equilibrium solution is stable, and that a one-spike solution drifts exponentially slowly towards the point in $\partial\Omega$ that maximizes the distance to the boundary.

In [45] a formal asymptotic analysis was done for (3.25) when $\tau = 0$ to derive an equation of motion for a spike on the boundary $\partial\Omega$ of a domain. Since the spike is localized, to leading order we have a spike on the boundary of a half-space. In view of the Neumann boundary conditions, the stability of the spike profile on an $O(1)$ time-scale is again determined by the infinite-line nonlocal eigenvalue problem (3.28). The following result was given in Proposition 2.1 of [45]:

Proposition 3.9. *Let $\varepsilon \to 0$ and assume that either $m = 2$ and $1 < p \le 3$, or $m = p + 1$. Then, the motion of a spike for (3.25) that is confined to the*

smooth boundary of a two-dimensional evolves according to

$$a \sim h^{q/(p-1)} w\left(\varepsilon^{-1}\left[(s-s_0(t))^2+\eta^2\right]^{1/2}\right)+O(\varepsilon)\,, \tag{3.32a}$$

$$s_0'(t) \sim \frac{4b}{3\pi}\varepsilon^3\kappa'(s_0)\,, \quad b \equiv \frac{\int_0^\infty \rho^2\left[w'(\rho)\right]^2\,d\rho}{\int_0^\infty \rho\left[w'(\rho)\right]^2\,d\rho}\,. \tag{3.32b}$$

Here $w(\rho)$ satisfies (1.7) when $N=2$, η is the distance from $x\in\Omega$ to $\partial\Omega$, and s is the corresponding orthogonal coordinate, which measures arclength along $\partial\Omega$ when $\eta=0$. In addition, κ is the curvature of $\partial\Omega$, taken with the sign convention that $\kappa>0$ for a circle.

This result shows that the speed of the spike is $O(\varepsilon^3)$, and that stable equilibrium points correspond to points on the boundary where κ has local maxima. An analogous result for the spike motion on the boundary of a three-dimensional domain is given in Proposition 3.1 of [45]. For the full GM model (1.1) it was proved in [18] that there is an equilibrium boundary spike solution that concentrates at a local maximum of the curvature of $\partial\Omega$ whenever the inhibitor diffusivity D in (1.1b) is sufficiently large. Therefore, for equilibrium boundary spike solutions, the shadow GM model closely predicts behavior in the full GM model for D large.

The result (3.32b) predicts that a spike is stationary on a flat segment of the boundary where $\kappa'=0$. In this case, as was shown in [45], the motion of a spike is exponentially slow and is determined by the local behavior of the boundary at the ends of the flat segment. Consider the two-dimensional case where $x=(x,y)$, and suppose that the spike is located on the straight-line boundary segment joining the points $(x_L,0)$ and $(x_R,0)$ as shown in Fig. 5. The spike is centered at $x_0=(\xi,0)$ where $x_L<\xi<x_R$. We decompose $\partial\Omega$ as $\partial\Omega=\partial\Omega_c\cup\partial\Omega_s$ where $\partial\Omega_s$ is the straight-line segment of the boundary and $\partial\Omega_c$ denotes the remaining curved part of $\partial\Omega$. The distance between the spike and $\partial\Omega_c$ is assumed to be a minimum at either of the two corners $(x_L,0)$ or $(x_R,0)$.

The local behavior of Ω_c near the corner points is critical to determining the motion. Near these corner points, we assume the local behavior

$$(x_L,0)\,; \quad y=\psi_L(x), \quad \psi_L'(x)\sim -K_L(x_L-x)^{\alpha_L}\,, \quad \text{as } x\to x_L^-, \tag{3.33a}$$

$$(x_R,0)\,; \quad y=\psi_R(x), \quad \psi_R'(x)\sim K_R(x-x_R)^{\alpha_R}\,, \quad \text{as } x\to x_R^+, \tag{3.33b}$$

where $\alpha_L>0$ and $\alpha_R>0$. When $\alpha_L=\alpha_R=1$, K_L and K_R are proportional to the curvature of $\partial\Omega_c$ at the left and right corners, respectively.

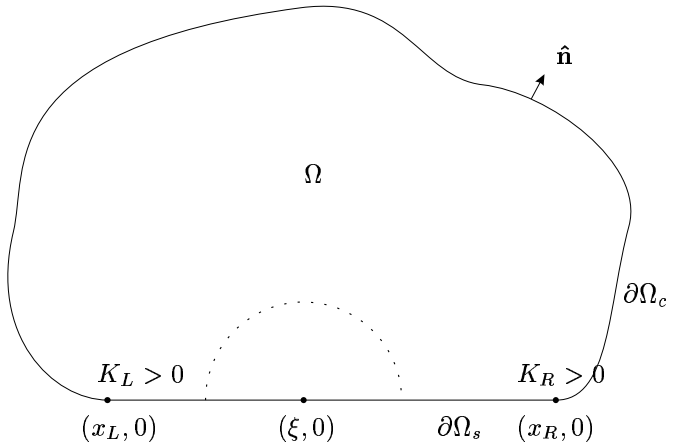

Figure 5. Plot of a two-dimensional domain Ω with a flat boundary segment. The spike is centered at $x = \xi$ on the flat segment. The dotted line indicates an approximate equipotential for a.

The following result characterizing the motion of a spike on the flat segment was derived in Proposition 5.2 of [45] using the projection method.

Proposition 3.10. *Let $\varepsilon \to 0$ and assume that either $m = 2$ and $1 < p \leq 3$, or $m = p + 1$. Assume that the distance between ξ and $\partial\Omega_c$ is a minimum at either of the two corners $(x_L, 0)$ or $(x_R, 0)$. Then, for $\varepsilon \to 0$, the x-coordinate, $\xi(t)$, of the center of a spike that is attached to the flat segment $\partial\Omega_s$ satisfies the asymptotic differential equation,*

$$\xi'(t) \sim \frac{2\varepsilon c^2}{\pi\beta}\left\{\frac{K_R}{x_R - \xi}\left(\frac{\varepsilon}{2}\right)^{\alpha_R+1}\Gamma(\alpha_R+1)\,e^{-2(x_R-\xi)/\varepsilon} - \frac{K_L}{\xi - x_L}\left(\frac{\varepsilon}{2}\right)^{\alpha_L+1}\Gamma(\alpha_L+1)\,e^{-2(\xi-x_L)/\varepsilon}\right\}. \tag{3.34}$$

Here c is given in (1.7b), $\beta \equiv \int_0^\infty \rho w'^2(\rho)\,d\rho$, and the constants K_L, K_R, α_L and α_R are defined in (3.33) in terms of the corner behavior of $\partial\Omega_c$.

A similar differential equation for the motion of a straight-line interface in a constant width neck region of a dumbbell-shaped domain was derived in [60]. The result (3.34) shows that there is a unique steady-state one-spike boundary solution on $x_L < \xi < x_R$ whenever K_L and K_R have the same sign. This solution is unstable when Ω is convex near $(x_L, 0)$ and $(x_R, 0)$ so that $K_R < 0$ and $K_L < 0$. It is stable when $K_L > 0$ and $K_R > 0$. If $K_L < 0$ and $K_R > 0$, then there is no steady-state and $\xi(t)$ will move exponentially slowly towards x_R. Similarly, $\xi(t)$ will move towards

x_L if $K_L > 0$ and $K_R < 0$. When the spike touches $(x_L, 0)$ or $(x_R, 0)$, its subsequent evolution is determined by (3.32b).

Question 3.7. Give a rigorous proof of the characterization of time-dependent spike motion on the boundary of the domain as given in Proposition 3.9–3.10 above, and in Proposition 3.1 of [45]. Formulate a numerical method that is able to numerically compute interior and boundary spike solutions to (3.25) over, possibly, exponentially long time-scales.

3.2. *Hopf Bifurcations for the Shadow GM Model*

We now analyze (3.25) when $\tau > 0$. A equilibrium one-spike solution is again given by (3.26). For this shadow GM problem, it was shown numerically in [78] that a Hopf bifurcation in the spike amplitude can occur when τ is large enough. Since this instability occurs on an $O(1)$ time-scale, for this problem we are not concerned with the exponentially small eigenvalues. By computing the full numerical solution to (3.25) for $N = 2$, in Fig. 6 we plot the amplitude $a_m \equiv a(0,t)$ of a spike centered at $r = |x| = 0$ versus t for two values of τ. This figure suggests that there is a Hopf bifurcation for some τ in $0.53 < \tau < 0.58$.

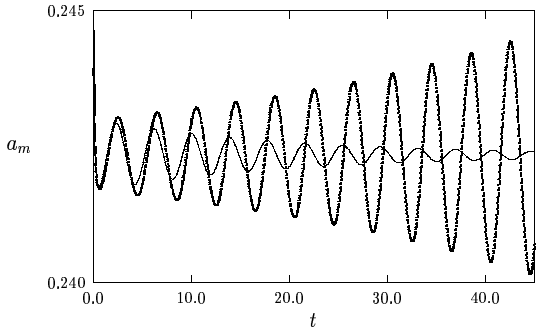

Figure 6. The Hopf bifurcation. We plot a at $x = 0$ versus t for $\tau = 0.53$ (solid curve) and $\tau = 0.58$ (heavy solid curve). The exponent set is $(p, q, m, s) = (2, 1, 2, 0)$, with $N = 2$, and $\varepsilon = 0.05$.

To analyze the Hopf bifurcation we must study the associated spectral problem. Upon linearizing (3.25) around the equilibrium solution in (3.26),

we obtain the following nonlocal eigenvalue problem in place of (3.28):

$$M_0\Phi \equiv L_0\Phi - \frac{mq}{s+1+\tau\lambda} w^p \left(\frac{\int_{\mathbb{R}^N} w^{m-1}\Phi\, dy}{\int_{\mathbb{R}^N} w^m\, dy} \right) = \lambda\Phi\,, \tag{3.35}$$

where $\Phi \to 0$ as $|y| \to \infty$ and L_0 is defined in (3.14b). This eigenvalue problem is more complicated than (3.28) since the multiplier of the nonlocal term now depends on $\tau\lambda$.

The spectrum of (3.35) was studied in [106], where the following result was obtained.

Proposition 3.11. *Assume that $m = 2$ and $1 < p \le 1 + 4/N$. Then, there exists a unique $\tau = \tau_0 > 0$ such that (3.35) has an eigenvalue $\lambda = i\lambda_I^0$, with $\lambda_I^0 > 0$. For all $\tau > \tau_0$ there are exactly two eigenvalues of (3.35) in the right half-plane $Re(\lambda) > 0$. In addition, there exists a τ_c with $\tau_c > \tau_0$ such that for any τ with $\tau > \tau_c$, these two eigenvalues are on the positive real axis, with one eigenvalue tending to ν_0 and the other eigenvalue tending to zero as $\tau \to \infty$. Here $\nu_0 > 0$ is the unstable eigenvalue of the local operator L_0. Alternatively, for any τ with $0 < \tau < \tau_0$ there are no eigenvalues of (3.35) in the right half-plane.*

The existence of a complex conjugate pair of eigenvalues for some $\tau = \tau_0$ was proved in Theorem 2.3 of [106]. The remainder of the proposition was proved in Lemma 3.1 and in Sec. 3 of [106]. Since there are no eigenvalues in the left half-plane when $0 < \tau < \tau_0$ and exactly two when $\tau > \tau_0$, this result shows a transversal crossing condition for τ near τ_0 and proves the existence of a Hopf bifurcation point. In Lemma 2.5 and Eq. (2.36) of [106], the following bounds on the frequency λ_I^0 were derived:

Proposition 3.12. *Assume that $m = 2$ and $1 < p \le 1 + 4/N$. Let ζ and $C_{N,p}$ be defined by*

$$C_{N,p} \equiv \left[\frac{N + (p+1)\,(1 - N/2)}{p+1} \right], \quad \zeta \equiv \frac{2q}{p-1} - (s+1) > 0\,. \tag{3.36}$$

Then, the Hopf bifurcation values τ_0 and $\lambda_I^0 > 0$ satisfy

$$\lambda_I^0 \ge \frac{\zeta(p-1)^2}{qC_{N,p}}, \quad \lambda_I^0 \le \frac{2q}{(s+1)} \left(\frac{\int_{\mathbb{R}^N} w^{2p}\, dy}{\int_{\mathbb{R}^N} w^2\, dy} \right)^{1/2}. \tag{3.37}$$

For the exponent set $(p, q, m, s) = (2, 1, 2, 0)$, in Fig. 7 we illustrate Proposition (3.11) by plotting the path of $\lambda = \lambda_R + i\lambda_I$ as τ is increased. This type of path in the spectrum is very similar to what was shown for

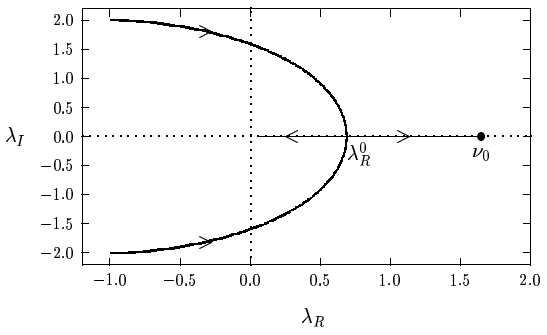

Figure 7. Plot of the path of $\lambda = \lambda_R \pm i\lambda_I$ for $(p, q, m, s) = (2, 1, 2, 0)$ with $N = 2$ (arrows indicate direction of increasing τ). There is a pair of pure imaginary eigenvalues when $\tau = \tau_0$. The complex conjugate pair merge onto the real axis at λ_R^0 when $\tau = \tau_c$. For $\tau > \tau_c$, one eigenvalue then tends to the eigenvalue $\nu_0 > 0$ of L_0 as $\tau \to \infty$.

the GS model in one spatial dimension in [25] and [26]. The existence of two real positive eigenvalues for $\tau \gg 1$ was proved in [16].

In Table 1 we give some numerical results for τ_0 and λ_I^0, obtained from full numerical solutions of (3.35) for different exponent sets (p, q, m, s) and dimension N. The lower and upper bounds on λ_I^0 predicted in (3.37) are also shown. Notice that the lower bound is actually quite close to the numerically computed value.

Table 1. Numerical values for τ_0, λ_I^0, and τ_c for different exponent sets (p, q, m, s) and dimension N for which $m = 2$ and $1 < p \leq 1 + 4/N$. The lower and upper bounds for λ_I^0 given in (3.37) are given in the fifth and sixth columns.

(p, q, m, s)	N	τ_0	λ_I^0	(lower bound)	(upper bound)	τ_c
$(2, 1, 2, 0)$	1	0.771	1.238	1.200	2.484	4.560
$(2, 1, 2, 0)$	2	0.561	1.593	1.500	3.230	3.338
$(2, 1, 2, 0)$	3	0.373	2.174	2.000	4.519	2.189
$(3, 2, 2, 0)$	1	0.304	2.859	2.667	5.842	1.800
$(3, 2, 2, 0)$	2	0.150	4.477	4.000	9.849	0.843
$(4, 2, 2, 0)$	1	0.149	2.525	2.143	6.628	0.471

We now discuss a few of the ideas that are needed for the proof of Proposition 3.11. As in the derivation of (3.18), the eigenvalues of (3.35)

are the roots of the function $g(\lambda) = 0$, where

$$g(\lambda) \equiv \frac{s+1+\tau\lambda}{qm} - f(\lambda)\,, \qquad f(\lambda) \equiv \frac{\int_{\mathbb{R}^N} w^{m-1}\,(L_0-\lambda)^{-1}\,w^p\,dy}{\int_{\mathbb{R}^N} w^m\,dy}\,. \tag{3.38}$$

The function $g(\lambda)$ is analytic in $\mathrm{Re}(\lambda) > 0$ except at the simple pole $\lambda = \nu_0$. In place of (3.19), the number M of zeroes of $g(\lambda)$ in $\mathrm{Re}(\lambda) > 0$ is

$$M = \frac{3}{2} + \frac{1}{\pi}\,[\arg g]_{\Gamma_I}\,. \tag{3.39}$$

Here $[\arg g]_{\Gamma_I}$ denotes the change in the argument of $g(\lambda)$ along the semi-infinite imaginary axis $\Gamma_I = i\lambda_I$, $0 \le \lambda_I < \infty$, traversed in the downwards direction. By letting $\lambda = i\lambda_I$, we find, in place of (3.20), that the eigenvalues of (3.35) along the positive imaginary axis are the roots of the coupled system $\tilde{g}_R = \tilde{g}_I = 0$, given by

$$\tilde{g}_R(\lambda_I) \equiv \frac{s+1}{qm} - \tilde{f}_R\,(\lambda_I)\,, \qquad \tilde{g}_I(\lambda_I) \equiv \frac{\tau\lambda}{qm} - \tilde{f}_I\,(\lambda_I)\,, \tag{3.40}$$

where $\tilde{f}_R$ and $\tilde{f}_I$ are defined in (3.20c).

Since $(s+1)/qm < (p-1)^{-1}$ from (1.2), we have that $\tilde{g}_R(0) < 0$ and $\tilde{g}_R \to (s+1)/qm > 0$ as $\lambda_I \to +\infty$. For $m = 2$ and $1 < p \le 1 + 4/N$, we have from Proposition 3.6 that $\tilde{f}_R' < 0$ for $\lambda_I > 0$, and hence there is a unique root to $\tilde{g}_R = 0$. If τ is sufficiently large, then $\tilde{g}_I > 0$ at the unique root of $\tilde{g}_R = 0$, and so we calculate that $[\arg g]_{\Gamma_I} = \pi/2$. Then, from (3.39) we get that $M = 2$ for τ sufficiently large. Alternatively, for τ small enough we have that $\tilde{g}_I < 0$ at the unique root of $\tilde{g}_R = 0$, so that $[\arg g]_{\Gamma_I} = -3\pi/2$, which yields $M = 0$. To show that there are two eigenvalues in the right half-plane along the positive real axis when τ is sufficiently large, we look for roots of $g(\lambda) = 0$ for $\lambda = \lambda_R > 0$. From (3.38), we get

$$g_R(\lambda_R) \equiv \frac{s+1+\tau\lambda_R}{qm} - f_R(\lambda_R)\,, \quad f_R(\lambda_R) \equiv \frac{\int_{\mathbb{R}^N} w^{m-1}\,(L_0-\lambda_R)^{-1}\,w^p\,dy}{\int_{\mathbb{R}^N} w^m\,dy}\,. \tag{3.41}$$

A simple calculation shows that $f_R(0) = 1/(p-1)$, so that $g_R(0) < 0$. In addition, we have that $f_R(\lambda_R) \to +\infty$ as $\lambda_R \to \nu_0^-$, where $\nu_0 > 0$ is the unique positive eigenvalue of L_0 (see Proposition 3.1). Hence, $g_R \to -\infty$ for $\lambda_R \to \nu_0^-$. Therefore, it is clear from (3.41) that for $\tau \to \infty$, there are two roots to (3.41). For $\tau \to \infty$, one root tends to ν_0^- while the other root tends to zero. These are the main ideas of the proof of Proposition 3.11.

Question 3.8. Can one determine more general conditions on the exponents (p, q, m, s) and on N for the existence of a unique Hopf bifurcation point for $\tau > 0$?

Question 3.9. Analyze the large-scale oscillatory motion for (3.25) for values of τ well-beyond the Hopf bifurcation point. Using a weakly nonlinear analysis determine whether the Hopf bifurcation is subcritical or supercritical. In the presence of the fast oscillation, derive an ODE for the slow motion of the center of the spike. Is the drift still exponentially slow?

3.3. *A Microwave Heating Model*

Another problem where nonlocal singularly perturbed PDE's arise is in the study of hot-spot formation in the microwave heating of ceramics (cf. [62], [63], [9], [10], and [11]). As shown in [62], when a thin cylindrical ceramic sample is placed in a resonant single-mode microwave cavity in such a way that the intensity of the electric field is constant along the axis of the cylinder, a localized region of elevated temperature, known as a hot-spot, can arise. The mechanism for the formation of a stable hot-spot is the detuning of the cavity that occurs as a result of a large increase in the electrical conductivity of the sample for high temperatures. Depending on the parameters, this detuning shifts the resonant point of the cavity, which reduces the strength of the electric field, and thereby stabilizes the temperature profile. In the small Biot number limit, and for a thin sample, the modeling of this detuning effect leads to a nonlocal reaction-diffusion equation for the dimensionless temperature $u(x,t)$ along the axis of the sample of the form (cf. [62]):

$$u_t = \varepsilon^2 u_{xx} - 2\left(u + b[(u+1)^4 - 1]\right) + \frac{p_c f(u)}{1 + \chi^2 \left[\int_{-1}^{1} f(u)\, dx\right]^2}\,, \quad |x| \le 1\,, \tag{3.42}$$

with $u_x = 0$ at $x = \pm 1$. Here $\varepsilon \ll 1$, $\chi > 0$, $p_c > 0$, and $b \ll 1$, and $f(u)$ is electrical conductivity of the sample, which is modeled as $f(u) = 1 + u^2$.

An equilibrium hot-spot solution has $u \to \infty$ as $\varepsilon \to 0$. The appropriate rescaling is $u = \varepsilon^{-2/3} U$ with $U = O(1)$ as derived in [9]. Using this rescaling in (3.42), and with $b \ll O(\varepsilon^2)$, we obtain the following rescaled problem

$$U_t = \varepsilon^2 U_{xx} - 2U + \frac{p_c U^2}{\chi^2 I_0^2}\,, \quad |x| \le 1\,; \qquad U_x(\pm 1, t) = 0\,, \tag{3.43}$$

where $I_0 \equiv \varepsilon^{-1} \int_{-1}^{1} U^2\, dx$. This problem has the form in (3.7). The equi-

librium hot-spot solution for (3.43) is given by

$$U \sim U_\varepsilon[x;x_0] \equiv \gamma w\left[\frac{\sqrt{2}(x-x_0)}{\varepsilon}\right], \quad \gamma^3 \equiv \left(\frac{p_c}{36\chi^2}\right), \quad I_0 = 3\sqrt{2}\left(\frac{p_c}{36\chi^2}\right)^{\frac{2}{3}}. \tag{3.44}$$

Here $w(y)$ is the solution (1.8) to Carrier's problem with $p = 2$.

Linearizing (3.43) around this equilibrium solution, we obtain the following finite-domain nonlocal eigenvalue problem:

$$M_\varepsilon\phi_\varepsilon \equiv \varepsilon^2\phi_{\varepsilon xx} + \left(-2 + \frac{2p_cU_\varepsilon}{\chi^2 I_0^2}\right)\phi_\varepsilon - \frac{4p_cU_\varepsilon^2}{\varepsilon\chi^2 I_0^3}\int_{-1}^{1} U_\varepsilon\phi_\varepsilon\, dx = \lambda^\varepsilon\phi_\varepsilon, \quad |x| \le 1, \tag{3.45}$$

with $\phi_{\varepsilon x}(\pm 1) = 0$. Letting, $\phi_\varepsilon(x) = \Phi(y)$, where $y = \sqrt{2}\varepsilon^{-1}(x - x_0)$, the discrete spectrum of (3.45) can be approximated by the spectrum of the corresponding infinite-line nonlocal eigenvalue problem

$$\Phi_{yy} - \Phi + 2w\Phi - \alpha w^2\left(\frac{\int_{-\infty}^{\infty} w\Phi\, dy}{\int_{-\infty}^{\infty} w^2\, dy}\right) = \frac{\lambda}{2}\Phi, \quad -\infty < y < \infty, \tag{3.46a}$$

where $\Phi \to 0$ as $|y| \to \infty$. The constant α in (3.46a) is

$$\alpha \equiv \frac{6\sqrt{2}\,p_c\,\gamma^3}{\chi^2 I_0^3}, \tag{3.46b}$$

where γ and I_0 are defined in (3.44).

This infinite-line problem has the form (3.14) with $p = m = 2$. Therefore, the second statement of Proposition 3.3 proves that any nonzero eigenvalue of (3.46a) satisfies $\mathrm{Re}(\lambda) < 0$ when $\alpha > 1$. A simple calculation using the expressions for γ and I_0 in (3.44) yields that $\alpha = 4$ for all $\chi > 0$ and $p_c > 0$. Therefore, the principal eigenvalue of (3.45) is exponentially small, and a hot-spot will exhibit metastable behavior. In this way, the following main result was derived in [50]:

Proposition 3.13. *For $\varepsilon \ll 1$, and for any $\chi > 0$ and $p_c > 0$, the exponentially small eigenvalue of (3.45) has the asymptotic estimate*

$$\lambda_0 \sim 120\left(e^{-2\sqrt{2}(1-x_0)/\varepsilon} + e^{-2\sqrt{2}(1+x_0)/\varepsilon}\right). \tag{3.47}$$

A metastable hot-spot solution to (3.43) is given by

$$u(x,t) \sim \frac{3\gamma}{2}\,sech^2\left(\frac{\varepsilon^{-1}[x - x_0(t)]}{\sqrt{2}}\right), \tag{3.48a}$$

where the hot-spot location $x_0(t)$ satisfies the differential equation,

$$\frac{dx_0}{dt} \sim 60\varepsilon\sqrt{2}\left(e^{-2\sqrt{2}(1-x_0)/\varepsilon} - e^{-2\sqrt{2}(1+x_0)/\varepsilon}\right). \tag{3.48b}$$

This shows that the equilibrium hot-spot solution centered at $x_0 = 0$ is unstable, and that the hot-spot tends to the closest of the two boundaries. As a remark, a similar analysis can be done for the generalized polynomial conductivity model $f(u) = 1 + c_1 u^p$. In place of (3.46a), the corresponding finite-domain nonlocal eigenvalue problem is

$$\Phi_{yy} - \Phi + 2w^{p-1}\Phi - 2pw^p\left(\frac{\int_{-\infty}^{\infty} w^{p-1}\Phi\, dy}{\int_{-\infty}^{\infty} w^p\, dy}\right) = \frac{\lambda}{2}\Phi\,, \quad -\infty < y < \infty\,. \tag{3.49}$$

The only result for the spectrum of this problem is given in the third statement of Proposition 3.3.

Question 3.10. Can a similar analysis be done for (3.49) and for the multi-dimensional version of (3.42)?

3.4. *A Flame-Front Evolution Model*

This problem concerns the evolution of a flame-front in a vertical channel. For a channel with a constant cross-section Ω in the $x \equiv (x_1, x_2)$ plane, and under certain physical conditions, the flame-front interface $z = Z(x_1, z_2, t)$ satisfies the nonlocal PDE (cf. [7], [92])

$$Z_t - \frac{1}{2}|\nabla Z|^2 = \varepsilon\triangle Z + Z - \frac{1}{|\Omega|}\int_\Omega Z\, dx\,, \quad x \in \Omega\,; \quad \partial_n Z = 0\,, \quad x \in \partial\Omega\,. \tag{3.50}$$

Here $\varepsilon \ll 1$, $|\Omega|$ is the area of the cross-section and ∂_n is the outward normal derivative. It is observed in physical experiments and numerical computations that the flame-front interface assumes a roughly paraboloidal shape and that the tip of the paraboloid moves very slowly.

The simpler one-dimensional problem in the slab geometry $\Omega = [0, 1]$ was studied in [7] and [92] by first converting (3.50) into a local problem by using the transformation $v = -Z_x$. This yields a convection-diffusion problem known as the Burgers-Sivashinsky equation

$$v_t + vv_x - v = \varepsilon v_{xx}\,, \qquad v(0,t) = v(1,t) = 0\,. \tag{3.51}$$

By analyzing (3.51), it was shown in [92] that the tip $x_0 = x_0(t)$ of a parabolic flame-front interface drifts exponentially slowly towards the closest point on the channel wall (i.e. either $x = 0$ or $x = 1$) according to the ODE

$$x_0' \sim \sqrt{\frac{2}{\pi\varepsilon}}\left[\left((1-x_0)^2+\frac{\pi^2\varepsilon}{3}\right)e^{-(1-x_0)^2/2\varepsilon} - \left((x_0^2+\frac{\pi^2\varepsilon}{3})\right)e^{-x_0^2/2\varepsilon}\right]. \tag{3.52}$$

The simple substitution $v = -Z_x$ to eliminate the nonlocal term for the one-dimensional case has no counterpart for the two-dimensional problem (3.50). However, the change of variables

$$Z = 2\varepsilon \log u\,, \tag{3.53}$$

readily reduces (3.50) to the nonlocal problem

$$u_t = \varepsilon\triangle u + u\left(\log u - \frac{1}{|\Omega|}\int_\Omega \log u\, dx\right), \quad x\in\Omega\,; \quad \partial_n u = 0\,, \quad x\in\partial\Omega\,, \tag{3.54}$$

which is a special case of (3.7). The corresponding local steady-state problem is $\varepsilon\triangle u + u\log u = 0$, which has a degenerate nonlinearity of the type studied in [21]. This leads to the following question:

Question 3.11. Can one analyze (3.54) and the spectrum of the linearized problem? In one-dimension, can one use (3.54) to give a rigorous proof of (3.52). Can the two-dimensional problem for a paraboloidal-shaped interface be analyzed? Investigate spike equilibria for Carrier's problem $\varepsilon^2 u'' + u\log u = 0$, and its multi-dimensional counterpart.

4. Dynamics and Equilibria of a Spike in an R-D System

We begin this section by giving some results for the dynamics and equilibrium locations for an interior one-spike solution to the GM model (1.1) with $\tau = 0$ in a bounded domain $\Omega \in \mathbb{R}^2$. The results in this section cover the range $D \gg O(\varepsilon^2)$, where D is not exponentially large as $\varepsilon \to 0$. The near-shadow limit where $D = O(e^{c/\varepsilon})$ for some $c > 0$ is discussed in §5.1.

Even in the simple case where $\tau = 0$, there are different dynamical laws of spike motion that hold for different ranges of D. For the shadow problem where $D = \infty$, we found above in Proposition 3.8 that a one-spike solution is metastable and that the spike drifts exponentially slowly towards the closest point on $\partial\Omega$. Alternatively, for D small with $\varepsilon^2 \ll D \ll 1$, we find below that the motion of an interior one-spike solution is again metastable, but

now the spike tends to a point in Ω that maximizes the distance function. In contrast, for $D \gg 1$, the motion of a one-spike solution is proportional to the gradient of the regular part of the Neumann Green's function for the Laplacian. Finally, for $D = O(1)$, the motion of a spike is proportional to the gradient of the regular part of the reduced wave Green's function. This second Green's function depends on D.

For $D \gg 1$ and $D = O(1)$, the equilibrium location of a one-spike solution is given by the zeroes of the gradient of the regular part of the Neumann Green's function and the reduced wave Green's function, respectively. In this way, we examine how both the shape of the domain and the inhibitor diffusivity D determine the possible equilibrium locations for a one-spike solution. For D small, we find that stable equilibrium spike locations tend to the centers of the disks of largest radii that can fit within the domain. Hence, for D small, there are two stable equilibrium locations for a dumbbell-shaped domain. In contrast, from the Neumann Green's function, we predict that for a family of dumbbell-shaped domains there is only one possible equilibrium location when D is sufficiently large. This change in the multiplicity of an equilibrium spike-layer location is explained from a certain bifurcation behavior of the zeroes of the gradient of the regular part of the reduced wave Green's function that occurs at a certain critical value of D.

The results below have been derived in [54] and [55]. There have been very few analytical studies of the dynamics of spikes for the GM model (1.1) or for other reaction-diffusion systems in $\mathbb{R}^2$. In [15] and [103] the motion of a one-spike solution for the GM model (1.1) was studied for $D \gg 1$. In [34] the metastable motion of a two-spike solution in $\mathbb{R}^2$ was studied in the weak interaction limit where $D = O(\varepsilon^2)$. This problem is equivalent to a one-spike solution in a half-space with a Neumann boundary condition. For this case, the spike interaction is repulsive, as was found in [34].

In the results below, there are two Green's functions that play a prominent role. The reduced wave Green's function $G(x; x_0)$ satisfies

$$\triangle G - \frac{1}{D} G = -\delta(x - x_0)\,, \quad x \in \Omega\,; \quad \partial_n G = 0\,, \quad x \in \partial\Omega\,. \tag{4.1}$$

The regular part $R(x; x_0)$ of this function is defined by

$$R(x, x_0) = G(x, x_0) + \frac{1}{2\pi} \log |x - x_0|\,. \tag{4.2}$$

Alternatively, the Neumann Green's function $G_m(x;x_0)$ satisfies

$$\triangle G_m = \frac{1}{|\Omega|} - \delta(x-x_0)\,, \;\; x\in\Omega\,; \;\; \partial_n G_m = 0, \;\; x\in\partial\Omega\,; \;\; \int_\Omega G_m\,dx = 0\,. \tag{4.3}$$

The regular part R_m of this Green's function is defined by

$$R_m(x,x_0) = \frac{1}{2\pi}\log|x-x_0| + G_m(x,x_0)\,. \tag{4.4}$$

In terms of R and R_m, we define $R_0 \equiv R(x_0,x_0)$ and

$$\nabla R_0 \equiv \nabla_x R(x,x_0)|_{x=x_0}\,, \quad \nabla R_{m0} \equiv \nabla_x R_m(x,x_0)|_{x=x_0}\,. \tag{4.5}$$

For $D \gg 1$, it is easy to see that these two Green's functions are related by

$$R(x,x_0) \sim \frac{D}{|\Omega|} + R_m(x,x_0) + O\left(D^{-1}\right)\,. \tag{4.6}$$

We begin with the first result that holds for $D \gg -\log\varepsilon$ as derived in [15] and in Proposition 3.2 of [103]:

Proposition 4.1. *Let $\varepsilon\to 0$ and $D \gg -\log\varepsilon$, and assume that the spike profile is stable on an $O(1)$ time-scale. Then, the motion of a one-spike solution for (1.1) in $\Omega\in\mathbb{R}^2$ is characterized by*

$$a(x,t) \sim H^{q/(p-1)} w\left[\varepsilon^{-1}|x-x_0|\right]\,, \quad H \sim \left(\frac{D\nu}{b}\right)^{1/\zeta}\,, \tag{4.7}$$

where $\nu \equiv -1/\log\varepsilon$, $b \equiv \int_0^\infty w^m(\rho)\rho\,d\rho$, and $\zeta > 0$ is given in (1.2). The spike location $x_0 = x_0(t)$ satisfies

$$\frac{dx_0}{dt} \sim -\left(\frac{2q|\Omega|}{p-1}\right)\frac{\varepsilon^2}{D}\nabla R_{m0}\,. \tag{4.8}$$

Here ∇R_{m0} is defined in (4.5).

The following result for $D \gg O(\varepsilon^2)$ is derived in Proposition 2.1 of [54]:

Proposition 4.2. *Let $\varepsilon\to 0$ and $D \gg O(\varepsilon^2)$, and assume that the spike profile is stable on an $O(1)$ time-scale. Then, the trajectory of an interior one-spike solution for (1.1) in $\Omega\in\mathbb{R}^2$ is given by*

$$\frac{dx_0}{dt} \sim -\left(\frac{4\pi q}{p-1}\right)\frac{\varepsilon^2}{-\log\varepsilon + 2\pi R_0}\nabla R_0\,, \tag{4.9}$$

where R_0 and its gradient are defined in (4.5).

For $D \gg 1$, we can use (4.6) in (4.9), to show that (4.9) reduces to (4.8). For $D \ll 1$, we can approximate R_0 by the distance function as outlined in Proposition 3.2 of [54]. More specifically, let $r(x) = \text{dist}(\partial\Omega, x)$. Suppose that x_0 is a local minimum of $R(x_0, x_0)$ for $D \ll 1$. Then, for $D \ll 1$, x_0 is a local maximum of $r(x)$. A more detailed result as given in Proposition 3.1 of [54] determines the following formula for the speed x_0':

Proposition 4.3. *Let $\varepsilon \to 0$ and $O(\varepsilon^2) \ll D \ll O(1)$, and assume that the spike profile is stable on an $O(1)$ time-scale. Assume that at some time t, there is a unique point $x_m \in \partial\Omega$ that is closest to x_0. Then, at that time t, the speed of a spike for (1.1) in $\Omega \in \mathbb{R}^2$ is given by*

$$\frac{dx_0}{dt} \sim -\frac{\sqrt{\pi\lambda}\, q}{p-1}\left(\frac{\varepsilon^2}{\log 2 - \gamma - \log[\varepsilon\lambda]}\right) r_m^{-1/2} e^{-2\lambda r_m}\left(1 - \frac{r_m}{\kappa_m}\right)^{-\frac{1}{2}} \hat{r}_m \,. \tag{4.10}$$

Here $\lambda \equiv D^{-1/2}$, γ is Euler's constant, $r_m = |x_m - x_0|$, $\hat{r}_m = (x_m - x_0)/r_m$, and κ_m is the curvature of $\partial\Omega$ at x_m. Since $dr_m/dt = -dx_0/dt \cdot \hat{r}_m > 0$ from (4.10), the spike moves away from the closest point on the boundary.

In Theorem 4.1 of [54], a complex variable method was used to determine an explicit formula for ∇R_{m0} for a certain class of mappings of the unit disk. From this formula, and from detailed boundary integral numerical computations, the following conjecture was made in [54] regarding the number of zeroes of ∇R_{m0}.

Conjecture 4.1. *Let Ω be any simply-connected bounded domain in $\mathbb{R}^2$, not necessarily convex, and assume that $\partial\Omega$ is smooth. Then, ∇R_{m0} has a unique root inside Ω. Thus, it is conjectured that for $D \gg 1$ there is a unique equilibrium location of an interior one-spike solution of (1.1), and that this location is stable.*

To illustrate the novelty of this conjecture consider a similar problem, but now for the Dirichlet Green's function G_d, which satisfies

$$\triangle G_d = -\delta(x - x_0) \quad x \in \Omega\,; \quad G_d = 0\,, \quad x \in \partial\Omega\,. \tag{4.11}$$

The regular part of G_d and its gradient are defined by

$$R_d(x, x_0) = G_d(x, x_0) + \frac{1}{2\pi}\log|x - x_0|\,, \quad \nabla R_{d0} \equiv \nabla\, R_d(x, x_0)|_{x=x_0}\,. \tag{4.12}$$

Many properties of R_d are given in the survey article [2]. The uniqueness of a root to $\nabla R_{d0} = 0$ in a *convex* domain was established in [43] and

[12]. Consider a class of possibly non-convex domains Ω, generated by the following map $f(z)$ of the unit disk $|z| = 1$, parameterized by b,

$$f(z) = \frac{(1-b^2)z}{z^2 - b^2}, \quad b > 1\,. \tag{4.13}$$

In Fig. 8 we plot Ω for several values of b. When $b \to \infty$, Ω is a perturbation of the unit circle. However, when $b \to 1^+$, Ω becomes the union of two disjoint circles each of radius $1/2$. It is easy to verify that Ω is non-convex when $1 < b < 1 + \sqrt{2}$. By using this map, it was proved in [43] that ∇R_{d0} can have multiple roots in a non-convex domain.

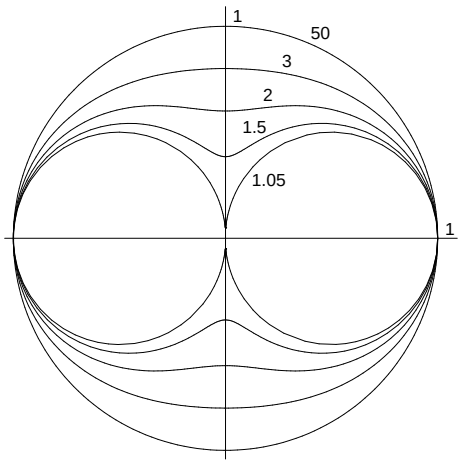

Figure 8. The boundary of $\Omega = f(B)$, with $f(z)$ as given in (4.13), where B is the unit disk. The values of b are as indicated.

From Conjecture 4.1 it follows that for D large enough, there is exactly one possible location for an interior one-spike equilibrium solution, and this location is stable. However, for a dumbbell-shaped domain such as shown in Fig. 8 for $1 < b < 1 + \sqrt{2}$, we know that when D is small enough, the only possible minima of the regular part R_0 of the reduced wave Green's function are near the centers of the lobes of the two dumbbells. In addition, R_0 has a saddle-point at the origin. For D small enough, the equilibria in the lobes of the dumbbell are stable, while the equilibrium at the origin is unstable. Hence, this suggests that a pitchfork bifurcation occurs for the zeroes of ∇R_0 as D is increased past some critical value D_c. As D approaches D_c from below, the two equilibria in the lobes of the dumbbell

should simultaneously merge into the origin. To investigate this effect, a boundary integral method was used in [55] to compute the zeroes of ∇R_0 as a function of $\lambda = D^{-1/2}$ for different values of the shape-parameter b in the class of mappings (4.13). The bifurcation diagram, as shown in Fig. 9, does indeed show a pitchfork bifurcation as predicted, with a subcritical bifurcation if b is small and a supercritical bifurcation if b is large.

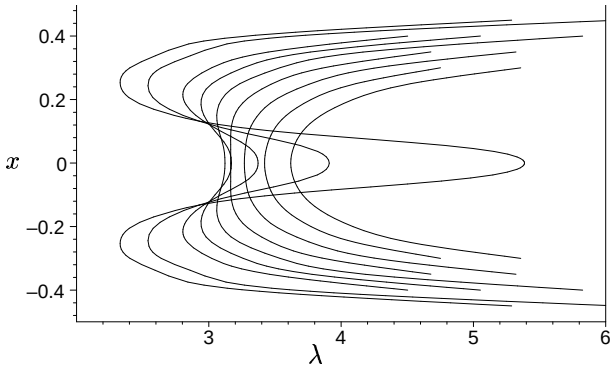

Figure 9. Plot of the bifurcation diagram for the spike equilibria versus $\lambda = D^{-1/2}$ for various values of the dumbbell shape-parameter b. The leftmost curve is $b = 1.15$. Successive curves from left to right correspond to increments in b of 0.05.

This numerical study, and Conjecture 4.1, shows that further work is required to understand the properties of the zeroes of ∇R_0 and ∇R_{m0}. The pitchfork bifurcation behavior for the zeroes of ∇R_0 in nonconvex domains having two axes of symmetry should be a generic feature.

Question 4.1. Can one determine general properties of the zeroes of the gradients of the regular parts of the Neumann Green's function and the reduced wave Green's function? Does Conjecture 4.1 hold?

Question 4.2. Do the zeroes of ∇R_0 have a subcritical bifurcation with respect to $\lambda = D^{-1/2}$ in a dumbbell-shaped domain, whenever the neck of the dumbbell is sufficiently thin, and a supercritical bifurcation in λ when a dumbbell-shaped domain is sufficiently close to a circular domain?

Question 4.3. Can one study the bifurcation behavior for an interior two-spike equilibrium solution as a function of D and the domain topology?

4.1. *The Near-Shadow System*

Next, we consider a one-spike solution for the near-shadow limit of the GM model (1.1) where D is exponentially large as $\varepsilon \to 0$. For the shadow problem where $D = \infty$, and under certain conditions on the exponents (p, q, m, s), it was shown in Sec. 3.1 that a one-spike profile is stable, but that the spike will drift towards the boundary with an asymptotically exponentially small speed as $\varepsilon \to 0$. The asymptotic equilibrium location of this metastable spike is determined by critical points of the distance function. However, when D is exponentially large, the spike location is determined by a balance between the Neumann Green's function R_m defined in (4.4) and the exponentially weak interaction between the far-field behavior of the spike and the boundary $\partial\Omega$ of the domain. In the one-dimensional case this balance leads to the following result (cf. [55]):

Proposition 4.4. *Let $\varepsilon \ll 1$, $\Omega = [-1, 1]$, and $x_0 \in (-1, 1)$. Assume that the spike profile is stable on an $O(1)$ time-scale. Then, when D is exponentially large as $\varepsilon \to 0$, the spike location x_0 satisfies the ODE*

$$\frac{dx_0}{dt} \sim \frac{4\varepsilon c^2}{\beta}\left(\frac{\varepsilon \sinh(2x_0/\varepsilon)}{2x_0} - \frac{D_c}{D}\right) e^{-2/\varepsilon} x_0 \,, \tag{4.14}$$

where D_c and β are defined by

$$D_c = \frac{\varepsilon^2 q \beta}{2c^2(p-1)} e^{2/\varepsilon} \,, \quad \beta \equiv \int_0^\infty \left[w'(y)\right]^2 dy \,. \tag{4.15}$$

This result shows that the spike at $x_0 = 0$ is stable when $D < D_c$, and is unstable when $D > D_c$. When $D < D_c$, there are two unstable equilibria, which are the nonzero roots of $2y/\sinh(2y) = D/D_c$ with $y = \varepsilon^{-1} x_0$.

Similar bifurcation behavior occurs for dumbbell-shaped domains. For these domains, an unstable spike for the shadow problem with $D = \infty$ can be located either in the neck or in one of the two lobes of the dumbbell. However, when D is exponentially large, the next result, as derived in Proposition 4.1 of [55], shows that the bifurcation behavior is such that the spike in the neck of the dumbbell becomes stable through a pitchfork bifurcation. A further result in [55] shows that the spikes in the lobes of the dumbbell tend to the boundary when D is exponentially large. Therefore, this suggests how Conjecture 4.1 arises from the near-shadow limit.

Proposition 4.5. *Let $\varepsilon \ll 1$ and consider the class of dumbbell-shaped domains generated by the mapping $f(z)$ given in (4.13). Assume that the*

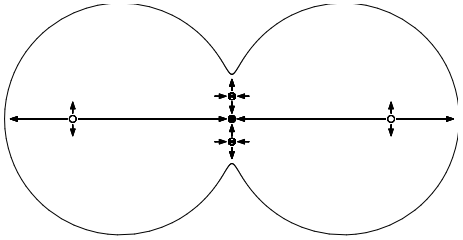

Figure 10. Plot of a dumbbell-shaped domain and the bifurcation behavior of spikes in the neck of the dumbbell when $D = O(e^{c/\varepsilon})$.

spike location $(0, y_0)$ *on the* y*-axis satisfies* $y_0 = O(\varepsilon)$. *Then, the local trajectory* $y_0(t)$ *satisfies*

$$\frac{dy_0}{dt} \sim \varepsilon^{1/2}\,\mu_0\, e^{-2y_m/\varepsilon}\left[\frac{\sinh(2y_0/\varepsilon)}{(2y_0/\varepsilon)} - \frac{D_c}{D}\right] y_0\,, \tag{4.16a}$$

where D_c *and* μ_0 *satisfy*

$$D_c \equiv \frac{\varepsilon^2\beta}{4c^2}\left(\frac{q}{p-1}\right)\left(\frac{\pi}{\varepsilon}\right)^{1/2}\left[y_m\left(1-\kappa_m y_m\right)\right]^{1/2} G_b e^{2y_m/\varepsilon}\,, \tag{4.16b}$$

$$\mu_0 \equiv \frac{8c^2}{\sqrt{\pi\beta}}\left[y_m\left(1-\kappa_m y_m\right)\right]^{-1/2}\,, \quad G_b \equiv \frac{(b^2-1)}{2(b^4-1)^2}\left[2b^6+3b^4+2b^2-1\right]\,. \tag{4.16c}$$

Here κ_m *is the curvature of the boundary at the point* $(0, y_m)$, *where*

$$\kappa_m \equiv \left(\frac{b^2+1}{b^2-1}\right)^3\left[1-\frac{8b^2}{(b^2+1)^2}\right]\,, \quad y_m \equiv \left(\frac{b^2-1}{b^2+1}\right)\,. \tag{4.16d}$$

Therefore, when $D > D_c$, $y_0 = 0$ is the unique, and unstable, equilibrium solution for (4.16a). For $D < D_c$, $y_0 = 0$ is stable, and there are two unstable equilibria with $|y_0| = O(\varepsilon)$, satisfying $2\zeta/\sinh(2\zeta) = D/D_c$ for $\zeta = y_0/\varepsilon$. Therefore, the local bifurcation is subcritical in D/D_c. In Fig. 10 we show the geometry and the bifurcation behavior indicated by Proposition 4.5.

Question 4.4. Provide a rigorous proof of Propositions 4.4 and 4.5. What is the behavior of equilibrium spikes that are $O(\varepsilon)$ close to the boundary?

Question 4.5. What is the relationship between k-spike equilibria of the shadow system (3.25) where $D = \infty$ and k-spike equilibria to the near-shadow system (1.1) where D is exponentially large.

4.2. *Pinning of a Spike*

For the GM model (1.1) with $\tau = 0$, we now examine the effect of spatial variations in the coefficients of the differential operators. We will consider two such problems. The first problem, in one space dimension, is

$$a_t = \varepsilon^2 a_{xx} - [1 + V(x)]\, a + \frac{a^p}{h^q}\,, \quad -1 < x < 1\,; \quad a_x(\pm 1, t) = 0\,, \quad (4.17a)$$

$$0 = D h_{xx} - \mu(x) h + \varepsilon^{-1} \frac{a^m}{h^s}\,, \quad -1 < x < 1\,; \quad h_x(\pm 1, t) = 0\,. \quad (4.17b)$$

Here $\mu(x) > 0$ and $V(x) > 0$ are precursor gradients (cf. [103]), and (p, q, m, s) satisfy (1.2). The second problem is in $\mathbb{R}^2$, and is given by

$$a_t = \varepsilon^2 \triangle a - [1 + V(x)]\, a + \frac{a^p}{h^q}\,, \quad x \in \Omega\,; \quad \partial_n a = 0 \quad x \in \partial\Omega\,, \quad (4.18a)$$

$$0 = D \triangle h - \mu(x) h + \varepsilon^{-2} \frac{a^m}{h^s}\,, \quad x \in \Omega\,; \quad \partial_n h = 0 \quad x \in \partial\Omega\,. \quad (4.18b)$$

In Corollary 2.2 of [103], the effect of $V(x)$ for a spatially independent μ was obtained for (4.17).

Proposition 4.6. *Let $\varepsilon \ll 1$ and suppose that the spike profile is stable on an $O(1)$ time-scale. Let $\mu(x) = \mu$ be a positive constant. Then, the motion of a one-spike solution for (4.17) is characterized by*

$$a(x,t) \sim H^{q/(p-1)}\, [1 + V(x_0)]^{1/(p-1)}\, w\left[\sqrt{1 + V(x_0)}\, \frac{(x - x_0)}{\varepsilon}\right]\,, \quad (4.19)$$

where $h(x_0) = H$ and H is given in Eq. (2.14b) of [103]. Moreover, $w(y)$ satisfies (1.8), $\theta \equiv \sqrt{\mu/D}$, and the spike location $x_0(t)$ satisfies

$$\frac{dx_0}{dt} \sim -\frac{\varepsilon^2 q \theta}{p-1} \left(\tanh\left[\theta(1 + x_0)\right] - \tanh\left[\theta(1 - x_0)\right]\right) - \frac{\varepsilon^2}{2} \left(\frac{p+3}{p-1}\right) \frac{V'(x_0)}{1 + V(x_0)}\,. \quad (4.20)$$

It is easy to see from (4.20) that if V is convex with a minimum at some point in $[-1, 1]$ then there exists a unique equilibrium solution to (4.20) and this equilibrium solution is stable. When $V(x)$ is not convex the situation is more complex. For instance suppose that $V(x)$ is a double-well potential of the form $V(x) = b(1 - x^2)^2$ with $b > 0$. Define ω by $\omega \equiv \frac{q\theta^2 \operatorname{sech}^2\theta}{p+3}$. Then, it readily follows that when $b/(1 + b) > \omega$, we have that $x_0 = 0$ is an unstable equilibrium solution to (4.20), and that there exists a stable equilibrium solution on each of the subintervals $-1 < x < 0$ and $0 < x < 1$.

Alternatively, if $\frac{b}{1+b} < \omega$, then $x_0 = 0$ is the only equilibrium solution to (4.20) and it is stable. This is a classic pitchfork bifurcation scenario.

The next result, given in Corollary 2.4 of [103], shows the effect of $\mu(x)$:

Proposition 4.7. *Let $\varepsilon \ll 1$ and suppose that the spike profile is stable on an $O(1)$ time-scale. Let $V(x) = 0$ and assume that $D \gg 1$. Then, the spike location for (4.17) satisfies*

$$\frac{dx_0}{dt} \sim -\frac{2\varepsilon^2 q}{D(p-1)} \left(\int_{-1}^{x_0} \mu(y)\, dy - \mu_a \right), \qquad \mu_a \equiv \frac{1}{2}\int_{-1}^{1} \mu(x)\, dx\,. \quad (4.21)$$

The results (4.20) and (4.21) show that the spike dynamics depends only on pointwise properties of $V(x)$, but on global properties of $\mu(x)$. The final result, given in Proposition 3.1 of [103], is for (4.18).

Proposition 4.8. *Let $\varepsilon \ll 1$ and suppose that the spike profile is stable on an $O(1)$ time-scale. Suppose that $D \gg -\log\varepsilon$ as $\varepsilon \to 0$. Then, the motion of a one-spike solution for (4.18) is characterized by*

$$a(x,t) \sim H^{q/(p-1)} \left[1 + V(x_0)\right]^{1/(p-1)} w\left[\sqrt{1+V(x_0)}\frac{|x-x_0|}{\varepsilon}\right], \quad (4.22)$$

where $h(x_0) = H$ and H is given in Eq. (3.9) of [103], and $w(y)$ satisfies (1.7) in $\mathbb{R}^2$. The spike location $x_0(t)$ satisfies the following gradient flow

$$\frac{dx_0}{dt} \sim -\frac{2\varepsilon^2}{(p-1)}\nabla W(x_0)\,, \quad \text{where} \quad W(x_0) \equiv \log\left[1 + V(x_0)\right]\,. \quad (4.23)$$

The spike motion is orthogonal to level curves of $W(x)$ and $dW(x_0)/dt < 0$ except at critical points of W.

When $D \gg -\log\varepsilon$, we observe from (4.23) that stable equilibria for the location of the spike occur at points where the potential $V(x)$ has a local minimum. Notice the qualitative similarity between this result and the result mentioned in Sec. 2.4 for Eq. (2.45).

Question 4.6. Can one derive an equation of motion for (4.18) when $D = O(1)$, that involves both ∇R_0 and ∇V, where R_0 is the reduced wave Green's function of (4.5)? If so, then a delicate competition will determine the possible equilibrium locations for an interior one-spike solution.

4.3. *Sudden Oscillatory Instabilities*

We now illustrate a dynamical instability that can occur for a one-spike solution to the GM model (1.1) in one space dimension when τ is sufficiently

large. For a one-spike solution on the $\Omega = [-1,1]$, it is known from (4.20) with $V(x) \equiv 0$, that when $\tau = 0$ the motion of a spike satisfies

$$\frac{dx_0}{dt} \sim -\frac{\varepsilon^2 q\theta}{p-1}\left(\tanh\left[\theta(1+x_0)\right] - \tanh\left[\theta(1-x_0)\right]\right) . \tag{4.24}$$

A simple analysis shows that this ODE is still asymptotically valid for $\tau > 0$ provided that the spike profile is stable. For certain ranges of τ and D, the spike profile may be stable for x_0 sufficiently close to the right endpoint $x = 1$, but may be unstable on an $O(1)$ time-scale due to a Hopf bifurcation in the spike amplitude that occurs at some critical value of x_0 near $x_0 = 0$. Since a spike moves slowly towards the origin under (4.24), this suggests that the spike will enter a zone of instability at some time t with $t = O(\varepsilon^{-2})$. The instability will initiate a rapid oscillation in the spike amplitude relative to a possible continued slow drift of the spike towards the origin. We call this phenomena a sudden oscillatory instability. This phenomenon was first observed in [95], and also occurs for the SC model (1.6) (cf. [95].

To study this instability, we construct a quasi-equilibrium one-spike solution to (1.1) in $\Omega = [-1,1]$. Then, we derive a nonlocal eigenvalue problem for the stability of the spike profile. A simple calculation shows that the quasi-equilibrium solution a_c, h_c is given for $\varepsilon \ll 1$ by

$$a_c \sim H^{q/(p-1)} w\left[\varepsilon^{-1}(x - x_0(t))\right] , \quad H = \left[G_0(x_0;x_0)\int_{-\infty}^{\infty} w^m\, dy\right]^{-1/\zeta} , \tag{4.25a}$$

$$h_c \sim G_0\left[x;x_0\right]/G_0\left[x_0;x_0\right] . \tag{4.25b}$$

Here $w(y)$ is the homoclinic solution in (1.8), ζ is given in (1.2), and $G_0(x;x_0)$ is the Green's function satisfying

$$DG_{0xx} - G_0 = -\delta(x - x_0) , \quad -1 < x < 1; \quad G_{0x}(\pm 1;x_0) = 0 . \tag{4.25c}$$

In Sec. 4.1 of [95] the following nonlocal eigenvalue problem was derived to study the stability of a_c and h_c on an $O(1)$ time-scale:

Proposition 4.9. *Let $0 < \varepsilon \ll 1$, $\tau \geq 0$, and $x_0 \in (-1,1)$. Then, the stability of the quasi-equilibrium profile (4.25) for the GM model (1.1) on $\Omega = [-1,1]$ is determined by the spectrum of the nonlocal eigenvalue problem*

$$L_0\Phi - \chi_m w^p\left(\frac{\int_{-\infty}^{\infty} w^{m-1}\Phi\, dy}{\int_{-\infty}^{\infty} w^m\, dy}\right) = \lambda\Phi , \quad -\infty < y < \infty , \tag{4.26a}$$

with $\Phi \to 0$ *as* $|y| \to \infty$. *Here* L_0 *is the local operator defined in (3.16), and the multiplier* χ_m *is defined by*

$$\chi_m = \chi_m(z; x_0) \equiv qm \left[s + \sqrt{1+z} \left(\frac{\beta(\theta_\lambda; x_0)}{\beta(\theta_0; x_0)} \right) \right]^{-1} , \tag{4.26b}$$

where the function $\beta(\xi; x_0)$ *is defined by*

$$\beta(\xi; x_0) \equiv \tanh\left[\xi(1+x_0)\right] + \tanh\left[\xi(1-x_0)\right] . \tag{4.26c}$$

Here z, θ_λ, *and* θ_0, *are given by*

$$z \equiv \tau\lambda , \qquad \theta_\lambda \equiv \theta_0\sqrt{1+z} , \qquad \theta_0 \equiv D^{-1/2} . \tag{4.26d}$$

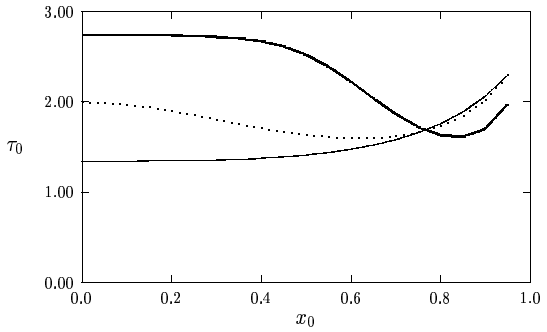

Figure 11. Plots of τ_0 versus x_0 for the GM model with $(p, q, m, s) = (2, 1, 2, 0)$. Here we have $D = 1.0$ (solid curve), $D = 0.5$ (dashed curve), and $D = 0.1$ (heavy solid curve).

This eigenvalue problem is very similar to (3.14) except that the constant multiplier α of the nonlocal term in (3.14) is replaced by the multiplier χ_m, which depends on x_0, on D, and on the product $\tau\lambda$. Consider the exponent set $(p, q, m, s) = (2, 1, 2, 0)$. Then, since $\chi_m > 1$ when $\tau = 0$, we conclude from the second statement of Proposition 3.3 that the spike profile is stable for $\tau = 0$. However, for each fixed D, the spike profile centered at x_0 will become destabilized due to a Hopf bifurcation when τ exceeds some critical value $\tau_0(x_0)$. By symmetry τ_0 is an even function of x_0 and so we need only consider $x_0 \in (0, 1)$. The results for $\tau_0(x_0)$ obtained from a numerical computation for different values of D are shown in Fig. 11. Since τ_0 is a monotone increasing function of x_0 for $x_0 > 0$ when $D = 1$,

by the discussion in the beginning of this subsection, a sudden oscillatory instability will occur for certain parameter values.

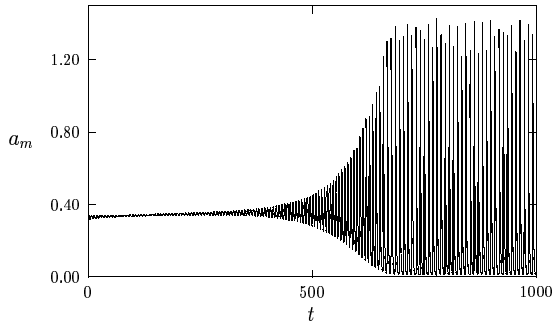

Figure 12. Plots of the spike amplitude $a_m = a(x_0, t)$ versus t for $D = 1.0$, $\varepsilon = 0.03$, $\tau = 1.35$, $x_0(0) = 0.6$, and $(p, q, m, s) = (2, 1, 2, 0)$.

To illustrate this, we take the parameter values $D = 1.0$, $\varepsilon = 0.03$, $\tau = 1.35$, $x_0(0) = 0.6$, and $(p, q, m, s) = (2, 1, 2, 0)$. Important values for $\tau_0(x_0)$ are $\tau_0(0.6) = 1.477$, $\tau_0(0) = 1.343$ and $\tau_0(0.35) = 1.36$. Since $\tau < \tau_0(0.6)$, the spike is initially stable. However, since $\tau_0(0) < \tau$, the slowly drifting spike will experience a sudden instability before it reaches the origin. To verify this prediction, full numerical solutions to (1.1) were computed. The theory is indeed confirmed in Fig. 12 where we plot the spike amplitude a_m defined by $a_m(t) \equiv a[x_0(t); t]$ versus t. The corresponding spike location $x_0(t)$ is plotted in Fig. 13. Before the onset of the instability, the spike motion is given asymptotically by (4.24).

Question 4.7. Can one analyze the large-scale spike oscillations for a slowly drifting spike beyond the Hopf bifurcation point? What is the ODE for spike motion after the onset of the oscillation? Can a similar phenomenon occur in a two-dimensional domain when τ is large enough?

5. Multi-Spike Solutions in Reaction-Diffusion Systems

In this section we begin by constructing multi-spike equilibrium solutions in one spatial dimension to the Gray-Scott (GS) model in the low feed-rate regime (1.5), the Gierer-Meinhardt model (GM) (1.1), and the Schnakenburg (SC) model (1.6). The analysis assumes semi-strong spike interactions

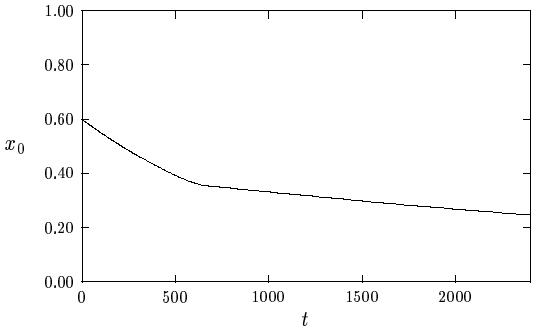

Figure 13. Plots of the spike location $x_0(t)$ versus t for $D = 1.0$, $\varepsilon = 0.03$, $\tau = 1.35$, $x_0(0) = 0.6$, and $(p, q, m, s) = (2, 1, 2, 0)$.

and is done for a one dimensional spatial domain. Two different types of spike patterns are constructed: symmetric patterns where the spikes have equal height, and asymmetric patterns where the spikes have different heights. The first study on the construction of k-spike symmetric patterns for (1.1) in one space dimension was done in [96]. For each of the three reaction-diffusion models, we show that each asymmetric pattern is characterized by two different spikes, B (big) and S (small). For a k-spike asymmetric equilibria, there are $k_1 > 0$ small spikes S and $k_2 = k - k_1 > 0$ large spikes B arranged in any order $SBBS \dots SBB$ across the interval. Neglecting the orientation of large and small spikes in a spike sequence, we show that there are $k - 1$ asymmetric k-spike equilibrium patterns that bifurcate from a symmetric k-spike solution branch at some critical value of the parameters.

We begin by constructing asymmetric multi-spike equilibria for the GM model (1.1) as done in [104]. A different approach was used in [28]. We first construct a symmetric one-spike equilibrium solution centered at the origin for (1.1) posed on a finite domain of length $2l$, where $l > 0$ is a parameter. Therefore, we look for an even solution to

$$\varepsilon^2 a_{xx} - a + \frac{a^p}{h^q} = 0\,, \quad -l < x < l\,; \quad a_x(\pm l) = 0\,, \tag{5.1a}$$

$$D h_{xx} - h + \varepsilon^{-1} \frac{a^m}{h^s} = 0\,, \quad -l < x < l\,; \quad h_x(\pm l) = 0\,. \tag{5.1b}$$

The basic idea is that we seek all values of l, labeled by $l_1, \dots, l_n$, such that $h(l_1) = , \dots, = h(l_n)$. For a certain range of the parameters, it is found that

there are exactly two such values of l. These "local" solutions are then used to obtain a global asymmetric pattern for (1.1) on $[-1,1]$.

The asymptotic solution to (5.1) is

$$a(x) \sim [h(0)]^{q/(p-1)}\, w\left(x/\varepsilon\right)\,, \tag{5.2}$$

where w is given in (1.8) of Sec. 1. Since a is localized near $x=0$, the term $\varepsilon^{-1}a^m/h^s$ in (5.1b) can be asymptotically approximated as a Dirac mass. Therefore, on $-l<x<l$, with $h'(\pm l)=0$, $h(x)$ satisfies

$$Dh'' - h = -\left[h(0)\right]^{\zeta+1}\left(\int_{-\infty}^{\infty}[w(y)]^m\,dy\right)\,\delta(x)\,,\quad -l<x<l\,, \tag{5.3}$$

where ζ is given in (1.2). The solution is

$$h(x) = [h(0)]^{\zeta+1}\left(\int_{-\infty}^{\infty}[w(y)]^m\,dy\right)\,G_l(x;0)\,, \tag{5.4}$$

where $G_l(x;0)$ is the Green's function satisfying

$$DG_{lxx} - G_l = -\delta(x)\,,\quad -l<x<l\,;\quad G_{lx}(\pm l;0)=0\,. \tag{5.5}$$

A simple calculation gives

$$G_l(x;0) = \frac{\cosh\left[(l-|x|)D^{-1/2}\right]}{2\sqrt{D}\sinh\left(lD^{-1/2}\right)}\,. \tag{5.6}$$

Setting $x=0$ in (5.4), we obtain

$$[h(0)]^{\zeta} = \left[G_l(0;0)\int_{-\infty}^{\infty}[w(y)]^m\,dy\right]^{-1}\,. \tag{5.7}$$

We can then write $h(l)$ as $h(l) = h(0)G_l(l;0)/G_l(0;0)$. From (5.6) and (5.7), we then determine $h(l)$ in terms of some constant C as

$$h(l) = C\beta_{gm}\left(lD^{-1/2}\right)\,. \tag{5.8}$$

The function, $\beta_{gm}(z)$, for $z>0$, is given by

$$\beta_{gm}(z) \equiv \frac{(\tanh z)^{1/\zeta}}{\cosh z}\,,\quad \zeta \equiv \frac{qm}{p-1} - (s+1) > 0\,. \tag{5.9}$$

We will analyze (5.8) below.

Symmetric and asymmetric spike patterns also occur in the SC model (1.6). The existence and stability of symmetric patterns in the SC model was studied in [49]. In [107] asymmetric spike patterns were constructed.

To construct these patterns, we first must calculate a symmetric one-spike solution centered at the origin for

$$\varepsilon^2 u_{xx} - u + vu^2 = 0\,, \quad -l < x < l\,; \quad u_x(\pm l) = 0\,, \tag{5.10a}$$

$$Dv_{xx} + \frac{1}{2} - \frac{b}{\varepsilon} vu^2 = 0\,, \quad -l < x < l\,; \quad v_x(\pm l) = 0\,. \tag{5.10b}$$

The asymptotic solution to (5.10a) is

$$u(x) \sim \frac{1}{v(0)} w\left(x/\varepsilon\right)\,, \tag{5.11}$$

where $w(y) = \frac{3}{2}\mathrm{sech}^2(y/2)$. Since u is localized near $x = 0$, the term $\varepsilon^{-1} bvu^2$ in (5.10b) is a multiple of a Dirac mass. Thus, for $\varepsilon \ll 1$, $v(x)$ satisfies

$$Dv^{''} + \frac{1}{2} - \frac{6b}{v(0)}\delta(x) = 0\,, \quad -l < x < l\,; \quad v^{'}(\pm l) = 0\,. \tag{5.12}$$

By integrating (5.12) we get $v(0) = 6b/l$. The solution to (5.12) is

$$v(x) = lG_n(x;0)\,, \tag{5.13}$$

where $G_n(x;0)$ is the Neumann Green's function satisfying

$$DG_{nxx} + \frac{1}{2l} - \delta(x) = 0\,, \quad -l < x < l\,; \quad G_{nx}(\pm l;0) = 0\,, \tag{5.14}$$

with $G_n(0;0) = 6bl^{-2}$. A simple calculation gives

$$G_n(x;0) = -\frac{x^2}{4lD} + \frac{l}{2D} + \frac{6b}{l^2} - \frac{1}{2D}\left(l - |x|\right)\,, \quad -l \le x \le l\,. \tag{5.15}$$

In terms of this solution, we can calculate $v(l) = lG_n(l;0)$ explicitly as

$$v(l) = \frac{r^2}{4D}\left[\beta_{sc}\left(l/r\right)\right]^{-1}\,, \qquad r \equiv \left[24bD\right]^{1/3}\,, \tag{5.16}$$

where the function $\beta_{sc}(z)$ is defined by

$$\beta_{sc}(z) \equiv \frac{z}{z^3 + 1}\,. \tag{5.17}$$

We now analyze some properties of β_{gm} and β_{sc} in (5.9) and (5.17), respectively, and show how these properties lead to the existence of asymmetric spike patterns.

The function $\beta_{gm}(z) > 0$ in (5.9) has a unique global maximum point at $z = z_{gm}$, where

$$z_{gm} = \log\left(\sqrt{\zeta^{-1}} + \sqrt{\zeta^{-1} + 1}\right)\,. \tag{5.18}$$

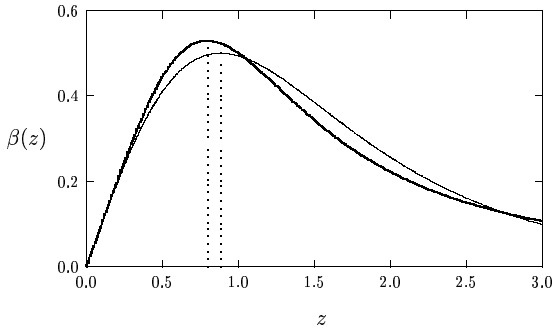

Figure 14. Plot of β_{gm} (heavy solid curve) versus z for the GM model with $\zeta = 1$. The solid curve is β_{sc} for the SC model. The maxima of β_{gm} and β_{sc} occur at z_{gm} and z_{sc} (dotted lines), respectively.

In addition, it satisfies $\beta_{gm}^{'}(z) > 0$ on $[0, z_{gm})$ and $\beta_{gm}^{'}(z) < 0$ on (z_{gm}, ∞). Therefore, given any $z \in (0, z_{gm})$, there exists a unique point $\tilde{z} = f_{gm}(z)$, with $\tilde{z} > z_{gm}$, such that $\beta_{gm}(z) = \beta_{gm}(\tilde{z})$.

Identical qualitative properties hold for the SC model. More specifically, the function $\beta_{sc}(z) > 0$ in (5.17) has a unique global maximum point at $z = z_{sc}$, where

$$z_{sc} = 2^{-1/3}\,. \tag{5.19}$$

In addition, $\beta_{sc}^{'}(z) > 0$ on $[0, z_{sc})$ and $\beta_{sc}^{'}(z) < 0$ on (z_{sc}, ∞). Therefore, given any $z \in (0, z_{sc})$, there exists a unique point $\tilde{z} = f_{sc}(z)$, with $\tilde{z} > z_{sc}$ such that $\beta_{sc}(z) = \beta_{sc}(\tilde{z})$. In Fig. 14 we plot β_{gm} and β_{sc}. One implication of these properties of β_{gm} and β_{sc} is the following:

Proposition 5.1. *Let $\xi > 0$ for the GM model. Given any l with $lD^{-1/2} < z_{gm}$, there exists a unique $\tilde{l}$, with $\tilde{l}D^{-1/2} \equiv \tilde{z} > z_{gm}$, such that $h(l) = h(\tilde{l})$. Similarly, for the SC model, given any l, with $l/r < z_{sc}$, there exists a unique $\tilde{l}$, with $\tilde{l}/r \equiv \tilde{z} > z_{sc}$, such that $v(l) = v(\tilde{l})$.*

We refer to solutions of length l and $\tilde{l}$ as S-type (small) and B-type (big) spikes, respectively. For both the GM and the SC models, we now show how to construct k-spike asymmetric equilibria on $-1 < x < 1$ with $k_1 > 0$ spikes of type S and $k_2 = k - k_1 > 0$ spikes of type B arranged in any particular order from left to right across the interval as

$$\text{SBSSB...B}\,, \qquad \text{with} \quad k_1 - \text{S's} \quad \text{and} \quad k_2 - \text{B's}\,. \tag{5.20}$$

For the GM model, we use translation invariance and the fact that $h(l) = h(\tilde{l})$ to glue S and B type spikes together to satisfy C^1 continuity for the inhibitor concentration h defined on $[-1, 1]$. A similar construction holds for the SC model. We use translation invariance and $v(l) = v(\tilde{l})$ to glue S and B type spikes together to satisfy a C^1 continuity for the global function v defined on $[-1, 1]$.

Since the support of an S-spike and a B-spike is $2l$ and $2\tilde{l}$, respectively, we get the length constraint $2k_1 l + 2k_2\tilde{l} = 2$. For the GM model, we have that $z = lD^{-1/2}$, $\tilde{z} = \tilde{l}D^{-1/2}$, and that $\beta_{gm}(z) = \beta_{gm}(\tilde{z})$. Therefore, for the GM model z and $\tilde{z}$ satisfy the coupled algebraic system

$$k_1 z + k_2\tilde{z} = D^{-1/2}\,, \quad \beta_{gm}(z) = \beta_{gm}(\tilde{z})\,. \tag{5.21}$$

Using the inverse function $\tilde{z} = f_{gm}(z)$ defined for $0 < z < z_{gm}$, we can reduce (5.21) to the study of the roots of the equation

$$f_{gm}(z) = \frac{D^{-1/2}}{k_2} - \frac{k_1 z}{k_2}\,, \tag{5.22a}$$

on $0 < z < z_{gm}$. In terms of the solution to (5.22a), l and $\tilde{l}$ are given by

$$l = zD^{1/2}\,, \quad \tilde{l} = f_{gm}(z)D^{1/2}\,. \tag{5.22b}$$

An identical construction can be done for the SC model. In place of (5.22), we obtain that

$$f_{sc}(z) = \frac{1}{rk_2} - \frac{k_1 z}{k_2}\,, \tag{5.23a}$$

on $0 < z < z_{sc}$, where l and $\tilde{l}$ are given by

$$l = zr\,, \quad \tilde{l} = f_{sc}(z)r\,. \tag{5.23b}$$

Here r is defined in (5.16)

Therefore, the problem of constructing asymmetric patterns for the GM and SC models has been reduced to the study of a single transcendental equation (5.22a) or (5.23a). To study these equations, we first use (5.9) and (5.17) to derive some key properties of the inverse functions $f_{gm}(z)$ and $f_{sc}(z)$. We summarize the result as follows:

Proposition 5.2. *For any $\zeta > 0$, $f_{gm}(z)$ is convex on $(0, z_{gm})$, $f'_{gm}(z) < -1$ on $(0, z_{gm})$, and $f'_{gm}(z_{gm}) = -1$. For the special case $\zeta = 1$, corresponding to the exponent set $(p, q, m, s) = (2, 1, 2, 0)$ for the GM model, we calculate explicitly that*

$$f_{gm}(z) \equiv \log\left[cschz + \coth z\right]\,, \qquad for \quad z \in [0, z_{gm})\,. \tag{5.24}$$

Similar properties hold for the SC model. In particular, $f_{sc}(z)$ is convex on $(0, z_{sc})$, $f_{sc}'(z) < -1$ on $(0, z_{sc})$, and $f_{sc}'(z_{sc}) = -1$. We calculate,

$$f_{sc}(z) = -\frac{z}{2} + \frac{\sqrt{z^2 + 4/z}}{2}\,. \tag{5.25}$$

We now determine conditions for which (5.22a) and (5.23a) have solutions on the interval $0 < z \le z_{gm}$ and $0 < z \le z_{sc}$, respectively. For the GM model, we must find the intersection points of $\tilde{z} = f_{gm}(z)$ with the straight line $\tilde{z} = -k_1 z/k_2 + k_2^{-1} D^{-1/2}$. A similar graphical analysis of (5.23a) holds for the SC model. The properties of $f_{gm}(z)$ and $f_{sc}(z)$ given in Proposition 5.2 show that there are two cases to consider:

$$\text{Case (i)} \quad k_1/k_2 \le 1\,; \qquad \text{Case (ii)} \quad k_1/k_2 > 1\,. \tag{5.26}$$

We readily obtain the first result for $k_1/k_2 \le 1$.

Proposition 5.3. *Let $k_1/k_2 \le 1$. Then, for the GM model, there exists a unique solution to (5.22a) on $z \in (0, z_{gm})$ when $D < D_{gm}(k)$, where*

$$D_{gm}(k) = \frac{1}{k^2 z_{gm}^2}\,, \qquad k = k_1 + k_2\,, \tag{5.27}$$

and z_{gm} satisfies (5.18). When $D = D_{gm}(k)$, then $z = \tilde{z} = z_{gm}$ and hence $l = \tilde{l} = 1/k$. In this case, we get a symmetric k-spike solution with spikes of equal height. A similar result holds for the SC model. When $k_1/k_2 \le 1$, there exists a unique solution to (5.23a) on $z \in (0, z_{sc})$ when $D < D_{sc}(k)$, where

$$D_{sc}(k) = \left[12bk^3\right]^{-1}\,, \qquad k = k_1 + k_2\,. \tag{5.28}$$

When $D = D_{sc}(k)$, we get $z = \tilde{z} = z_{sc}$ and $l = \tilde{l} = 1/k$, which yields a symmetric k-spike solution with spikes of equal height.

Since $f_{gm}'(z) < -1$ for $0 < z < z_{gm}$ and $f_{sc}'(z) < -1$ for $0 < z < z_{sc}$, with f_{gm} and f_{sc} convex, there can be solution multiplicity to (5.22a) and (5.23a) when $k_1/k_2 > 1$. In particular, as D is decreased from a large value, the straight line of slope $-k_1/k_2$ first intersects the curve $\tilde{z} = f_{gm}(z)$ at a point of tangency at the critical value $D = D_{gm}^*$. As D is decreased slightly below D_{gm}^*, there are exactly two roots to (5.22a) until D is decreased to the value $D_{gm}(k)$. For D below $D_{gm}(k)$ there is only one solution to (5.22a). For the GM model with $\zeta = 1$, this result is illustrated in Fig. 15. We summarize our result as follows:

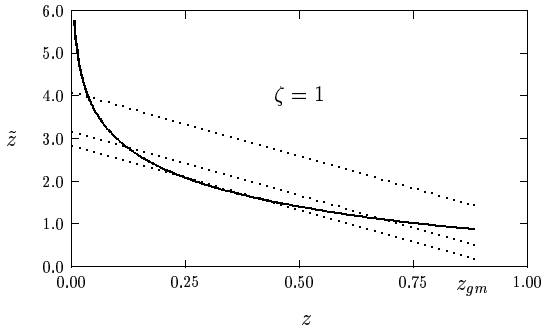

Figure 15. Plot of the graphical solution to (5.22a) when $\zeta = 1$, $k_1 = 3$, and $k_2 = 1$. Depending on D, $\tilde{z} = f_{gm}(z)$ (solid) will intersect the straight line in (5.22a) (dotted lines) at either zero, one, or two points. When $D = D^*_{gm}$ the straight line is tangent to $f_{gm}(z)$. When $D = D_{gm}(k)$ the straight line intersects $f_{gm}(z)$ at $z = z_{gm}$.

Proposition 5.4. *Consider the GM model with $k_1/k_2 > 1$. Then, there exists a critical value $D^*_{gm} > D_{gm}(k)$ such that the solution multiplicity for (5.22a) on $z \in (0, z_{gm})$ is as follows:*

$$\begin{aligned} &\textit{If } D > D^*_{gm} && \text{there are no solutions}, \\ &\textit{If } D_{gm}(k) < D < D^*_{gm} && \text{there are exactly two solutions}, \\ &\textit{If } D < D_{gm}(k) && \text{there is exactly one solution}. \end{aligned} \tag{5.29}$$

The critical value D^*_{gm} is the value of D where there is a double root to (5.22a). For a GM model with $\zeta = 1$, we calculate explicitly that

$$D^*_{gm} = \left[k_1 \sinh^{-1}\left(\frac{k_2}{k_1}\right) + k_2 \sinh^{-1}\left(\frac{k_1}{k_2}\right) \right]^{-2}, \quad \textit{for} \quad k_1/k_2 > 1\,. \tag{5.30}$$

An identical solution multiplicity result holds for the SC model except that z_{gm}, $D_{gm}(k)$, and D^*_{gm}, are to be replaced with z_{sc}, $D_{sc}(k)$, and D^*_{sc}, respectively, where

$$D^*_{sc} = \frac{1}{24b}\left[k_2 f_{sc}(z_*) + k_1 z_*\right]^{-3}. \tag{5.31a}$$

Here z_* is defined by

$$z_* = \left[\frac{2(1+\gamma^2) - 2\sqrt{(1+\gamma^2)^2 - (1-\gamma^2)}}{(1-\gamma^2)} \right]^{1/3}, \quad \gamma \equiv 1 - \frac{2k_1}{k_2}. \tag{5.31b}$$

In summary, consider a particular fixed ordering of k_1 spikes of type S and k_2 spikes of type B across the interval. For $k_1 \leq k_2$, and for the GM or the SC models, there is only one asymmetric spike pattern with the particular ordered sequence when D is below $D_{gm}(k)$. However, when there are more S (small) than B (big) spikes in the sequence, then for some range of D there are exactly two such patterns that have the same ordering. For the GM model we obtain the following result for asymmetric patterns (see Proposition 2.1 of [104]):

Proposition 5.5. *For the range of D in Proposition 5.4, let l and $\tilde{l}$ be determined from (5.22). Then, for $\varepsilon \to 0$, the activator concentration a for an asymmetric equilibrium k-spike pattern for (1.1) with k_1 spikes of type S and $k_2 = k - k_1$ spikes of type B is given by*

$$a(x) \sim \sum_{j=1}^{k} \left[h_{l_j}\right]^{q/(p-1)} w\left[\varepsilon^{-1}(x - x_j)\right] , \quad h_{l_j} \equiv \left(\frac{2\sqrt{D}\,\tanh\left(l_j D^{-1/2}\right)}{\int_{-\infty}^{\infty} [w(y)]^m \, dy} \right)^{1/\zeta} . \tag{5.32}$$

Here for each j, $l_j = l$ or $l_j = \tilde{l}$. The value $l_j = l$ must occur $k_1 > 0$ times, while $l_j = \tilde{l}$ must occur $k_2 = k - k_1 > 0$ times. The small and large spikes can be arranged in any sequence. The spike locations x_j are given by

$$x_1 = l_1 - 1 , \quad x_k = 1 - l_k , \quad x_{j+1} = x_j + l_{j+1} + l_j , \quad j = 1, \ldots, k-2 . \tag{5.33}$$

The symmetric k-spike solution occurs when $l_j = 1/k$ for $j = 1, \ldots, k$.

In Fig. 16 we illustrate this result for the GM model by plotting a 5-spike asymmetric pattern of the form SBBSB for a specific parameter set.

The result in Proposition 5.3 shows that asymmetric spike patterns bifurcate off of the symmetric patterns at the value $D = D_{gm}(k)$ for $k \geq 2$. To illustrate this result graphically, in Fig. 17 we plot a bifurcation diagram of an L_1 type- norm of a, defined by $|a|_1 \equiv \sum_{j=1}^{k} h_{l_j}^{\gamma}$, versus D for both symmetric and asymmetric k-spike patterns. The portions of the branches that are unstable to $O(1)$ instabilities are indicated by the dashed lines in this figure. Some stability results are given below.

A similar result follows for the construction of asymmetric spike patterns in the SC model (see Proposition 1 of [107]):

Proposition 5.6. *For the range of D in Proposition 5.4, let l and $\tilde{l}$ be determined from (5.23). Then, for $\varepsilon \to 0$, the u component for an asymmetric equilibrium k-spike pattern for (1.6) with k_1 spikes of type S and*

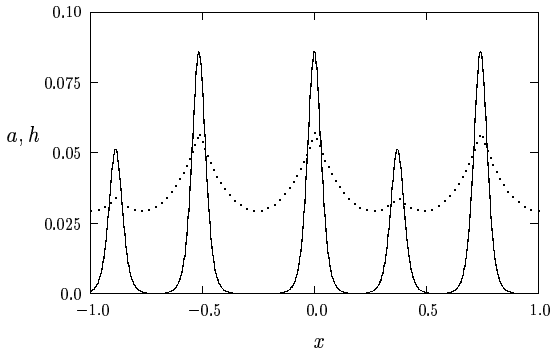

Figure 16. Plot of a (solid curve) and h (dotted curve) for a 5-spike asymmetric pattern of the type SBBSB for the GM model (1.1). The parameter values are $\varepsilon = .02$, $D = .04$, and $(p, q, m, s) = (2, 1, 2, 0)$.

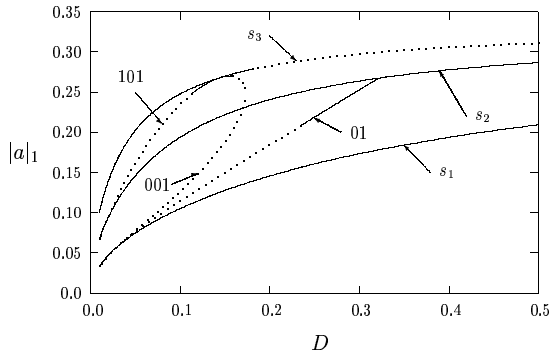

Figure 17. Plot of $|a|_1 \equiv \sum_{j=1}^{k} h_{l_j}^{\gamma}$ versus D for the GM model with $(p, q, m, s) = (2, 1, 2, 0)$ and for solutions with $k = 1, 2, 3$ spikes. The k-spike symmetric branch is s_k. The asymmetric patterns SB, BSB, and SSB are labeled by 01, 101, and 001, respectively. The dashed portions of these branches are unstable with on an $O(1)$ time-scale.

$k_2 = k - k_1$ spikes of type B is given by

$$u(x) \sim \sum_{j=1}^{k} v_j^{-1} w\left[\varepsilon^{-1}(x - x_j)\right], \quad v_j = \frac{6b}{l_j}. \tag{5.34}$$

Here l_j and x_j for $j = 1, \ldots, k$ are given in Proposition 5.5. The symmetric k-spike solution is found by setting $l_j = 1/k$ for $j = 1, \ldots, k$ in (5.34).

5.1. *Gray-Scott Model (Low Feed-Rate): Equilibrium*

The asymptotic construction of symmetric and asymmetric k-spike equilibria to the GS model in the low feed-rate regime (1.5) has many similarities with that for the GM model, except that now the equilibria can exhibit a saddle-node bifurcation structure.

We follow [56] by first constructing symmetric k-spike equilibria to (1.5) for $\varepsilon \ll 1$. The spike locations x_j, for $j = 1, \ldots, k$, for such a pattern satisfy

$$x_j = -1 + \frac{(2j-1)}{k}\,, \qquad j = 1, \ldots, k\,. \tag{5.35}$$

Since the spikes have equal height, then $u(x_j) = U$, for some constant U.

In the inner region near the j^{th} spike, we let $y = \varepsilon^{-1}(x - x_j)$. In each inner region, we get that $u \sim U + O(\varepsilon)$. Therefore, from (1.5a), the leading-order inner solution for ν is $\nu \sim [\tilde{A}U]^{-1} w(y)$, where $w(y)$ is given in (1.8) with $p = 2$.

Approximating the term $\varepsilon^{-1} u\nu^2$ in (1.5b) as a multiple of a Dirac mass, and using $\int_{-\infty}^{\infty} w^2 dy = 6$, we get that the outer solution for u satisfies

$$Du_{xx} + (1-u) - \frac{6}{\tilde{A}^2 U} \sum_{j=1}^{k} \delta(x - x_j) = 0\,, \quad u_x(\pm 1) = 0\,. \tag{5.36}$$

The solution to (5.36) is

$$u(x) = 1 - \frac{6}{\tilde{A}^2 U} \sum_{j=1}^{k} G(x; x_j)\,, \tag{5.37}$$

where $G(x; x_j)$ is the Green's function, satisfying

$$DG_{xx} - G = -\delta(x - x_j)\,, \qquad -1 < x < 1\,; \qquad G_x(\pm 1; x_j) = 0\,. \tag{5.38}$$

We define $a_g \equiv \sum_{i=1}^{k} G(x_j; x_i)$, where the x_j satisfy (5.35). By solving (5.38) explicitly, the find that a_g is independent of j and is given by

$$a_g \equiv \sum_{i=1}^{k} G(x_j; x_i) = \left[2\sqrt{D} \tanh\left(\theta_0/k\right) \right]^{-1}\,. \tag{5.39}$$

Setting $u(x_j) = U$ in (5.37), we obtain a quadratic equation for U

$$U(U-1) = -\frac{6a_g}{\tilde{A}^2}\,. \tag{5.40}$$

By solving this equation, the following result was derived in [56]:

Proposition 5.7. *Let $\varepsilon \to 0$, with $\tilde{A} = O(1)$ and $D = O(1)$ in (1.5). Then, when $\tilde{A} > \tilde{A}_{ke}$, there are two symmetric k-spike equilibrium solutions to (1.5) given asymptotically by*

$$\nu_{\pm}(x) \sim \frac{1}{\tilde{A}U_{\pm}} \sum_{j=1}^{k} w\left[\varepsilon^{-1}(x - x_j)\right] , \tag{5.41}$$

where $w(y) = \frac{3}{2}sech^2(y/2)$. We label ν_+ and ν_- as the large and small solution, respectively. Here $U_{\pm}$, and the saddle-node bifurcation value $\tilde{A}_{ke} = \sqrt{24a_g}$ are given by

$$U_{\pm} \equiv \frac{1}{2}\left[1 \pm \sqrt{1 - \frac{\tilde{A}_{ke}^2}{\tilde{A}^2}}\right] , \quad \tilde{A}_{ke} \equiv \sqrt{\frac{12\theta_0}{\tanh\left(\theta_0/k\right)}} , \qquad \theta_0 \equiv D^{-1/2} . \tag{5.42}$$

We now construct asymmetric k-spike equilibria, where the spikes can have different heights. The analysis, given in Sec. 2.1 of [56], is very similar to that for the GM and SC models given above. The idea is to construct a symmetric one-spike equilibrium to (1.5) centered at $x = 0$ on a domain $-l < x < l$ with $u_x(\pm l) = 0$. The goal is to find all different values of l, labeled by $l_1, \ldots, l_n$, such that $u(l_1) = , \ldots, = u(l_n)$. Once again we find that there are only two types of spikes S and B.

A straightforward calculation shows that $u(l)$ is given by

$$u(l) = E_{\pm}(z) \equiv 1 + \frac{1}{2}\mathrm{sech}(z)\left[-1 \pm \sqrt{1 - \frac{\coth(z)}{\tilde{A}_0^2}}\right] , \quad \text{for } z > z_0 , \tag{5.43a}$$

where

$$z \equiv \theta_0 l , \quad \theta_0 \equiv D^{-1/2} , \quad z_0 \equiv \frac{1}{2}\log\left[\frac{\tilde{A}_0^2 + 1}{\tilde{A}_0^2 - 1}\right] , \quad \tilde{A} \equiv \sqrt{12\theta_0}\tilde{A}_0 . \tag{5.43b}$$

Clearly $E_{\pm}(z) > 0$ for $z > z_0$. For $z > z_0$, it is easy to see that $E_+(z)$ is monotonically increasing. Therefore, asymmetric patterns cannot be obtained with $E_+(z)$.

A simple calculation as given in Proposition 2.2 of [56] shows that $E_-(z_0) < 1$ with $E_-'(z) < 0$ for $z_0 < z < z_{gs}$, and $E_-'(z) > 0$ for $z > z_{gs}$. Moreover, $E_-(z) \to 1$ as $z \to \infty$. The point z_{gs} where $E_-(z)$ has its minimum value is the unique root of

$$\tilde{A}_0 = [\tanh z]^{-1/2}[\tanh(2z)]^{-1} . \tag{5.44}$$

In Fig. 18 we plot E_- versus z for $z \geq z_0$ when $\tilde{A}_0 = 3$.

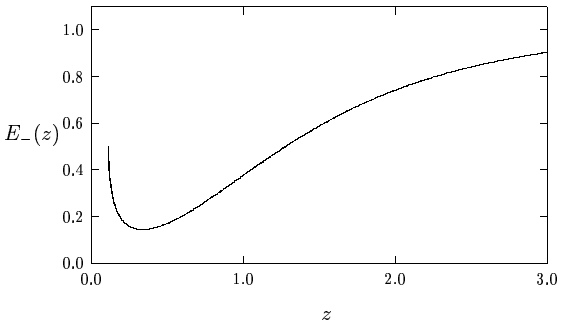

Figure 18. Plot of E_- versus z for $z \geq z_0$ when $\tilde{A}_0 = 3$.

Therefore, when $\tilde{A}_0 > 1$, we conclude that for any z in $z_0 < z < z_{gs}$, there exists a unique $\tilde{z} = f_{gs}(z)$, with $\tilde{z} > z_{gs}$, such that $E_-(z) = E_-(\tilde{z})$. Since $z = \theta_0 l$ and $\tilde{z} = \theta_0 \tilde{l}$, the implication of this result is that for any l with $z_0 < l\theta_0 < z_{gs}$, there exists a unique $\tilde{l}$, with $\tilde{l}\theta_0 > z_{gs}$, such that $u(l) = u(\tilde{l})$. This implies that in any asymmetric pattern of this form using $E_-(z)$ there are again only two types of spikes S and B. Therefore, in place of (5.23), we obtain that

$$f_{gs}(z) = \frac{\theta_0}{k_2} - \frac{k_1 z}{k_2}\,, \tag{5.45a}$$

on $z_0 < z < z_{gs}$. In terms of the solution to (5.45a), we get

$$l = z\theta_0^{-1}\,, \quad \tilde{l} = f_{gs}(z)\theta_0^{-1}\,. \tag{5.45b}$$

To recover the symmetric k-spike equilibrium solutions, we set $z = f_{gs}(z) = \theta_0/k$. This has a solution only when $z = z_{gs}$. Therefore, setting $z = \theta_0/k$ in (5.44), we we obtain the critical value of $\tilde{A}_0$ for the emergence of the asymmetric branch. This leads to the following bifurcation result:

Proposition 5.8. *Let l and $\tilde{l}$ be found from (5.45) for a given $\tilde{A} > \sqrt{12\theta_0}$ and $\theta_0 = D^{-1/2}$. Then, for $\varepsilon \to 0$, the ν component of an asymmetric equilibrium k-spike pattern for (1.5) with k_1 spikes of type S and $k_2 = k - k_1$*

spikes of type B is given by

$$\nu_-(x) \sim \sum_{j=1}^{k} \frac{1}{\tilde{A}U(l_j)} w\left[\frac{(x-x_j)}{\varepsilon}\right], \quad U(l_j) \equiv \frac{1}{2}\left(1-\sqrt{1-\frac{12\theta_0\coth(\theta_0 l_j)}{\tilde{A}^2}}\right). \tag{5.46}$$

Here for each j, $l_j = l$ or $l_j = \tilde{l}$. The value $l_j = l$ must occur $k_1 > 0$ times, while $l_j = \tilde{l}$ must occur $k_2 = k - k_1 > 0$ times. The spike locations x_j are given by (5.33). Finally, the asymmetric k-spike equilibrium solutions bifurcate from the k-spike symmetric small equilibrium solution branch of Proposition 5.7 at the value $\tilde{A} = \tilde{A}_{ka}$, where

$$\tilde{A}_{ka} \equiv \tilde{A}_{ke}\left[\tanh\left(\frac{2\theta_0}{k}\right)\right]^{-1}. \tag{5.47}$$

Here $\tilde{A}_{ke}$ is the saddle-node bifurcation value given in (5.42).

To display our results graphically in a bifurcation diagram it is convenient to define a norm of ν by $|\nu|_2 \equiv \left(\varepsilon^{-1}\int_{-1}^{1}\nu^2\,dx\right)^{1/2}$. For symmetric and asymmetric spike patterns, a simple calculation using (5.46) shows that

$$|\nu|_2 \sim \frac{\sqrt{6k}}{\tilde{A}U_\pm} \ \text{(symm)}, \quad |\nu|_2 \sim \frac{1}{\tilde{A}}\left(\frac{6k_1}{[U(l)]^2}+\frac{6k_2}{\left[U(\tilde{l})\right]^2}\right) \ \text{(asymm)}. \tag{5.48}$$

In Fig. 19 we plot the symmetric and asymmetric solution branches for $k = 1, \ldots, 4$ when $D = 0.75$. It is easy to see that an asymmetric branch with k_1 small spikes asymptotes to the symmetric branch with $k - k_1$ spikes as $\tilde{A} \to \infty$. There are several questions suggested by these calculations.

Question 5.1. What general properties of a reaction-diffusion system will, necessarily, lead to asymmetric patterns involving ony two types of spikes in the semi-strong spike interaction regime?

Question 5.2. Can one find singularly perturbed reaction-diffusion systems having similar asymmetric patterns, but that now involve three or more types of spikes?

5.2. *Gray-Scott Model (High Feed-Rate): Equilibrium*

We now construct k-spike symmetric spike patterns for the GS model in the high feed-rate regime (1.3). In this regime, where $A = O(1)$, the scalings

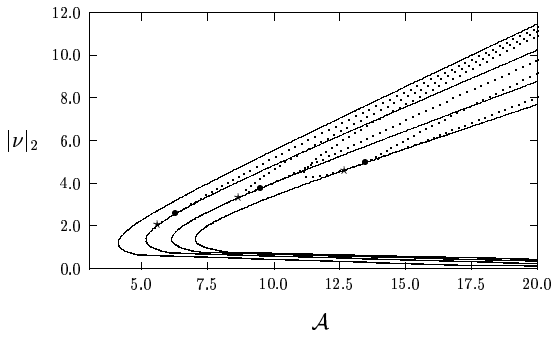

Figure 19. Bifurcation diagram of symmetric (solid curves) and asymmetric (dotted curves) spike patterns in the low feed-rate regime $A = \tilde{A}\varepsilon^{1/2}$ for $D = 0.75$ and $k = 1, 2, 3, 4$. The saddle-node values $\tilde{A}_{ke}$ increase with k.

for equilibria are $v = O(\varepsilon^{-1})$ and $u = O(\varepsilon)$ (cf. [57]). Although we will only give results for spike patterns on the interval $[-1, 1]$, other essentially one-dimensional patterns can be constructed. Specifically, in [72] and [58], the existence and stability of radially symmetric solutions, known as ring solutions, was investigated.

In [57] it was shown that k-spike equilibria can be constructed in terms of the solutions $V(y) > 0$ and $U(y) > 0$ to a *core problem* defined by

$$V'' - V + V^2 U = 0\,, \qquad U'' = UV^2\,, \qquad 0 < y < \infty\,, \tag{5.49a}$$

$$V'(0) = U'(0) = 0\,; \quad V \to 0\,, \quad U \sim By\,, \quad \text{as} \quad y \to \infty\,, \tag{5.49b}$$

where B is related to A by

$$B \equiv A \tanh\left(\theta_0/k\right)\,, \quad \theta_0 = D^{-1/2}\,. \tag{5.49c}$$

The precise result, as given in Proposition 3.1 of [57], is as follows:

Proposition 5.9. *Let $\varepsilon \to 0$, $A = O(1)$, $\varepsilon A/\sqrt{D} \ll 1$, and suppose that (5.49) has a solution. Then, the v-component for a k-spike equilibrium solution to (1.3) is given by*

$$v \sim \frac{\sqrt{D}}{\varepsilon} \sum_{j=1}^{k} \left(V\left[\varepsilon^{-1}(x - x_j)\right] + O\left(\frac{\varepsilon A}{\sqrt{D}}\right)\right)\,. \tag{5.50}$$

In the j^{th} inner region, defined by $|x - x_j| = O(\varepsilon)$, we also have that $u \sim \frac{\varepsilon}{A\sqrt{D}} U\left[\varepsilon^{-1}(x - x_j)\right]$.

The core problem (5.49) was studied qualitatively and numerically in [57] in terms of B. We first determine some analytical properties of (5.49). By integrating (5.49a) from $0 < y < \infty$, and using (5.49b), we get

$$\int_0^\infty V^2 U \, dy = \int_0^\infty V \, dy = B \, . \tag{5.51}$$

To determine a good parameterization of the solution branch for (5.49), we define $U_0 \equiv U(0)$ and $V_0 \equiv V(0)$. Then, we can readily derive that

$$\frac{V_0^2}{2} + \int_0^\infty \frac{U}{3} \left[V^3\right]' \, dy = \frac{V_0^2}{2} - \frac{U_0 V_0^3}{3} - \int_0^\infty \frac{1}{3} V^3 U' \, dy = 0 \, . \tag{5.52}$$

This gives,

$$\int_0^\infty V^3 U' \, dy = V_0^2 \left[\frac{3}{2} - U_0 V_0\right] \, . \tag{5.53}$$

Since $U' > 0$ on $0 < y < \infty$, we get the key inequality that

$$0 < \gamma < \frac{3}{2} \, , \qquad \gamma \equiv U_0 V_0 \, . \tag{5.54}$$

In [57] numerical solutions to (5.49) were computed for which V has a single maximum at $y = 0$ as $\gamma \to 3/2$ from below. By using Euler continuation a resulting curve $B = B(\gamma)$ was computed. This limiting solution for V asymptotically matches onto the solution constructed in the low feed-rate regime in Sec. 5.1. It was found in [57] that the curve $B = B(\gamma)$ is double-valued with $B \to 0$ as $\gamma \to 0$ and as $\gamma \to 3/2$, and it has a saddle-node bifurcation point at the maximum value B_c of B given by $B_c = 1.347$, where $\gamma = \gamma_c = 1.02$. This critical value of B was also computed in [74]. We refer to the range $\gamma_c < \gamma < 3/2$ and $0 < \gamma < \gamma_c$ as the *primary* and *secondary* branches of the $B = B(\gamma)$ bifurcation diagram. Using (5.49c), these results show that equilibrium k-spike solutions in the high feed-rate regime exist only when A is small enough. The equilibrium result, derived in Proposition 3.2 of [57], is summarized as follows:

Proposition 5.10. *Let $\varepsilon \ll 1$, $A = O(1)$, and $\varepsilon A/\sqrt{D} \ll 1$. Then, there will be no k-spike equilibrium solution to (1.3) that merges onto the low feed-rate regime solution when*

$$A > A_{pk} \equiv 1.347 \coth\left(\frac{1}{k\sqrt{D}}\right) \, . \tag{5.55}$$

In Fig. 20 we plot the norm $|v|_2$, defined by $|v|_2^2 \equiv \int_{-1}^{1} v^2\,dx$ versus A when $D = 0.1$. This norm can be evaluated asymptotically using (5.50) as

$$|v|_2^2 \sim \varepsilon^{-1} k D \int_{-\infty}^{\infty} V^2\,dy\,. \tag{5.56}$$

Notice that the saddle-node bifurcation values A_{pk} occur at approximately the same value when $D \ll 1$, since for k fixed we have that $\tanh\left(1/k\sqrt{D}\right) \approx 1$ for $D \ll 1$. This is called the *lining-up property* of saddle-node equilibria.

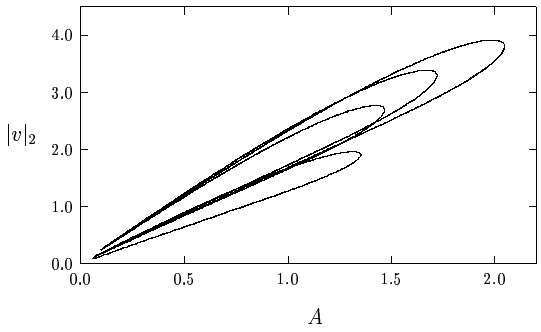

Figure 20. Bifurcation diagram of $|v|_2$ versus A when $A = O(1)$ for k-spike solutions to the GS model in the high feed-rate regime with $\varepsilon = 0.02$, $D = 0.1$, and $k = 1, \ldots, 4$. The saddle-node values A_{pk} increase with k.

In [57] the limiting behavior of (5.49) was studied asymptotically for $\gamma \to 3/2$ from below and for $\gamma \to 0$ from above. The main result of this analysis is that on the secondary branch of the $B = B(\gamma)$ bifurcation diagram a one-spike solution to (5.49) splits into a two-spike solution where the spikes are separated by $O(-\log B)$ as $B \to 0$. This multi-bump behavior is closely related to a phenomenon known as pulse-splitting, as described in [32], [82], [83], [81], [98], and [57].

For $\gamma \to 3/2$ from below, the following result obtained in Proposition 4.1 of [57] shows that the solution matches onto the low feed-rate regime solution:

Proposition 5.11. *Along the primary branch, the core problem (5.49) has a solution where $\gamma \to 3/2$ from below as $\delta \to 0$, where $\delta = 1/U(0) \ll 1$. This solution has the form*

$$V \sim \delta w(y) + O(\delta^2)\,, \quad U \sim \delta^{-1} + O(\delta)\,, \tag{5.57a}$$

where $w(y)$ satisfies (1.8) with $p = 2$. We have that $B \sim 3\delta$, and that

$$\gamma \equiv U_0 V_0 \sim \frac{3}{2} - \frac{11B^2}{48}, \quad \text{as} \quad B \to 0. \tag{5.57b}$$

Alternatively, as $\gamma \to 0$ from above, the solution V has two bumps. This behavior, as derived in Proposition 4.2 of [57] is characterized as follows:

Proposition 5.12. *Let $\delta = 1/U_0 \ll 1$. Then, along the secondary branch, the core problem (5.49) has a solution where $\gamma \equiv U_0 V_0 \to 0$ from above as $\delta \to 0$. This solution has the form*

$$V \sim \delta \left[w(y - y_1) + w(y + y_1) \right], \quad U \sim \frac{1}{\delta} + O(\delta), \tag{5.58a}$$

where $w(y)$ satisfies (1.8) when $p = 2$. We have that $B \sim 6\delta$ as $\delta \to 0$, and

$$\gamma \equiv U_0 V_0 \sim \sqrt{2} B / \sqrt{5}, \quad y_1 \sim -\log B + O(1), \quad \text{as } B \to 0. \tag{5.58b}$$

The existence of multi-bump solutions to the core problem along the secondary branch is closely related to a similar multi-bump phenomena for the modified version (2.45) of Carrier's problem, as discussed in Sec. 2.4.

Question 5.3. Can one determine rigorous properties of multi-bump solutions to the core problem and of the $B = B(\gamma)$ bifurcation curve? In particular, can we prove the existence of a saddle-node bifurcation and determine analytical bounds for the saddle-node value?

5.3. *Stability of Multi-Spike Equilibria: One Dimension*

In this subsection we give some results for the stability of symmetric k-spike patterns for the GS model (1.5) in the low feed-rate regime and the GM model (1.1). For each of these models, there are two types of eigenvalues in the spectrum of the linearization. There are eigenvalues that are $O(1)$ as $\varepsilon \to 0$, referred to as the *large* eigenvalues, and eigenvalues of order $O(\varepsilon^2)$, referred to as the *small* eigenvalues. The large eigenvalues are associated with the initiation of profile instabilities, whereby the spike amplitudes will either oscillate, typically with a common frequency and phase, or else undergo a competition instability leading to the monotonic annihilation of spikes in a spike sequence. Alternatively, the small eigenvalues of order

$O(\varepsilon^2)$, determine the stability with respect to translations of the spike profile, and are associated with the bifurcation of asymmetric branches of spike equilibria off of the symmetric branches.

We first consider the stability of symmetric k-spike patterns for the GS model (1.5) with respect to the large eigenvalues. To analyze the stability of these solutions we let $u(x,t) = u_\pm(x) + e^{\lambda t}\eta(x)$, and $\nu(x,t) = \nu_\pm(x) + e^{\lambda t}\phi(x)$, where $\nu_\pm$ and $u_\pm$ are defined in Proposition 5.8 with $l_j = 1/k$. Here ϕ is a localized eigenfunction of the form

$$\phi(x) \sim \sum_{j=1}^{k} c_j \Phi\left[\varepsilon^{-1}(x - x_j)\right] , \tag{5.59}$$

for some coefficients c_j to be found, and $\int_{-\infty}^{\infty} w(y)\Phi(y)\,dy \neq 0$. A lengthy derivation leading to Proposition 3.2 of [56], yields the following spectral problem for $\Phi(y)$:

Proposition 5.13. *Let $0 < \varepsilon \ll 1$. Then, with $\Phi = \Phi(y)$, the $O(1)$ eigenvalues determining the stability of k-spike symmetric equilibria in the GS model (1.5) satisfy the nonlocal eigenvalue problem*

$$L_0\Phi - \chi_{gs} w^2 \left(\frac{\int_{-\infty}^{\infty} w\Phi\,dy}{\int_{-\infty}^{\infty} w\,dy} \right) = \lambda\Phi\,, \quad -\infty < y < \infty\,; \quad \Phi \to 0\,, \quad \text{as } |y| \to \infty\,. \tag{5.60}$$

Here $w(y)$ is the homoclinic solution (1.8) with $p = 2$, and L_0 is the local operator $L_0\Phi \equiv \Phi'' - \Phi + 2w\Phi$. The multiplier $\chi_{gs} = \chi_{gs}(z;j)$ is defined by

$$\chi_{gs} \equiv 2s_g \left(s_g + \frac{\sqrt{1+z}}{\tanh(\theta_0/k)} \left[\tanh(\theta_\lambda/k) + \frac{(1 - \cos[\pi(j-1)/k])}{\sinh(2\theta_\lambda/k)} \right] \right)^{-1} , \tag{5.61}$$

where $z \equiv \tau\lambda$, $\theta_\lambda \equiv \theta_0\sqrt{1+z}$, and $\theta_0 \equiv D^{-1/2}$. Here s_g is defined in terms of $U_\pm$, given in (5.42), by

$$s_g = \frac{1 - U_\pm}{U_\pm}\,, \quad 0 < s_g < \infty\,. \tag{5.62}$$

The coefficients $\boldsymbol{c}^t = (c_1, \ldots, c_k)$ in (5.59) are given by

$$\boldsymbol{c}_1^t = \frac{1}{\sqrt{k}}(1, \ldots, 1)\,; \quad c_{l,j} = \sqrt{\frac{2}{k}} \cos\left(\frac{\pi(j-1)}{k}(l - 1/2) \right) , \quad j = 2, \ldots, k\,. \tag{5.63}$$

The method for deriving (5.60) is similar to the approach used in [80] for studying the stability of pulses in the Fitzhugh-Nagumo model. Notice that the small solution ν_- corresponds to the range $1 < s_g < \infty$, while the large solution corresponds to $0 < s_g < 1$. The saddle-node bifurcation value $\tilde{A}_{ke}$ corresponds to $s_g = 1$. Using (5.42), we can write $\tilde{A}$ as

$$\frac{\tilde{A}}{\tilde{A}_{ke}} = \frac{(1+s_g)}{2\sqrt{s_g}}\,. \tag{5.64}$$

As in the derivation (3.16)–(3.18), there is an equivalent formulation of (5.60) which states that the eigenvalues of (5.60) with $\int_{-\infty}^{\infty} w\Phi\,dy \neq 0$ are the union of the zeros of the functions $g_j(\lambda) = 0$ for $j = 1, .., k$, where

$$g_j(\lambda) \equiv C_j(\lambda) - f(\lambda)\,, \quad f(\lambda) \equiv \frac{\int_{-\infty}^{\infty} w\,(L_0-\lambda)^{-1}\,w^2\,dy}{\int_{-\infty}^{\infty} w^2\,dy}\,, \quad C_j(\lambda) \equiv \frac{1}{\chi_{gs}}\,. \tag{5.65}$$

Notice that this reformulation is very similar to (3.18). By analyzing the zeroes of $g_j(\lambda)$ in the right half-plane $\mathrm{Re}(\lambda) \geq 0$ in a similar way as in Sec. 3, the main stability result for multi-spike solutions is as follows (cf. Proposition 3.10 and 3.13 of [56]:

Proposition 5.14. *The large solution u_+, ν_+ is unstable for any $0 < s_g < 1$, $k \geq 1$, and $D > 0$. Next, let $k \geq 1$, and consider the k-spike small solution u_-, ν_-, where $s_g > 1$. For $\tilde{A} > \tilde{A}_{kL}$, the solution is stable on an $O(1)$ time-scale when $0 < \tau < \tau_{hL}$. Alternatively, for $\tilde{A}_{ke} < \tilde{A} < \tilde{A}_{kL}$, the small solution is unstable for any $\tau > 0$. The threshold $\tilde{A}_{kL}$ is given analytically by*

$$\tilde{A}_{kL} = \frac{\tilde{A}_{ke}\left((\gamma_k/2) + 2\sinh^2(\theta_0/k)\right)}{\left(\left[(\gamma_k/2) + 2\sinh^2(\theta_0/k)\right]^2 - (\gamma_k/2)^2\right)^{1/2}}\,, \quad \gamma_k \equiv 1 + \cos\left(\frac{\pi}{k}\right)\,. \tag{5.66}$$

Notice that $\tilde{A}_{kL} = \tilde{A}_{ke}$ when $k = 1$.

Let $\tilde{A}$ satisfy $\tilde{A} > \tilde{A}_{kL}$. Then, as τ increases beyond τ_{hL}, a Hopf bifurcation in the spike amplitudes was computed numerically in [56]. The threshold τ_{hL} is given by the *minimum value* of the set τ_j, $j = 1, .., k$, for which $g_j(\lambda) = 0$, $j = 1, .., k$, has complex conjugate roots on the imaginary axis. Let $\lambda = \pm i\lambda_h$ be the corresponding value of λ. Then, as was shown in [56], the unstable eigenfunction generically has the form of a *synchronous*

oscillatory instability with

$$\nu = \nu_- + \delta e^{i\lambda_h t}\phi + \text{c.c}\,, \quad \phi(x) = \sum_{n=1}^{k} \Phi\left[\varepsilon^{-1}(x - x_n)\right]\,, . \tag{5.67}$$

Here c.c denotes complex conjugate and $\delta << 1$. In other words, the instability threshold is set by the $j = 1$ mode in (5.61), for which $c_n = 1$ for $n = 1, \ldots, k$. This type of instability is illustrated in Fig. 21.

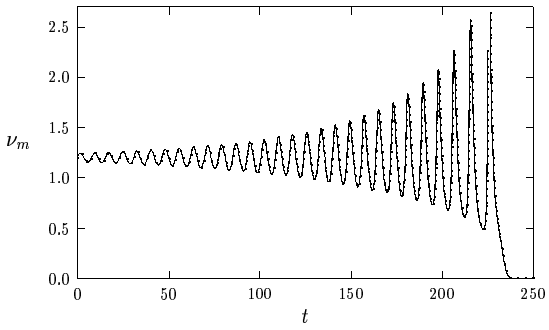

Figure 21. Synchronous Oscillatory Instability: Plot of the spike amplitudes for $k = 3$, $D = 0.75$, $\tilde{A} = 8.86$, $\tau = 7.6$ and $\varepsilon = 0.01$. The amplitudes of the spikes trace out identical trajectories after a short initial transient.

Alternatively, suppose that $\tilde{A}_{ke} < \tilde{A} < \tilde{A}_{kL}$. Then, for any $\tau > 0$, the dominant initial instability was shown in [56] to correspond to the $j = k$ mode in (5.61). This instability has the form

$$v = v_- + \delta e^{\lambda_{Rk} t}\phi\,, \quad \phi(x) = \sum_{n=1}^{k} c_n \Phi\left[\varepsilon^{-1}(x - x_n)\right]\,, \tag{5.68a}$$

where

$$c_n = \cos\left(\frac{\pi(k-1)}{k}\,(n - 1/2)\right)\,, \quad n = 1, .., k\,. \tag{5.68b}$$

Here $\delta \ll 1$, and $\lambda_{Rk} > 0$ is the unique root of $g_k(\lambda_R) = 0$. Since $\sum_{n=1}^{k} c_n = 0$, this instability locally conserves the sum of the heights of the spikes. Hence, it is referred to as a *competition instability.* The numerical experiments in Sec. 3.3 of [56] show that this instability leads to a spike competition process whereby certain spikes in a spike sequence are ultimately annihilated. This type of instability is illustrated in Fig. 22.

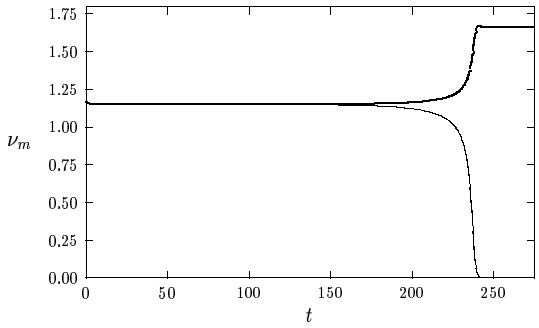

Figure 22. Competition Instability: Plot of th spike amplitudes $\nu_m \equiv \nu(x_j, t)$ versus t for $k = 3$, $D = 0.75$, $\tilde{A} = 8.6$, $\varepsilon = 0.01$, and $\tau = 2.0$. The middle spike is annihilated, and the other two spikes have a common amplitude.

An interesting limiting case of (5.60) is to take the limit where $\tilde{A} \gg 1$, but $\tilde{A} \ll O(\varepsilon^{-1/2})$. This represents the intermediate limit between the GS model in the low feed-rate regime (1.5) and the high feed-rate regime (1.3). This intermediate regime was first studied in the pioneering works of [25]–[27], and [29]. In this intermediate regime there are no longer any competition instabilities, and there is a scaling law for the Hopf bifurcation. The main result as given in [56] is as follows:

Proposition 5.15. *Let $\varepsilon \ll 1$, $D = O(1)$, and $O(1) \ll \tilde{A} \ll O(\varepsilon^{-1/2})$. Then, the k-spike equilibrium small solution u_-, ν_-, is stable with respect to the large eigenvalues when $\tau < \tau_H$, where*

$$\tau_H \sim \frac{\tilde{A}^4 D}{9} \tanh^4(\theta_0/k)\, \tau_{0h} \left(1 - \frac{6\theta_0}{\tilde{A}^2 \tanh(\theta_0/k)}\right)^2 + o(1)\,. \qquad (5.69)$$

Here $\tau_{0h} = 1.748$ is the minimum value of τ_0 for which the nonlocal eigenvalue problem

$$\Phi'' - \Phi + 2w\Phi - \frac{2w^2}{1+\sqrt{\tau_0 \lambda}} \left(\frac{\int_{-\infty}^{\infty} w\Phi\, dy}{\int_{-\infty}^{\infty} w\, dy}\right) = \lambda\Phi\,, \quad -\infty < y < \infty\,, \qquad (5.70)$$

with $\Phi \to 0$ as $|y| \to \infty$, has a pair of pure imaginary eigenvalues.

This limiting eigenvalue problem was studied [25], [26], and [73]. As for the small eigenvalues, the following result was obtained in Proposition 4.4 of [56]:

Proposition 5.16. *Let $\varepsilon \ll 1$, and $\tau = O(1)$. For $k = 1$, the small solution u_- and ν_- is always stable with respect to the small eigenvalue. For $k > 1$, and for the small solution u_-, ν_-, one small eigenvalue satisfies $\lambda_k < 0$, and so is stable. The other small eigenvalues λ_j, for $j = 1, \ldots, k-1$ are negative at a fixed value of D if and only if $\tilde{A}$ satisfies*

$$\tilde{A} > \tilde{A}_{kS}\,, \quad \tilde{A}_{kS} \equiv \tilde{A}_{ke}\left[\tanh\left(\frac{2\theta_0}{k}\right)\right]^{-1}. \tag{5.71}$$

Here $\tilde{A}_{ke}$ are the existence thresholds of (5.42).

By comparing (5.71) with (5.47) of Proposition 5.8 it follows that $k-1$ branches of asymmetric equilibria bifurcate from the symmetric k-spike branch when $k-1$ small eigenvalues simultaneously cross through zero.

Competition and synchronous oscillatory instabilities also occur for the GM model (cf. [105]). By linearizing around a symmetric k-spike pattern, the following nonlocal eigenvalue problem was found to determine the stability of the solution on an $O(1)$ time-scale (see Proposition 2.3 of [105]):

Proposition 5.17. *Let $0 < \varepsilon \ll 1$. Then, the $O(1)$ eigenvalues determining the stability of k-spike symmetric equilibria in the GM model (1.1) satisfy the nonlocal eigenvalue problem*

$$L_0\Phi - \chi_{gm} w^p \left(\frac{\int_{-\infty}^{\infty} w^{m-1}\Phi\, dy}{\int_{-\infty}^{\infty} w^m\, dy}\right) = \lambda\Phi\,, \quad -\infty < y < \infty\,, \tag{5.72}$$

with $\Phi \to 0$ as $|y| \to \infty$. Here $w(y)$ is the homoclinic solution in (1.8), and L_0 is the local operator $L_0\Phi \equiv \Phi'' - \Phi + pw^{p-1}\Phi$. The multiplier χ_{gm} is

$$\chi_{gm} = qm\left(s + \frac{\sqrt{1+z}}{\tanh(\theta_0/k)}\left[\tanh(\theta_\lambda/k) + \frac{(1-\cos[\pi(j-1)/k])}{\sinh(2\theta_\lambda/k)}\right]\right)^{-1}, \tag{5.73}$$

where $z \equiv \tau\lambda$, $\theta_\lambda \equiv \theta_0\sqrt{1+z}$, and $\theta_0 \equiv D^{-1/2}$.

By comparing the eigenvalue problems in Propositions 5.13 and 5.17, an interesting *spectral equivalence principle* is found to hold. Namely, the GS model has the same nonlocal eigenvalue problem as a GM model with exponent set $(2, s_g, 2, s_g)$.

As described above for the GS model, there are two types of instabilities of k-spike patterns with $k > 1$: synchronous oscillatory instabilities and competition instabilities. Competition instabilities, due to real positive

eigenvalues in the spectrum of (5.72), will only occur when

$$D > D_k \equiv \frac{4}{k^2}\left(\log\left[a_k + \sqrt{a_k^2 - 1}\right]\right)^{-2} \qquad k = 2, 3, \dots , \tag{5.74}$$

where $a_k \equiv 1 + \left[1 + \cos\left(\frac{\pi}{k}\right)\right]\zeta^{-1}$, and ζ is defined in (1.2). This result was given in [47] and Proposition 2.6 of [105]. Finally, it was shown in Proposition 11 of [47] that there are $k-1$ eigenvalues that simultaneously cross through zero when $D = D_{gm}$, where D_{gm} was the threshold given in Proposition 5.3 for the bifurcation of asymmetric k-spike branches from a symmetric k-spike branch. Many further results on the spectrum of (5.72) are given in [105]. Similar results have been found in [49] for the SC model (1.6).

There are several key open problems related to the stability of k-spike patterns in one spatial dimension. Although, the existence of a Hopf bifurcation value is guaranteed, it appears to be difficult to establish a transversal crossing condition as was done for the shadow GM model in Sec. 3.2. This leads to the first question.

Question 5.4. Can one give a rigorous proof that there is a unique value of τ where the GM model (1.1) and the GS model (1.5) have a Hopf bifurcation?

The theory described above is based solely on the linearization around a symmetric k-spike patterns. The stability of asymmetric patterns is largely open.

Question 5.5. What are the stability properties of asymmetric spike equilibria for the GM model (1.1) and the GS model (1.5) as a function of $\tau > 0$?.

Question 5.6. Is the Hopf bifurcation subcritical or supercritical? Can one perform a weakly nonlinear theory to determine the local behavior of the bifurcating solutions?

Finally, there are many questions relating to the dynamics of quasi-equilibrium spike patterns for the GM and the GS models. The dynamics of spikes for $\tau = 0$ was studied for the GM model in [48], while a two-spike evolution for the GS model (1.5) was analyzed in [23] and [24]. This leads to the next question.

Question 5.7. Determine the dynamical behavior of k-spike quasi-equilibria for the GM and GS models and the coarsening behavior of these

solutions whereby spikes are annihilated through synchronous oscillations or competition instabilities.

In addition to some of the one-dimensional results given here, there have been a few key studies of the existence and stability of k-spike patterns in the two-dimensional GM and GS models (cf. [19], [113], [114], [115], and [116]). However, there are still many open problems in this direction, including studying the dynamics of multi-spike patterns in multi-dimensional domains.

6. Concluding Remarks

This survey has focussed only on some questions and results related to scalar quasilinear problems and to reaction-diffusion systems with semi-strong spike interactions. For each of our problems involving semi-strong interactions, one of the components of the reaction can be approximated by the solution to either (2.2) or (2.47), while the other component varies on the length scale of the domain.

Alternatively, there have been several studies of spike behavior for systems having weak spike interactions. These systems are characterized by a localization of both components of the reaction. For the Gray-Scott model (1.3) with weak spike interactions, where $D = O(\varepsilon^2)$, spike-replication and chaotic behavior was analyzed in the pioneering studies of [82], [83], [98], and [81]. The initial numerical study of [86] was in the weak interaction regime. For the GM model (1.1) with $D = O(\varepsilon^2)$, the spikes also exhibit self-replication behavior (cf. [30], [95]), and multi-bump phenomena (cf. [20]). Exponentially weak interactions of localized structures were studied for general classes of systems in [32], [33], and [90].

Acknowledgments

I am very grateful to Prof. Chen Hua of Wuhan University and Prof. Roderick Wong of the City University of Hong Kong for inviting me to participate in the meeting in Wuhan, China, in October 2003, and for inviting me to write this survey. It is my great pleasure to acknowledge the contributions of my collaborator Juncheng Wei and my former graduate students David Iron, Theodore Kolokolnikov, and Xiaodi Sun to most of the work described herein. This work was supported by NSERC grant 81541.

References

1. S. Ai, J . Math. Anal. Appl., **277**, No. 2, (2003), pp. 405–422.

2. C. Bandle, M. Flucher, SIAM Rev., **38**, No. 2, (1996), pp. 191–238.
3. P. Bates, N. Fusco, J. Differential Equations, **160**, No. 2, (2000), pp. 283–356.
4. P. Bates, J. Shi, J. Funct. Anal., **196**, No. 2, (2002), pp. 211–264.
5. G. Bellettini, G. Fusco, Asymptot. Anal. **26**, No. 3-4, (2001), pp. 307–357.
6. G. Bellettini, G. Fusco, Asymptot. Anal., **33**, No. 1, (2003), pp. 9–50.
7. H. Berestycki, S. Kamin, G. Sivashinsky, Interfaces Free Bound. **3**, No. 4, (2001), pp. 361–392.
8. H. Berestycki, J. Wei, Ann. Sc. Norm. Super. Pisa Cl. Sci (5), **2**, No. 1, (2003), pp. 199–230.
9. A. Bose, G. Kriegsmann, Methods Appl. Anal., **5**, No. 4, (1998), pp. 351–366.
10. A. Bose, G. Kriegsmann, Methods Appl. Anal., **7**, No. 2, (2000), pp. 295–311.
11. A. Bose, SIAM J. Math. Anal., **31**, No. 2, (2000), pp. 431–454.
12. L. A. Caffarelli, A. Friedman, Duke Math. J., **52**, No. 2, (1985), pp. 431–456.
13. G. Carrier, C. Pearson, *Ordinary Differential Equations*, Blaisdell Publishing Co., Waltham, MA, (1968). (Reprinted in SIAM's *Classics in Applied Mathematics*, series, Vol. **6**, SIAM, Philadelphia, (1991)).
14. X. Chen, M. Kowalczyk, Adv. Differential Equations, **6**, No. 7, (2001), pp. 847–872.
15. X. Chen, M. Kowalczyk, SIAM. J. Math. Anal., **33**, No. 1, (2001), pp. 172–193.
16. E. N. Dancer, Methods Appl. Anal., **8**, No. 2, (2001), pp. 245–256.
17. P. De Groen, G. Karadzhov, Electron. J. Differential Equations, No. 50, (2002), pp. 1–22.
18. M. Del Pino, P. Felmer, M. Kowalczyk, Commun. Pure Appl. Anal., **1**, No. 4, (2002), pp. 437–456.
19. M. Del Pino, M. Kowalczyk, J. Wei, Ann. Inst. H. Poincare, Anal. Non Lineaire, **20**, No. 1, (2003), pp. 53–85.
20. M. Del Pino, M. Kowalczyk, X. Chen, Commun. Contemp. Math. **3**, No. 3, (2001), pp. 419–439.
21. M. Del Pino, P. Felmer, Indiana Univ. Math. J., **48**, No. 3, (1999), pp. 883–898.
22. M. Del Pino, P. Felmer, K. Tanaka, Nonlinearity, **15**, No. 5, (2002), pp. 1653–1671.
23. A. Doelman, W. Eckhaus, T. J. Kaper, SIAM J. Appl. Math., **61**, No. 3, (2000), pp. 1080–1102.
24. A. Doelman, W. Eckhaus, T. J. Kaper, SIAM J. Appl. Math., **61**, No. 6, (2000), pp. 2036–2061.
25. A. Doelman, R. A. Gardner, T. J. Kaper, Phys. D, **122**, No. 1-4, (1998), pp. 1–36.
26. A. Doelman, R. A. Gardner, T. Kaper, Mem. Amer. Math. Soc., **155**, No. 737, (2002), xii+64 pp.
27. A. Doelman, R. A. Gardner, T. Kaper, Indiana U. Math. Journ., **50**, No. 1, (2001), pp. 443-507.
28. A. Doelman, T. Kaper, H. van der Ploeg, Methods Appl. Anal., **8**, No. 3, (2001), pp. 387–414.
29. A. Doelman, T. J. Kaper, P. Zegeling, Nonlinearity, **10**, No. 2, (1997),

pp. 523–563.
30. A. Doelman, H. van der Ploeg, SIAM J. Appl. Dyn. Syst., **1**, No. 1, (2002), pp. 65–104.
31. G. Domokos, P. Holmes, R. Soc. Lond. Proc. Ser. A. Math. Phys. Eng. Sci., **459**, No. 2034, (2003), pp. 1535–1561.
32. S. Ei, Y. Nishiura, K. Ueda, Japan J. Indust. Appl. Math., **18**, No. 2, (2001), pp. 181–205.
33. S. Ei, J. Dynam. Differential Equations, **14**, No. 1, (2002), pp. 85–137.
34. S. Ei, J. Wei, Japan J. Indust. Appl. Math., **19**, No. 2, (2002), pp. 181–226.
35. P. Freitas, Proc. Roy. Soc. Edinburgh Sect. A, **124**, No. 1, (1994), pp. 169–188.
36. A. Gierer, H. Meinhardt, Kybernetik, **12**, (1972), pp. 30–39.
37. P. Gray, S. K. Scott, Chem. Eng. Sci. **39**, (1984), pp. 1087–1097.
38. C. Gui, Commun. in Part. Diff. Eq., **21**, No. 5-6, (1996), pp. 787–820.
39. C. Gui, Duke Math. J., **84**, No. 3, (1996), pp. 739–769.
40. C. Gui, J. Wei, J. Differential Equations, **158**, No. 1, (1999), pp. 1–27.
41. C. Gui, J. Wei, Canad. J. Math., **52**, No. 3, (2000), pp. 522–538.
42. C. Gui, J. Wei, M. Winter, Ann. Inst. H. Poincare Anal. Non Lineaire, **17**, No. 1, (2000), pp. 47–82.
43. B. Gustafsson, Duke Math. J., **60**, No. 2, (1990), pp. 303–311.
44. D. Iron, M. J. Ward, SIAM J. Appl. Math., **60**, No. 3, (2000), pp. 778–802.
45. D. Iron, M. J. Ward, European. J. Appl. Math., **11**, No. 5, (2000), pp. 491–514.
46. D. Iron, M. J. Ward, Math. Comput. Simulation, **55**, No. 4-6, (2001), pp. 419–431.
47. D. Iron, M. J. Ward, J. Wei, Phys. D, **150**, No. 1-2, (2001), pp. 25–62.
48. D. Iron, M. J. Ward, SIAM J. Appl. Math., **62**, No. 6, (2002), pp. 1924–1951.
49. D. Iron, J. Wei, M. Winter, to appear, J. Math. Biology, (2004).
50. D. Iron, M. J. Ward, Analysis and Applications, **2**, No. 1, (2004), pp. 1–50.
51. W. Kath, C. Knessl, B. Matkowsky, Stud. Appl. Math., **77**, No. 1, (1987), pp. 61–88.
52. W. Kelley, J. Math. Anal. Appl., **255**, No. 2, (2001), pp. 678–697.
53. W. Kelley, IMA J. Appl. Math., **60**, No. 1, (1998), pp. 91–108.
54. T. Kolokolnikov, M. J. Ward, European J. Appl. Math., **14**, No. 5, (2003), pp. 513–545.
55. T. Kolokolnikov, M. J. Ward, to appear, Discrete Contin. Dyn. Syst. Ser. B., (2004).
56. T. Kolokolnikov, M. Ward, J. Wei, submitted, Mem. Amer. Math. Soc., (2003).
57. T. Kolokolnikov, M. Ward, J. Wei, submitted, Phys. D, (2003).
58. T. Kolokolnikov, J. Wei, submitted, European J. Appl. Math., (2003).
59. M. Kowalczyk, Duke Math J., **98**, No. 1, (1999), pp. 59–111.
60. M. Kowalczyk, J. Differential Equations, **138**, No. 1, (1997), pp. 55–85.
61. E. Knobloch, Outstanding Problems in the Theory of Pattern Formation, book chapter in *Nonlinear Dynamics and Chaos. Where Do We Go From Here?*, edited by S. J. Hogan et al., Institute of Physics Publishing, Bristol,

U.K. (2003).
62. G. Kriegsmann, IMA J. Appl. Math. **59**, No. 2, (1997), pp. 123–148.
63. G. Kriegsmann, IMA J. Appl. Math., **66**, No. 1, (2001), pp. 1–32.
64. M. Kuwamura, S. Ei, M. Mimura, Japan J. Indust. Appl. Math., **9**, No. 1, (1992), pp. 35–77.
65. M. Kwong, Arch. Rational Mech. Anal., **105**, No. 3, (1989), pp. 243–266.
66. C. Lange, Stud. Appl. Math., **68**, No. 3, (1983), pp. 227–257.
67. J. Y. Lee, M. J. Ward, Stud. Appl. Math., **94**, No. 3, (1995), pp. 271–326.
68. C. S. Lin, W. M. Ni, I. Takagi, J. Diff. Eq., **72**, (1988), pp. 1-27.
69. A. D. MacGillivray, R. Braun, G. Tanouglu, Stud. Appl. Math., **104**, No. 4, (2000), pp. 293–311.
70. H. Meinhardt, *Models of Biological Pattern Formation*, Academic Press, London, (1982).
71. H. Meinhardt, *The Algorithmic Beauty of Sea Shells*, Springer-Verlag, Berlin, (1995).
72. D. Morgan, T. Kaper, submitted, Phys. D, (2003).
73. C. Muratov, V. V. Osipov, SIAM J. Appl. Math., **62**, No. 5, (2002), pp. 1463–1487.
74. C. Muratov, V. V. Osipov, J. Phys. A: Math Gen. **33**, (2000), pp. 8893–8916.
75. K. Nagasaki, T. Suzuki, Asymptotic Anal., **3**, No. 2, (1990), pp. 173–188.
76. W. M. Ni, I. Takagi, Comm. Pure Appl. Math., **44**, No. 7, (1991), pp. 819–851.
77. W. M. Ni, I. Takagi, Duke Math. J., **70**, No. 2, (1993), pp. 247–281.
78. W. M. Ni, Notices Amer. Math. Soc., **45**, No. 1, (1998), pp. 9–18.
79. W. M. Ni, J. Wei, Comm. Pure. Appl. Math., **48**, No. 7, (1995), pp. 731–768.
80. Y. Nishiura, in Dynamics Reported: Expositions in Dynamical Systems Volume 3 (editors: C. K. R. T. Jones, U. Kirchgraber), Springer-Verlag, New York, (1995).
81. Y. Nishiura, Methods Appl. Anal., **8**, No. 2, (2001), pp. 321–332.
82. Y. Nishiura, D. Ueyama, Phys. D, **130**, No. 1-2, (1999), pp. 73–104.
83. Y. Nishiura, D. Ueyama, Phys. D, **150**, No. 3-4, (2001), pp. 137–162.
84. R. O'Malley Jr., J. Math. Anal. Appl., **54**, No. 2, (1976), pp. 449–466.
85. C.H. Ou, R. Wong, Stud. Appl. Math., **111**, No. 4, (2003), pp. 377–408.
86. J. E. Pearson, Science, **216**, (1993), pp. 189–192.
87. L. Reyna, M. J Ward, European J. Appl. Math., **5**, No. 4, (1994), pp. 495-523.
88. S. Rosenbalt, R. Szeto, Stud. Appl. Math., **63**, No. 2, (1980), pp. 99–117.
89. B. Sandstede, Trans. Amer. Math. Soc., **350**, No. 2, (1998), pp. 429–472.
90. J. Schnakenberg, J. Theoret. Biology, **81**, (1979), pp. 389–400.
91. B. Sleeman, M. J. Ward, J. Wei, submitted, SIAM J. Appl. Math., (2004).
92. X. Sun, M. J. Ward, European J. Appl. Math., **10**, No. 1, (1999), pp. 27–53.
93. X. Sun, M. J. Ward, Methods Appl. Anal., **8**, No. 2, (2001), pp. 333–347.
94. X. Sun, IMA J. Numer. Anal., **21**, No. 4, (2001), pp. 817–842.
95. W. Sun, T. Tang, M. J. Ward, J. Wei, Stud. Appl. Math., **111**, No. 1, (2003), pp. 41–84.
96. I. Takagi, J. Differential Equations, **61**, No. 2, (1986), pp. 208–249.
97. A. Turing, Phil. Trans. Roy. Soc. B, **237**, (1952), pp. 37–72.

98. D. Ueyama, Hokkaido Math J., **28**, No. 1, (1999), pp. 175–210.
99. Z. Wang, J. Differential Equations, **159**, No. 1, (1999), pp. 102-137.
100. M. J. Ward, Stud. Appl. Math., **87**, No. 2, (1992), pp. 95–135.
101. M. J. Ward, Stud. Appl. Math., **97**, No. 2, (1996), pp. 103-126.
102. M. J. Ward, book chapter in *Analyzing Multiscale Phenomena Using Singular Perturbation Methods*, (J. Cronin, R. O'Malley editors), Proceedings of Symposia in Applied Mathematics, Vol. 56, AMS Short Course (1998), pp. 151–184.
103. M. J. Ward, D. McInerney, P. Houston, D. Gavaghan, P. Maini, SIAM J. Appl. Math., **62**, No. 4, (2002), pp. 1297–1328.
104. M. J. Ward, J. Wei, European J. Appl. Math., **13**, No. 3, (2002), pp. 283–320.
105. M. J. Ward, J. Wei, J. Nonlinear Science, **13**, No. 2, (2003), pp. 209–264.
106. M. J. Ward, J. Wei, to appear, European J. Appl. Math., (2004).
107. M. J. Ward, J. Wei, Stud. Appl. Math., **109**, No. 3, (2002), pp. 229–264.
108. J. Wei, European J. Appl. Math., **10**, No. 4, (1999), pp. 353–378.
109. J. Wei, J. Differential Equations, **134**, No. 1, (1997), pp. 104–133.
110. J. Wei, Tohoku Math. J., **50**, No. 2, (1998), pp. 159–178.
111. J. Wei, Proc. Roy. Soc. Edinburgh Sect. A, **131**, No. 6, (2001), pp. 1457–1480.
112. J. Wei, Phys. D. **148**, No. 1-2, (2001), pp. 20-48.
113. J. Wei, M. Winter, J. Differential Equations, **178**, No. 2, (2002), pp. 478–518.
114. J. Wei, M. Winter, J. Nonlinear Science, **11**, No. 6, (2001), pp. 415–458.
115. J. Wei, M. Winter, Internat. J. Bifur. Chaos Appl. Sci. Engrg., **13**, No. 6, (2003), pp. 1529-1543.
116. J. Wei, M. Winter, Stud. Appl. Math., **110**, No. 1, (2003), pp. 63-102.
117. J. Wei, M. Winter, Phys. D, **176**, No. 3-4, (2003), pp. 147–180.